Gamma rays from the inner galaxy and the galactic halo region

Focus on recent work with:
Hu, **IC**, Zhong, arXiv:2602.20252 (PRD accepted)
IC, Hu, Zhong, in prep. 260X.XXXXX

Mention some earlier results from:
IC, Zhong, McDermott, Surdutovich, PRD **105**, 103023 (2022)
McDermott, Zhong, **IC** MNRAS Letters, **522,** L21-L25 (2023)
Also ongoing work in Zhong & **IC** PRD 109, 123017 (2024)

Ilias Cholis, 07/01/2026

third dimension (not shown) — energy

The Fermi-LAT Gamma-ray SKY

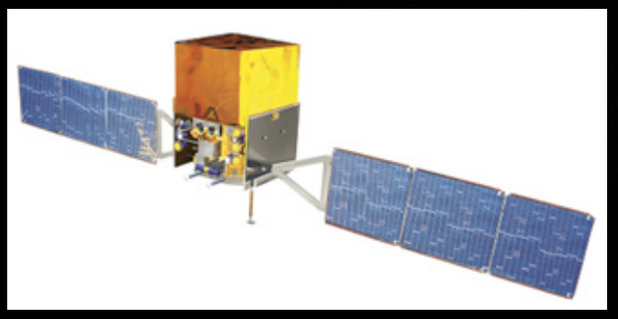

latitude, b→

Galactic Halo Region

Inner Galaxy

Galactic Center

←Galactic longitude, ℓ

third dimension (not shown) — energy

The Fermi-LAT Gamma-ray SKY

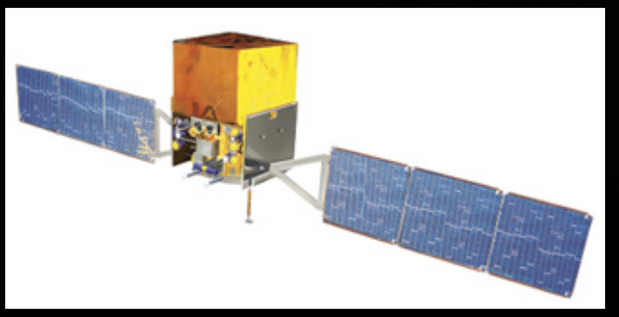

latitude, b→

Sources for the observed gamma-rays are:

i)Galactic Diffuse Emission: decay of pi0s (and other mesons) from pp (NN) collisions in the ISM, bremsstrahlung radiation off CR e, Inverse Compton scattering: up-scattering of CMB and IR, optical photons from CR e

ii)from point sources (galactic or extra galactic)

iii)Extragalactic Isotropic

iv)"extended sources"(Fermi Bubbles, Geminga, Vela ...)

iv)misidentified CRs (isotropic due to diffusion of CRs in the Galaxy)

Modeling the ISM galactic production and propagation uncertainties for cosmic rays

$$\frac{\partial \psi(r,p,t)}{\partial t} = \overset{\text{sources}}{q(r,p,t)} + \overset{\text{diffusion}}{\vec{\nabla}\cdot(D_{xx}\vec{\nabla}\psi)} + \overset{\text{re-acceleration}}{\frac{\partial}{\partial p}\left[p^2 D_{pp}\frac{\partial}{\partial p}\left(\frac{\psi}{p^2}\right)\right]} + \overset{\text{convection}}{\frac{\partial}{\partial p}\left[\frac{p}{3}(\vec{\nabla}\cdot\vec{V})\psi\right]}$$

Modeling the ISM galactic production and propagation uncertainties for cosmic rays

$$\frac{\partial \psi(r,p,t)}{\partial t} = \underbrace{q(r,p,t)}_{\text{sources}} + \underbrace{\vec{\nabla}\cdot(D_{xx}\vec{\nabla}\psi)}_{\text{diffusion}} + \underbrace{\frac{\partial}{\partial p}\left[p^2 D_{pp}\frac{\partial}{\partial p}\left(\frac{\psi}{p^2}\right)\right]}_{\text{re-acceleration}} + \underbrace{\frac{\partial}{\partial p}\left[\frac{p}{3}(\vec{\nabla}\cdot\vec{V})\psi\right]}_{\text{convection}}$$

Voyager 1 (ISM) proton flux:

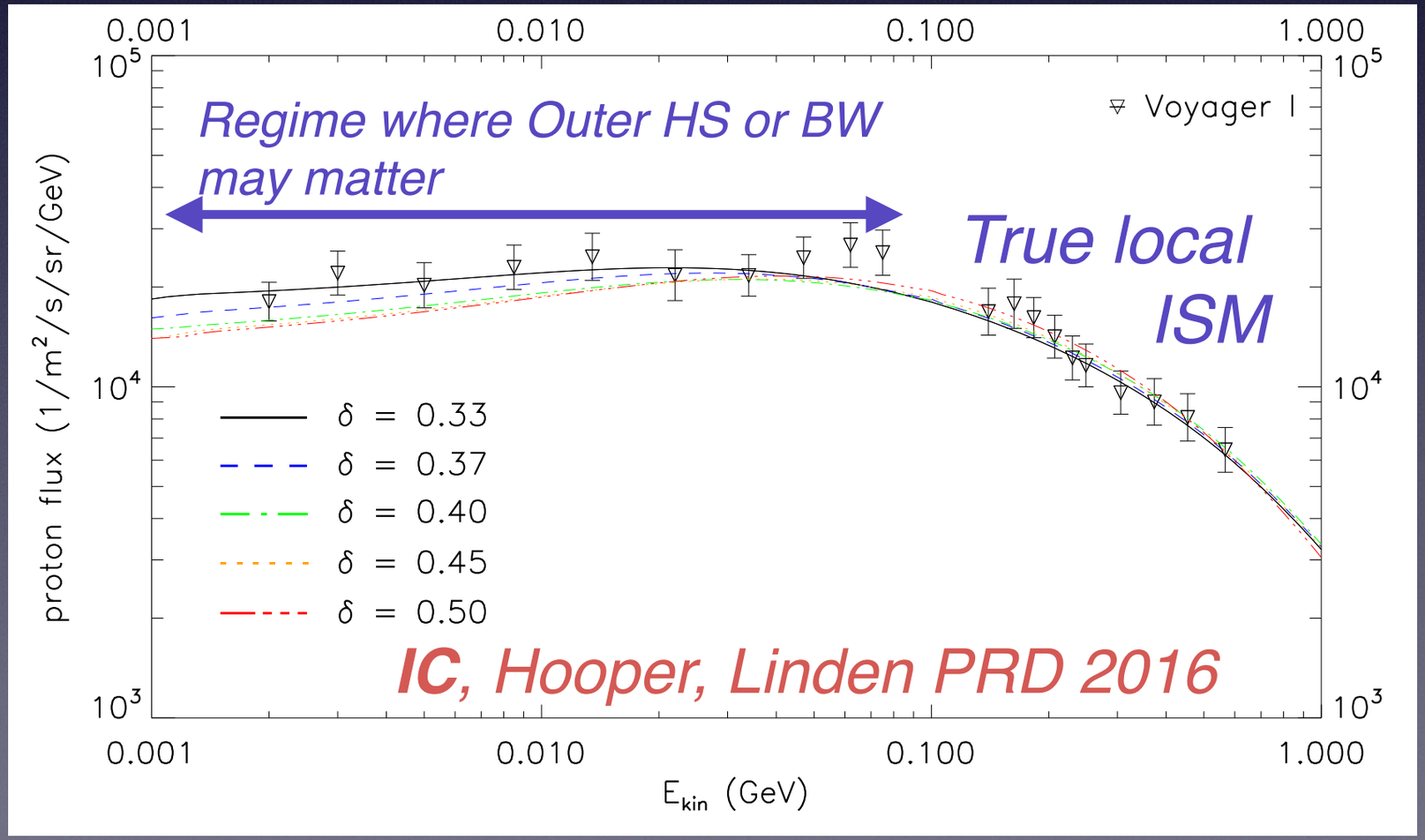

We use GALPROP a numerical solver build by Moskalenko, Strong et al. as a starting point and build several models that are in agreement with CR measurements

Cross-checking with the PROTON data that account for the majority of observed cosmic rays; monthly AND total (i.e ISM & Solar Modulation):

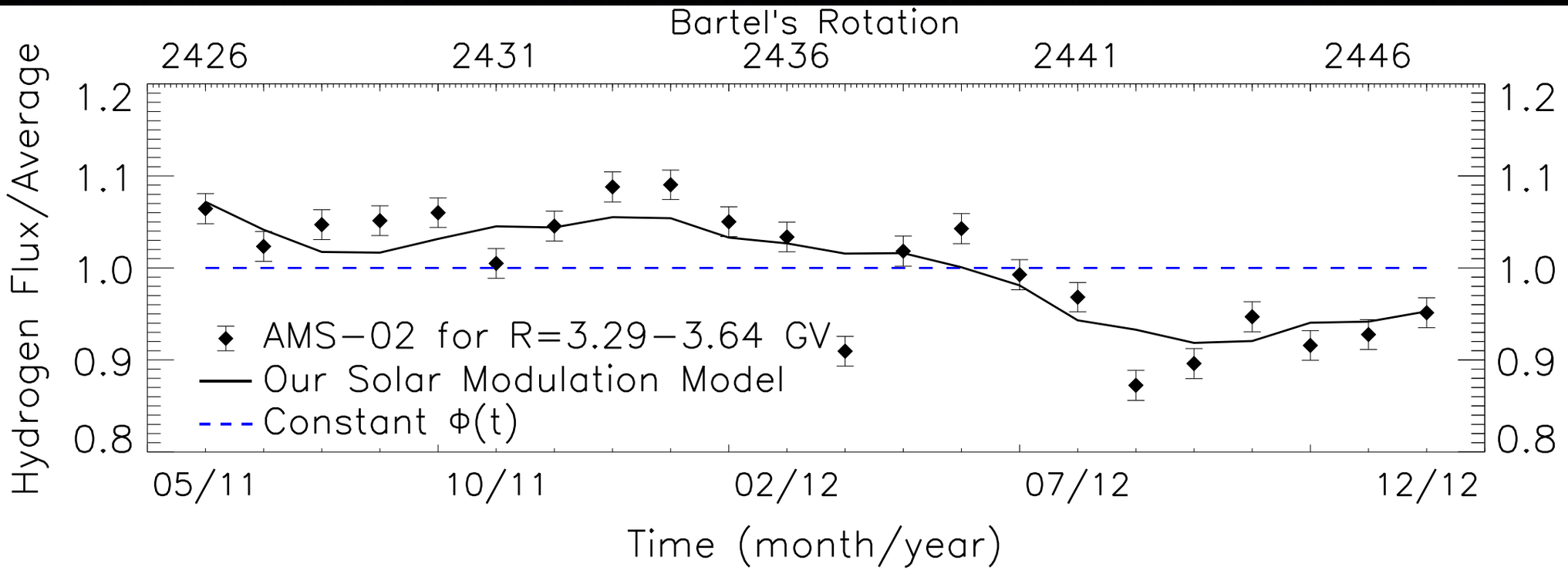

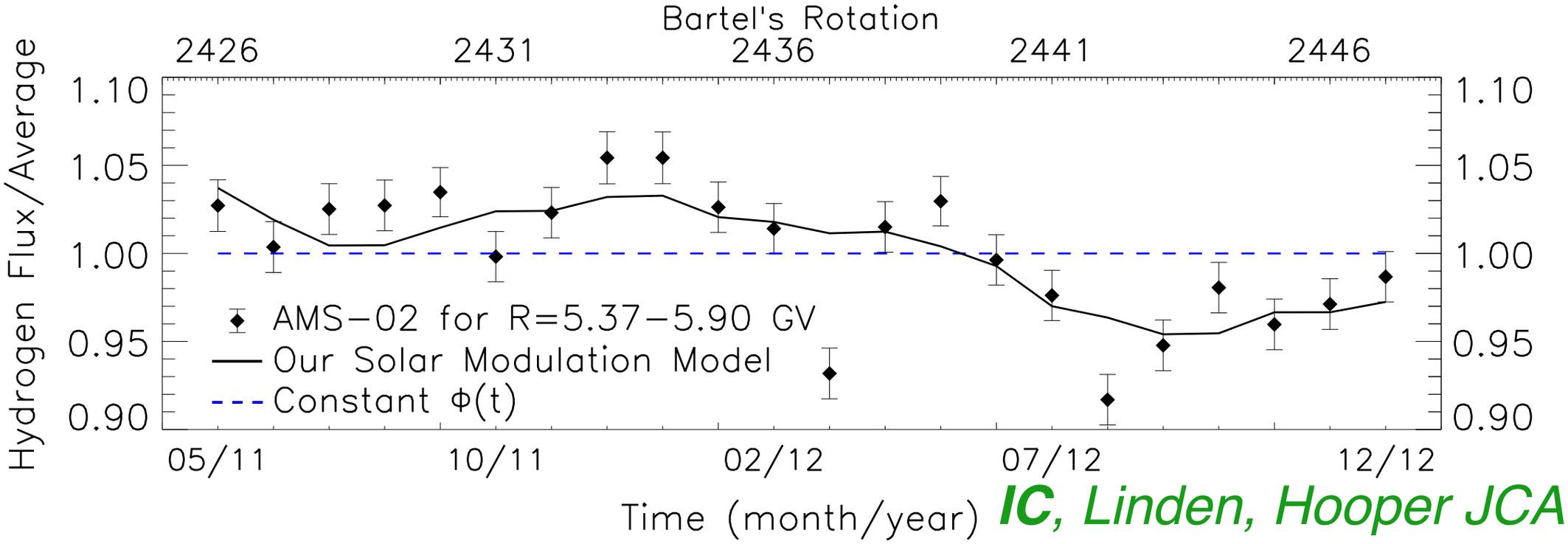

***IC**, Linden, Hooper JCAP 2022*

Constraining the form of the Modulation potential and the ISM p spectrum in a recursive manner.

*Also **IC**, McKinnon PRD **106**, 063021 2022*

Repeating for multiple Cosmic-Ray species we can constrain the physical processes affecting the cosmic-ray production & propagation

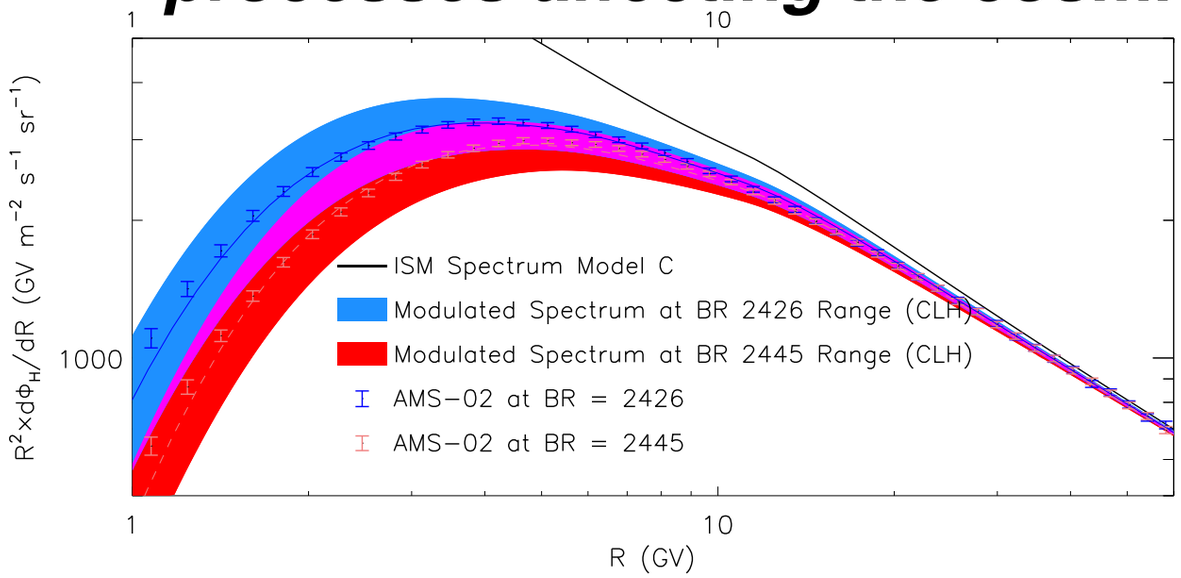

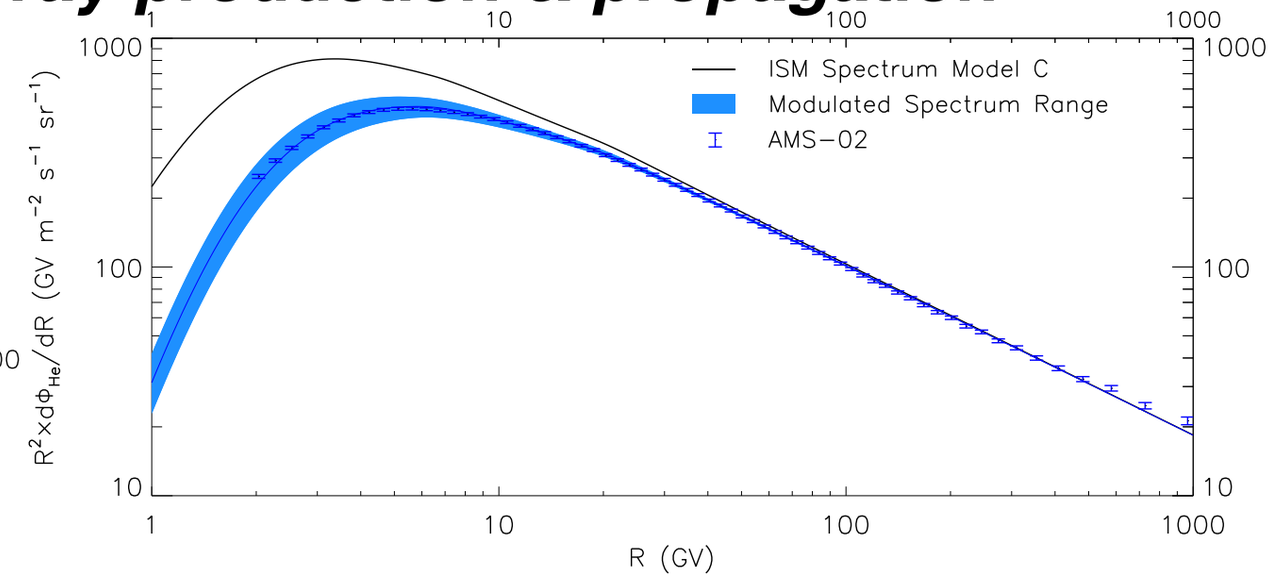

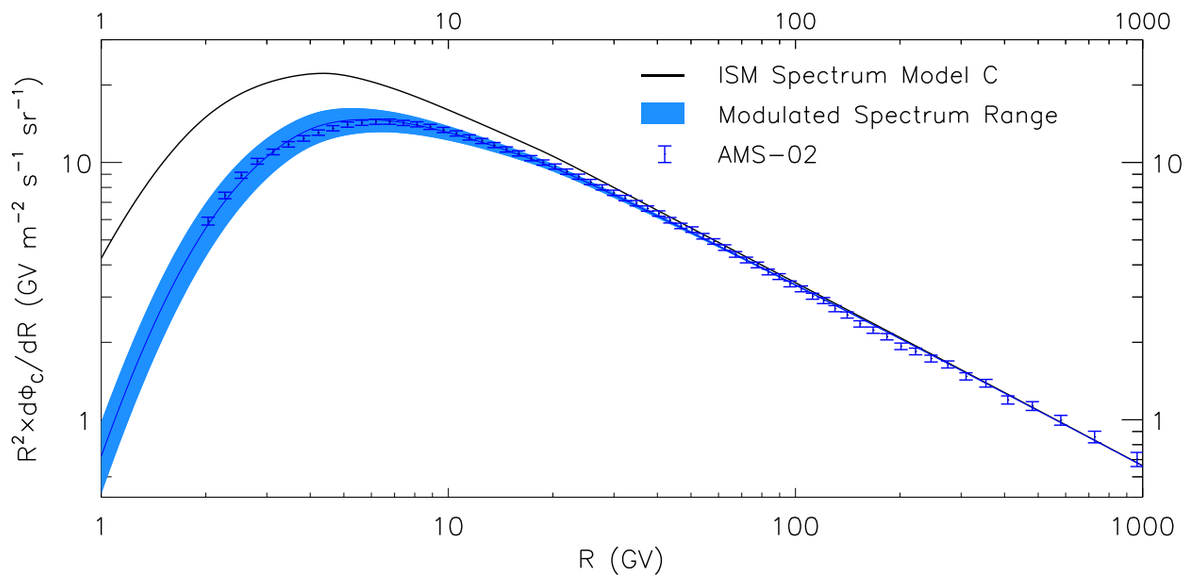

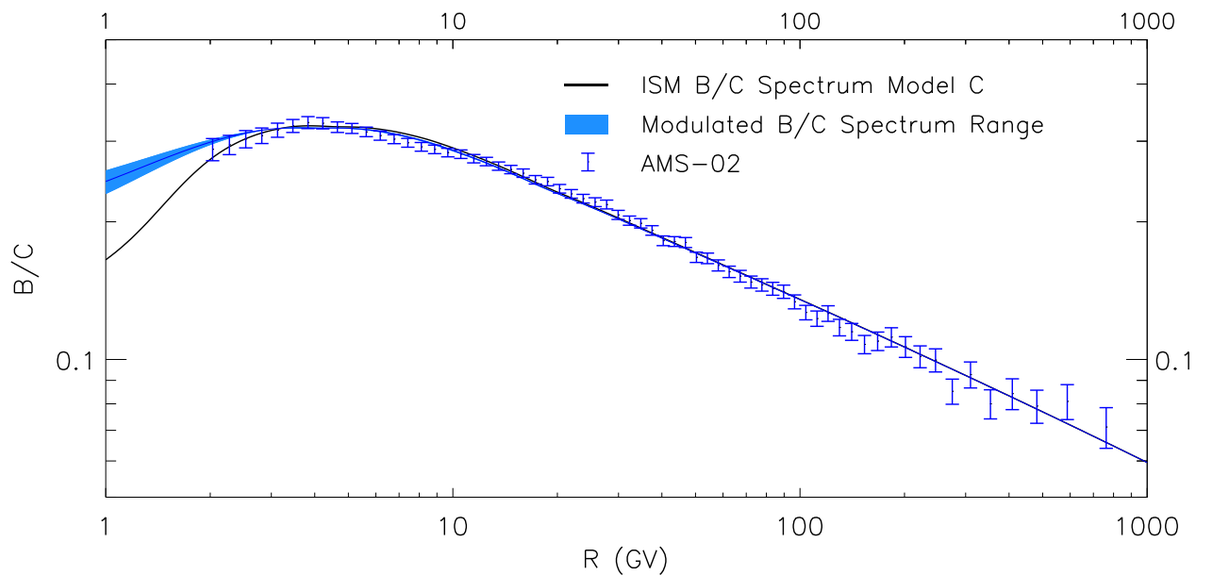

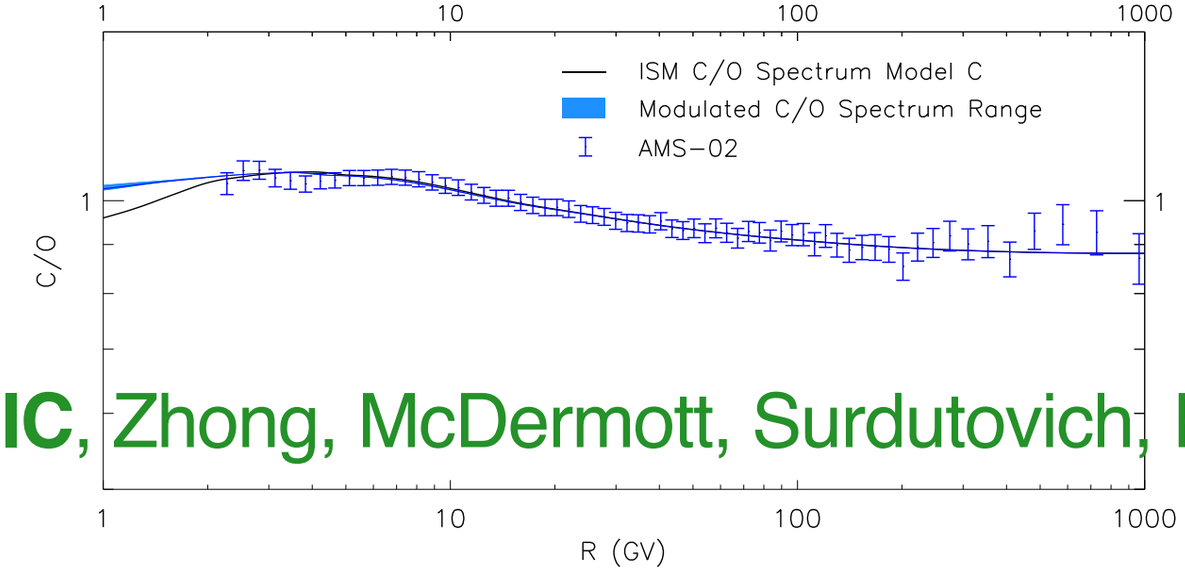

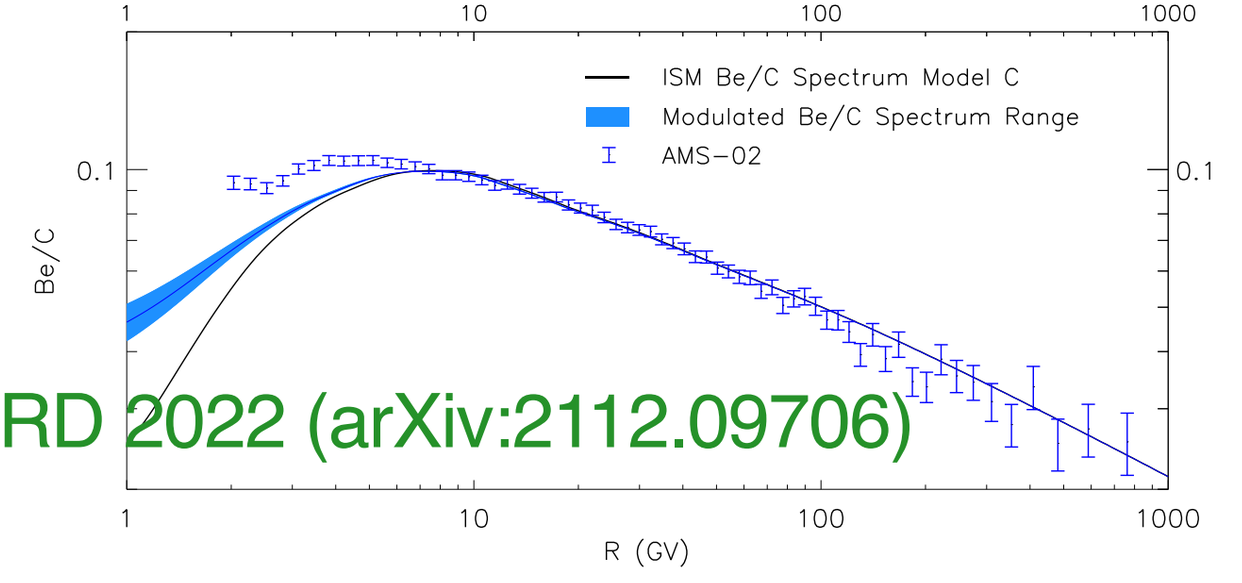

IC, Zhong, McDermott, Surdutovich, PRD 2022 (arXiv:2112.09706)

The ISM propagation conditions that fit the local spectra

TABLE I. The cosmic-ray propagation assumptions (CR model), determined by the diffusion index δ, the diffusion scale height z_L, the normalization of the diffusion co-efficient D_0, the Alfvén velocity v_A, the galactic convection gradient dv_c/dv, the injection indices α_1, α_2, α_3, and the rigidity breaks R_{br_1} and R_{br_2} for cosmic-ray hydrogen and helium isotopes. In the last five columns, the first values refer to hydrogen injection properties and the second values to helium.

CR model	δ	z_L (kpc)	$D_0 \times 10^{28}$ (cm^2/s)	v_A (km/s)	$dv_c/d\|z\|$ (km/s/kpc)	α_1 H/He	R_{br_1} H/He (GV)	α_2 H/He	R_{br_2} H/He (GV)	α_3 H/He
A	0.33	5.7	6.70	30.0	0	1.74/1.70	6.0/7.4	2.04/2.16	14.0/21.5	2.41/2.39
B	0.37	5.5	5.50	30.0	2	1.72/1.74	6.0/8.0	2.00/2.14	12.4/21.0	2.38/2.375
C	0.40	5.6	4.85	24.0	1	1.69/1.65	6.0/6.7	2.00/2.13	12.4/20	2.38/2.355
D	0.45	5.7	3.90	24.0	5.5	1.69/1.68	6.0/7.0	1.99/2.12	12.4/18.7	2.355/2.34
E	0.50	6.0	3.10	23.0	9	1.71/1.68	6.0/7.2	2.02/2.14	11.2/17.5	2.38/2.33
F	0.43	3.0	1.85	20.0	2	1.68/1.74	6.0/10.5	2.08/2.09	13.0/21.0	2.41/2.33

This is a starting point.

The ISM propagation conditions that fit the local spectra

TABLE I. The cosmic-ray propagation assumptions (CR model), determined by the diffusion index δ, the diffusion scale height z_L, the normalization of the diffusion co-efficient D_0, the Alfvén velocity v_A, the galactic convection gradient dv_c/dv, the injection indices α_1, α_2, α_3, and the rigidity breaks R_{br_1} and R_{br_2} for cosmic-ray hydrogen and helium isotopes. In the last five columns, the first values refer to hydrogen injection properties and the second values to helium.

CR model	δ	z_L (kpc)	$D_0 \times 10^{28}$ (cm^2/s)	v_A (km/s)	$dv_c/d\|z\|$ (km/s/kpc)	α_1 H/He	R_{br_1} H/He (GV)	α_2 H/He	R_{br_2} H/He (GV)	α_3 H/He
A	0.33	5.7	6.70	30.0	0	1.74/1.70	6.0/7.4	2.04/2.16	14.0/21.5	2.41/2.39
B	0.37	5.5	5.50	30.0	2	1.72/1.74	6.0/8.0	2.00/2.14	12.4/21.0	2.38/2.375
C	0.40	5.6	4.85	24.0	1	1.69/1.65	6.0/6.7	2.00/2.13	12.4/20	2.38/2.355
D	0.45	5.7	3.90	24.0	5.5	1.69/1.68	6.0/7.0	1.99/2.12	12.4/18.7	2.355/2.34
E	0.50	6.0	3.10	23.0	9	1.71/1.68	6.0/7.2	2.02/2.14	11.2/17.5	2.38/2.33
F	0.43	3.0	1.85	20.0	2	1.68/1.74	6.0/10.5	2.08/2.09	13.0/21.0	2.41/2.33

This is a starting point. For the inner galaxy we allow for greater ranges to account for uncertainties on the ISM conditions of the inner galaxy. As:

TABLE II. Galactic diffuse model parameters z_L is in kpc, D_0 is in $\times 10^{28}$ cm^2/s, v_A is in km/s, $dv_c/d|z|$ is in km/s/kpc. N^p and N^e are the cosmic-ray proton and electron differential flux dN/dE normalizations at the galactocentric distance of 8.5 kpc. They are defined at 100 and 34.5 GeV for the protons and electrons respectively and are in units of $\times 10^{-9}$ cm^{-2} s^{-1} sr^{-1} MeV^{-1}. See text for full details.

Name	z_L	D_0	δ	v_A	$dv_c/d\|z\|$	S^N/S^e	α_1^p/α_2^p	α_1^e/α_2^e	N^p/N^e	B-field	ISRF	H2	HI	HII
I	4.0	5.00	0.33	32.7	55	Pul/Pul	1.35/2.33	1.5/2.25	4.13/3.33	200030050	1.36,1.36,1.0	9	5	1
II	6.0	7.1	0.33	50.0	0	Pul/SNR	1.89/2.30	1.40/2.10	2.40/2.20	050100020	1.0,1.0,1.0	2*	1	1
III	5.6	4.85	0.40	40.0	0	Pul/Pul	1.50/1.90	1.5/2.25	2.40/1.55	200050040	1.4,1.4,1.0	9	4	1
VI	6.0	2.00	0.33	0	200	Pul/SNR	1.60/2.10	1.6/2.30	2.32/5.70	200030050	1.4,1.4,1.0	9	5	1
X	10.0	8.00	0.33	32.2	50	Pul/SNR	1.40/1.80	1.4/2.35	1.90/3.20	200040050	1.4,1.4,1.0	0	5	2
XV	6.0	7.10	0.33	50.0	0	Pul/SNR	1.89/2.30	1.40/2.10	2.40/2.20	050100020	1.0,1.0,1.0	0	5	2
...														
LXXX	5.6	4.85	0.40	40.0	0	Pul/Pul	1.50/1.90	1.5/2.25	2.40/1.55	200050040	1.4,1.4,1.0	0	4	3

Every model predicts its own unique combination of diffuse emission maps:

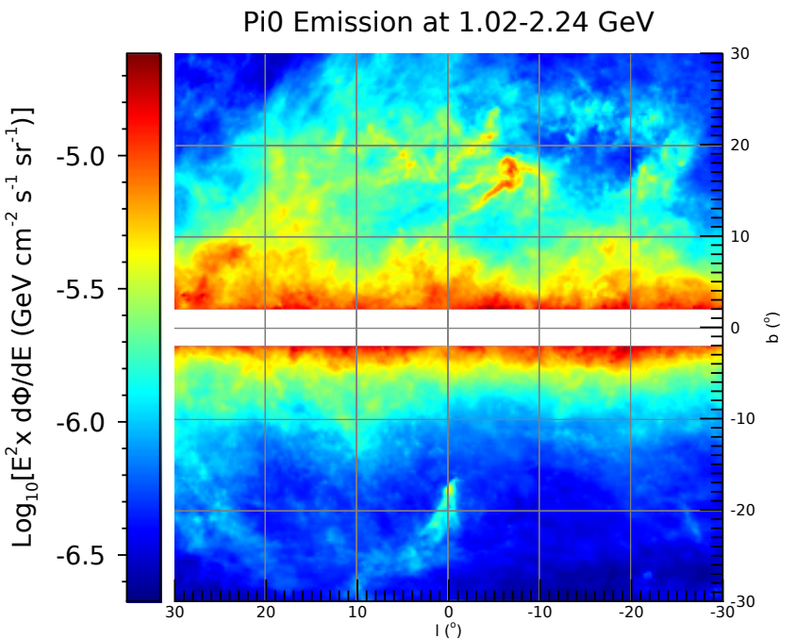

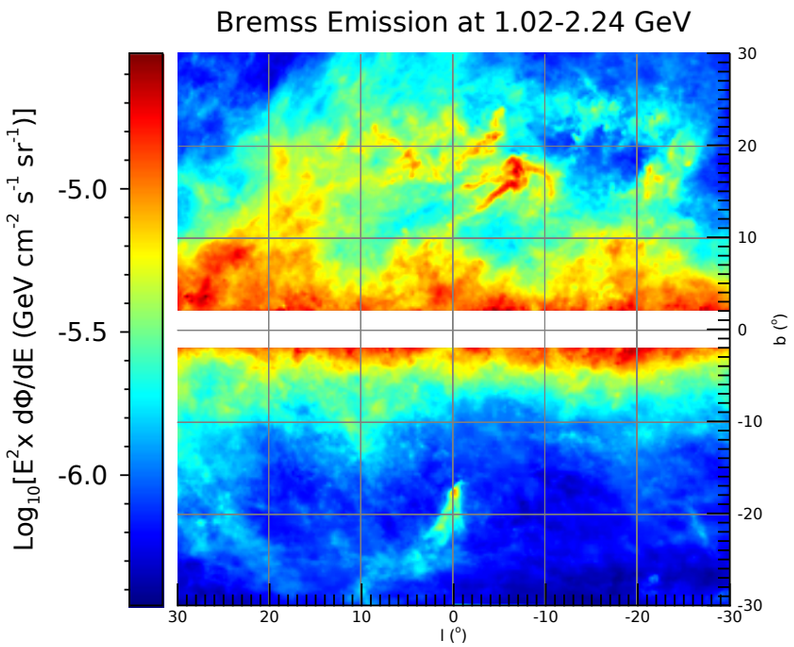

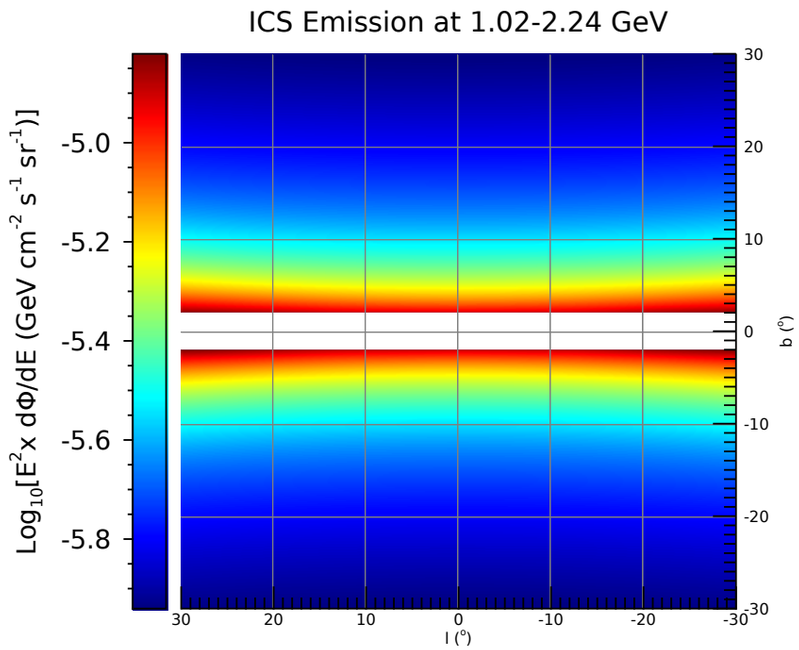

And energy evolution:

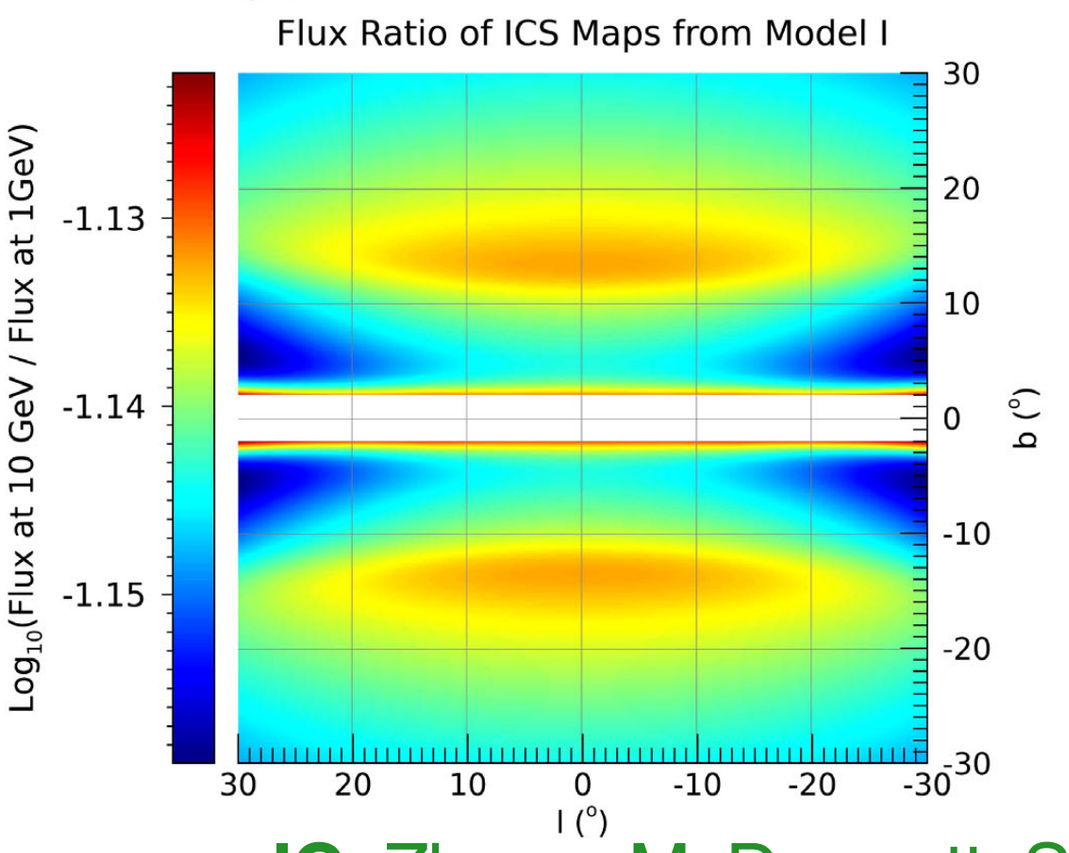

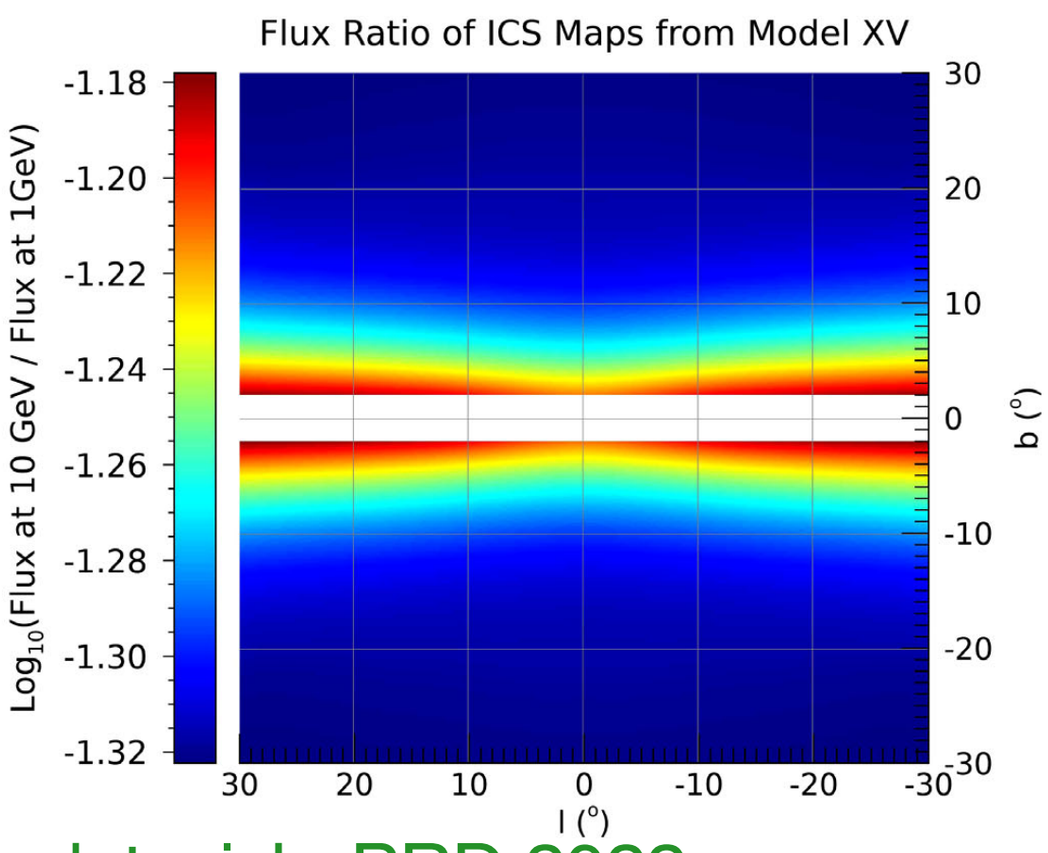

IC, Zhong, McDermott, Surdutovich, PRD 2022

Pi0 Emission at 1.02-2.24 GeV

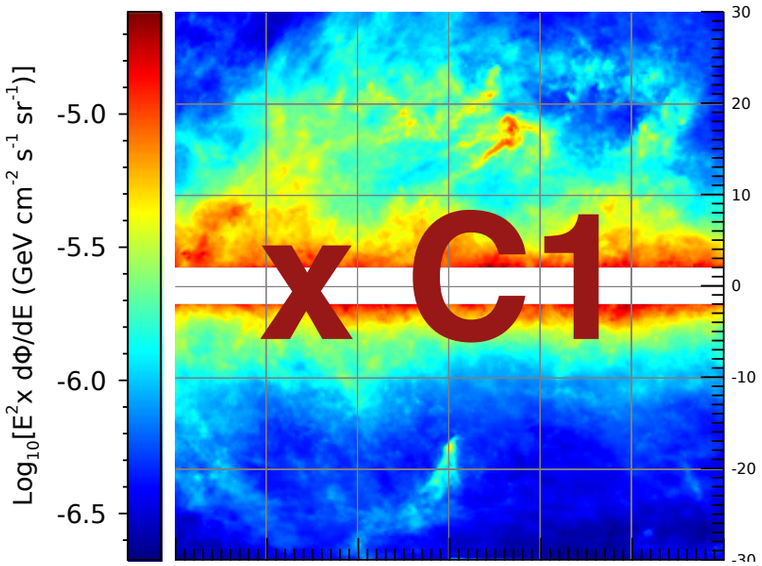

Bremss Emission at 1.02-2.24 GeV

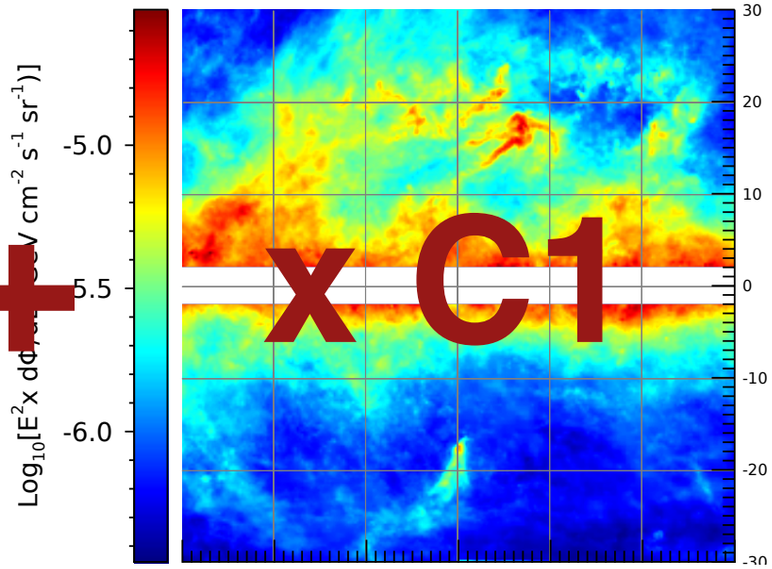

ICS Emission at 1.02-2.24 GeV

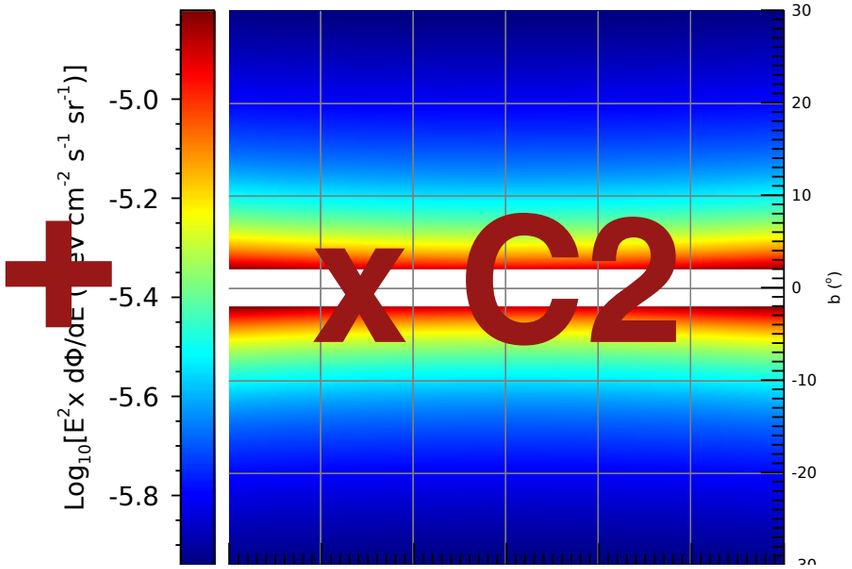

Bubbles Emission at 1.02-2.24 GeV

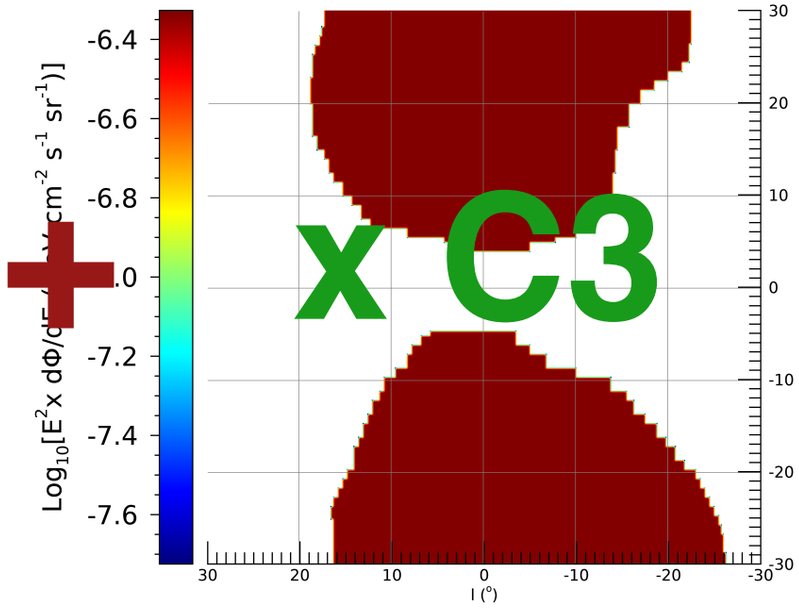

Isotropic Emission at 1.02-2.24 GeV

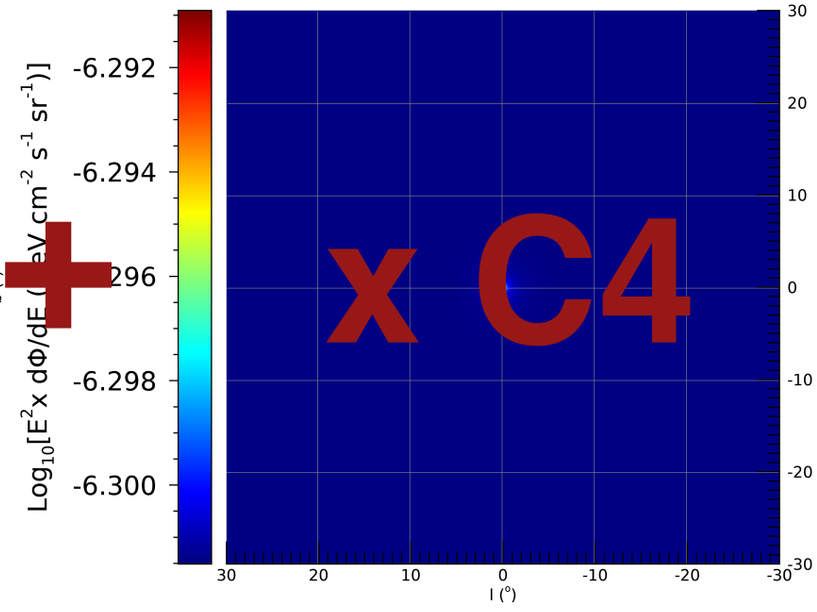

Dark Matter Emission at 1.02-2.24 GeV

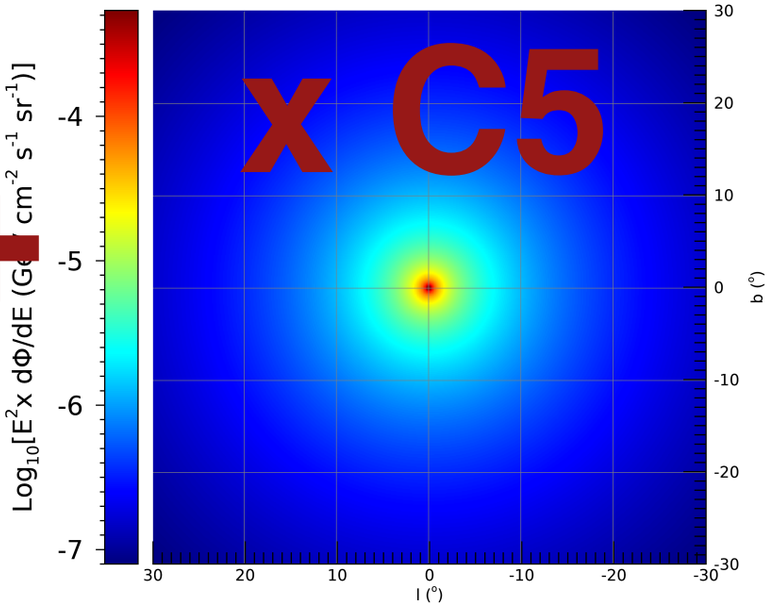

Pi0 Emission at 1.02-2.24 GeV

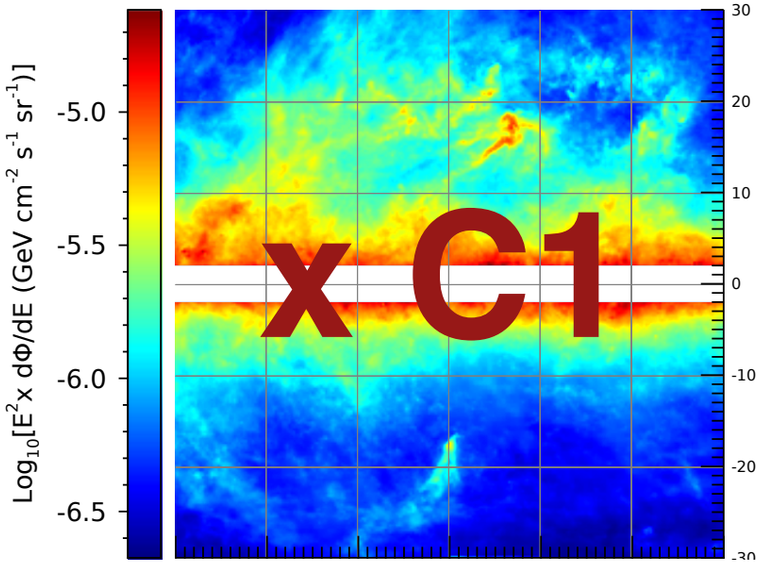

Bremss Emission at 1.02-2.24 GeV

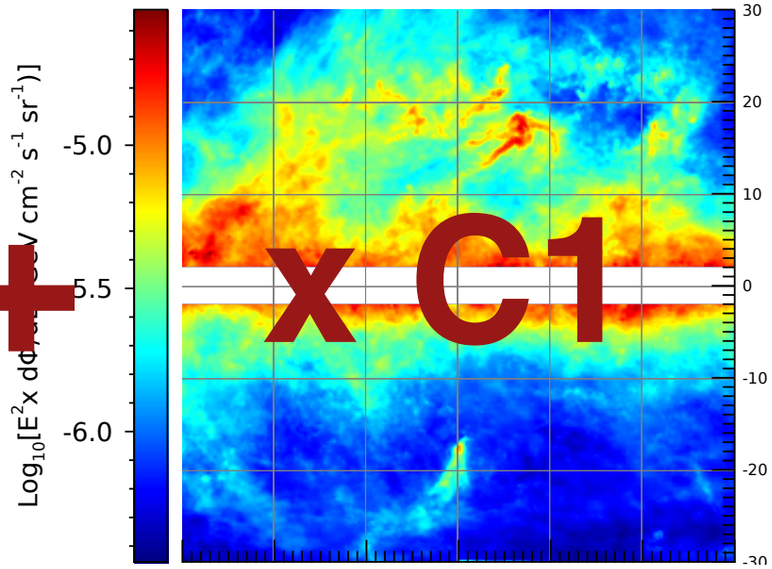

ICS Emission at 1.02-2.24 GeV

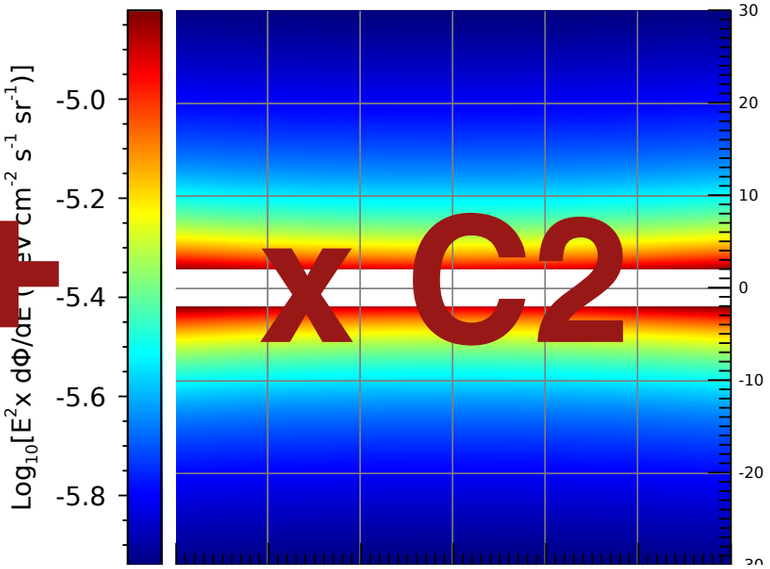

Bubbles Emission at 1.02-2.24 GeV

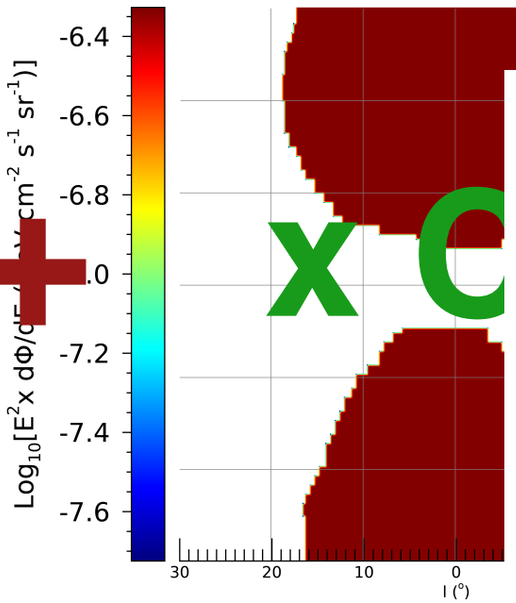

Isotropic Emission at 1.02-2.24 GeV

Dark Matter Emission at 1.02-2.24 GeV

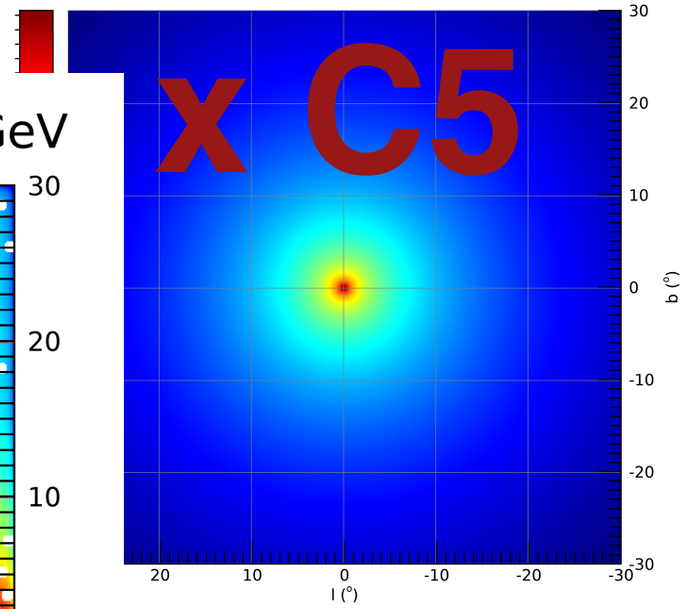

Composite Emission w PSF at 1.02-2.24 GeV

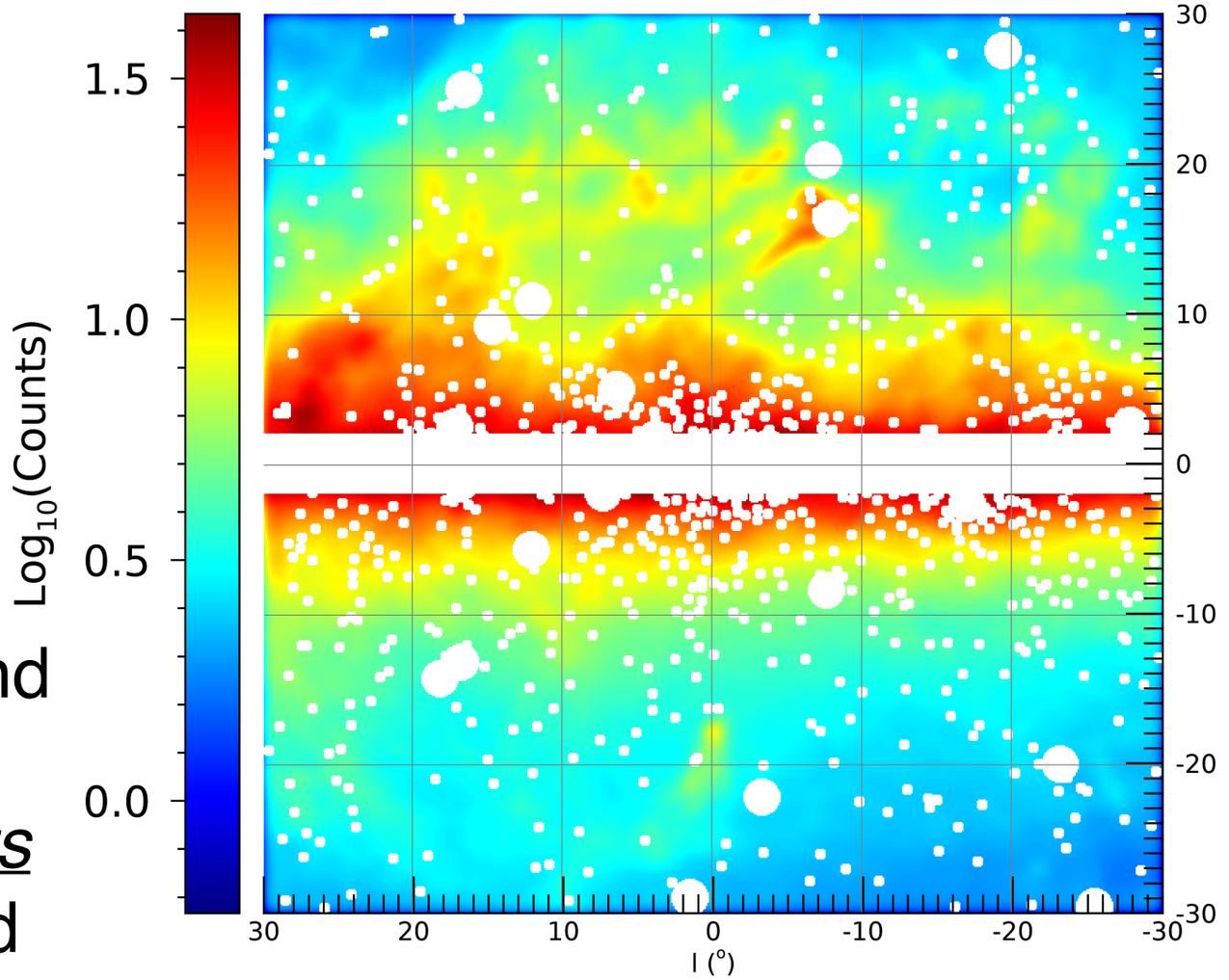

Adding properly and accounting for *instrumental effects* as the point spread function and the non-uniform exposure (also masking-out bright point sources)

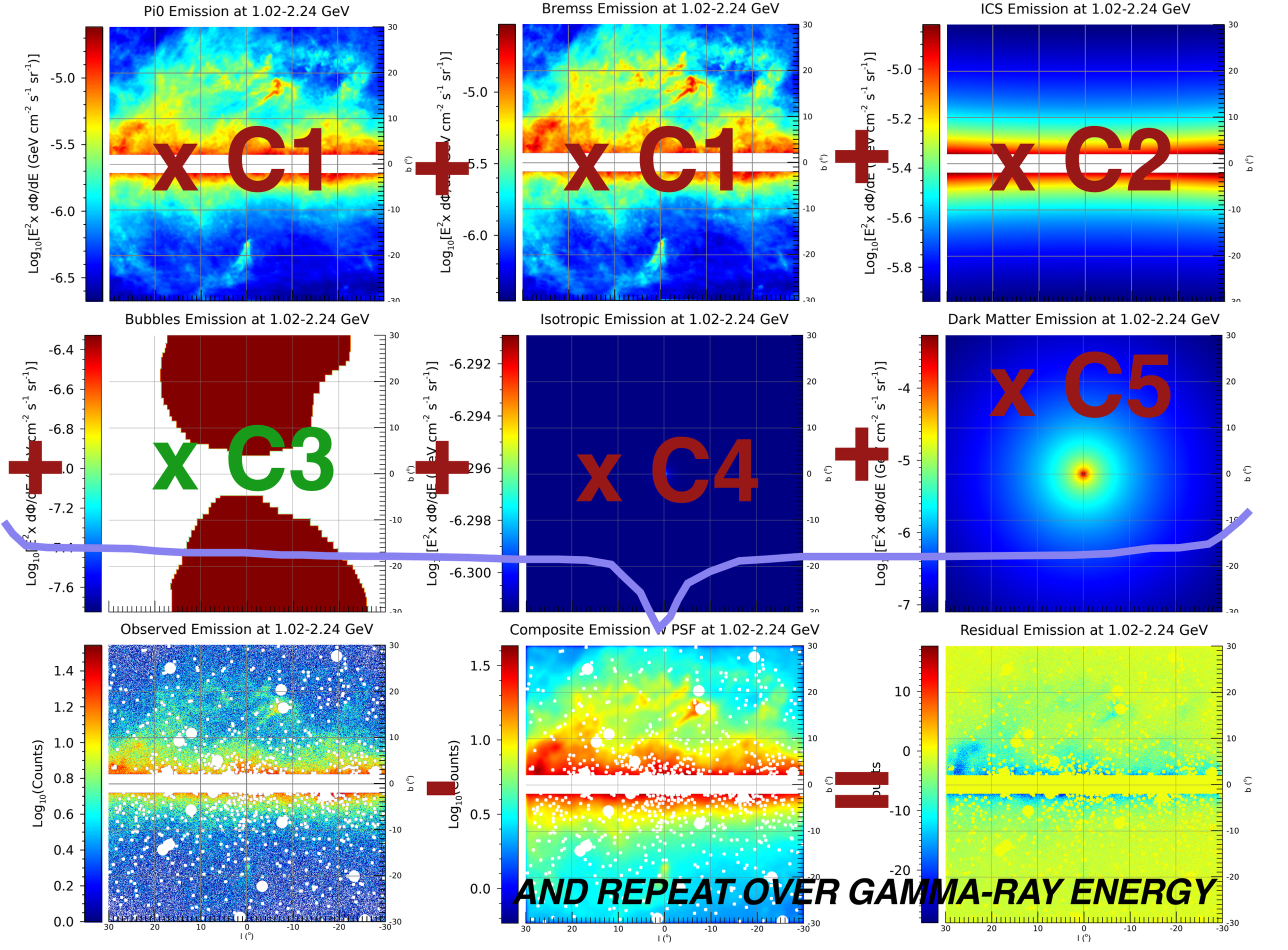
Pi0 Emission at 1.02-2.24 GeV
Bremss Emission at 1.02-2.24 GeV
ICS Emission at 1.02-2.24 GeV
x C1
x C1
x C2
Bubbles Emission at 1.02-2.24 GeV
Isotropic Emission at 1.02-2.24 GeV
Dark Matter Emission at 1.02-2.24 GeV
x C3
x C4
x C5
Observed Emission at 1.02-2.24 GeV
Composite Emission w PSF at 1.02-2.24 GeV
Residual Emission at 1.02-2.24 GeV
AND REPEAT OVER GAMMA-RAY ENERGY
l (°)
b (°)

Looking for excesses in the galactic center

Using Templates:

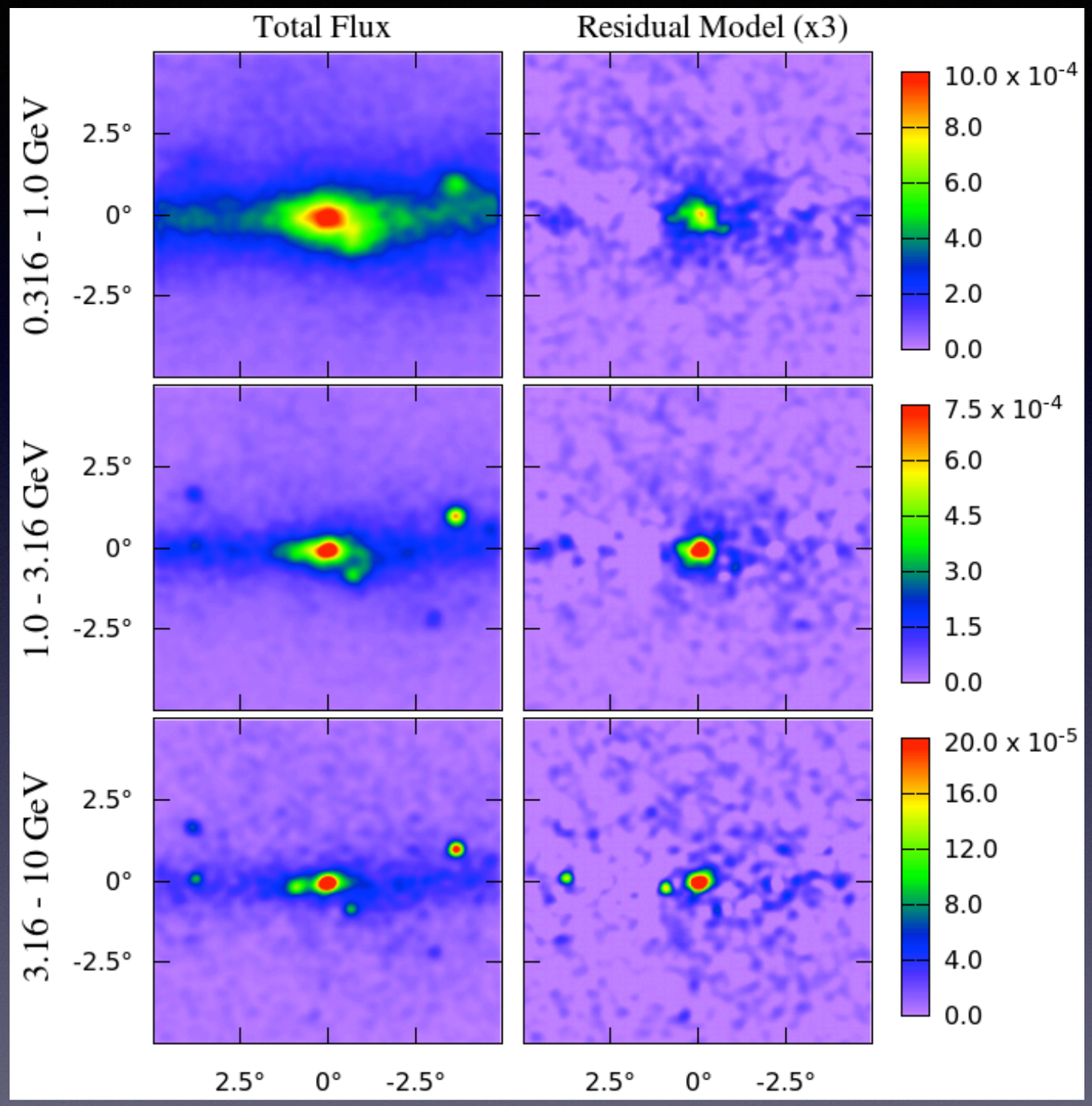

Daylan, Finkbeiner, Hooper, Linden, Portilo, Rodd, Slatyer, PoDU 2015

Claim:

- A clear excess emission in the galactic center emerges
- Excess emission cuts-off at ~10 GeV (is in some dis-agreement with later findings)

Will call this excess emission the ***Galactic Center Excess (GCE)***

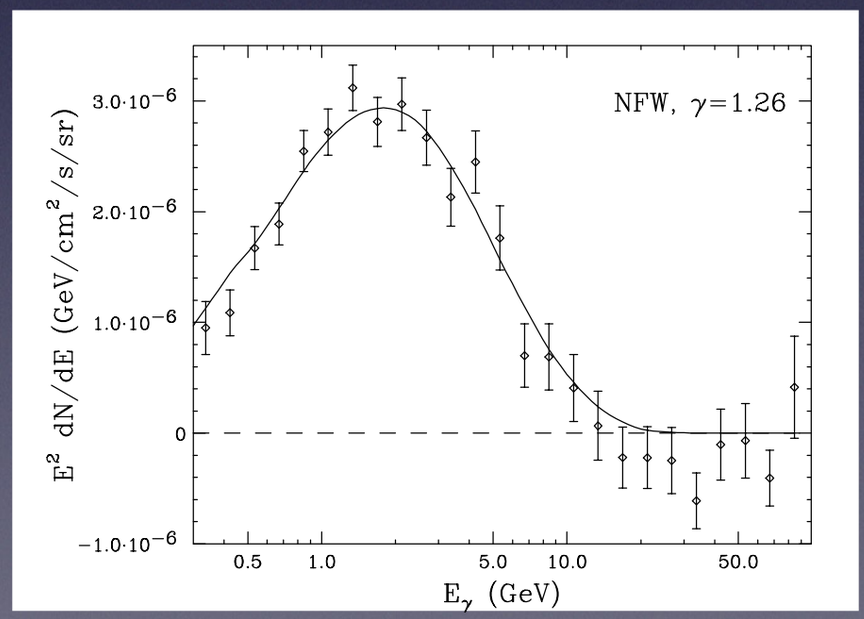

Also: Hooper & Goodenough PRL 2011, Abazajian JCAP 2011, Hooper & Linden PRD 2011, Gordon & Macias PRD 2014, Zhou et al. PRD 2015, Ajello et al. ApJ 2016

Going to High Latitudes (Inner Galaxy)

Advantages of looking further away from the center:

i)For a DM signal, you now have a prediction on the spectrum and its normalization based on the DM distribution.

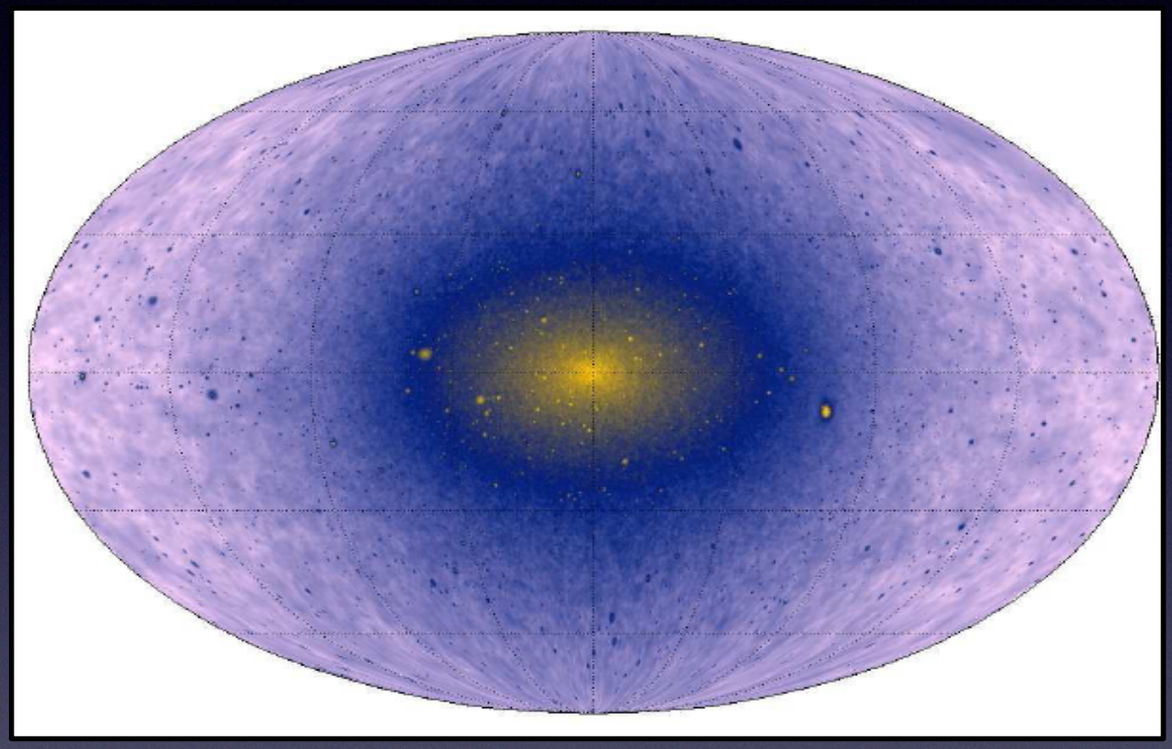

ii) Different region on the galactic sky suffers from different uncertainties in the background gamma-ray flux.

iii) A region that does not have too many very young and energetic sources that might affect the CR propagation on a local scale. That relates to avoiding the stronger inhomogeneities in diffusion, that exist along the disk. Similar argument for the interstellar radiation field.

Modeling the background gamma-ray sky: Interplay with Cosmic-Rays & the ISM

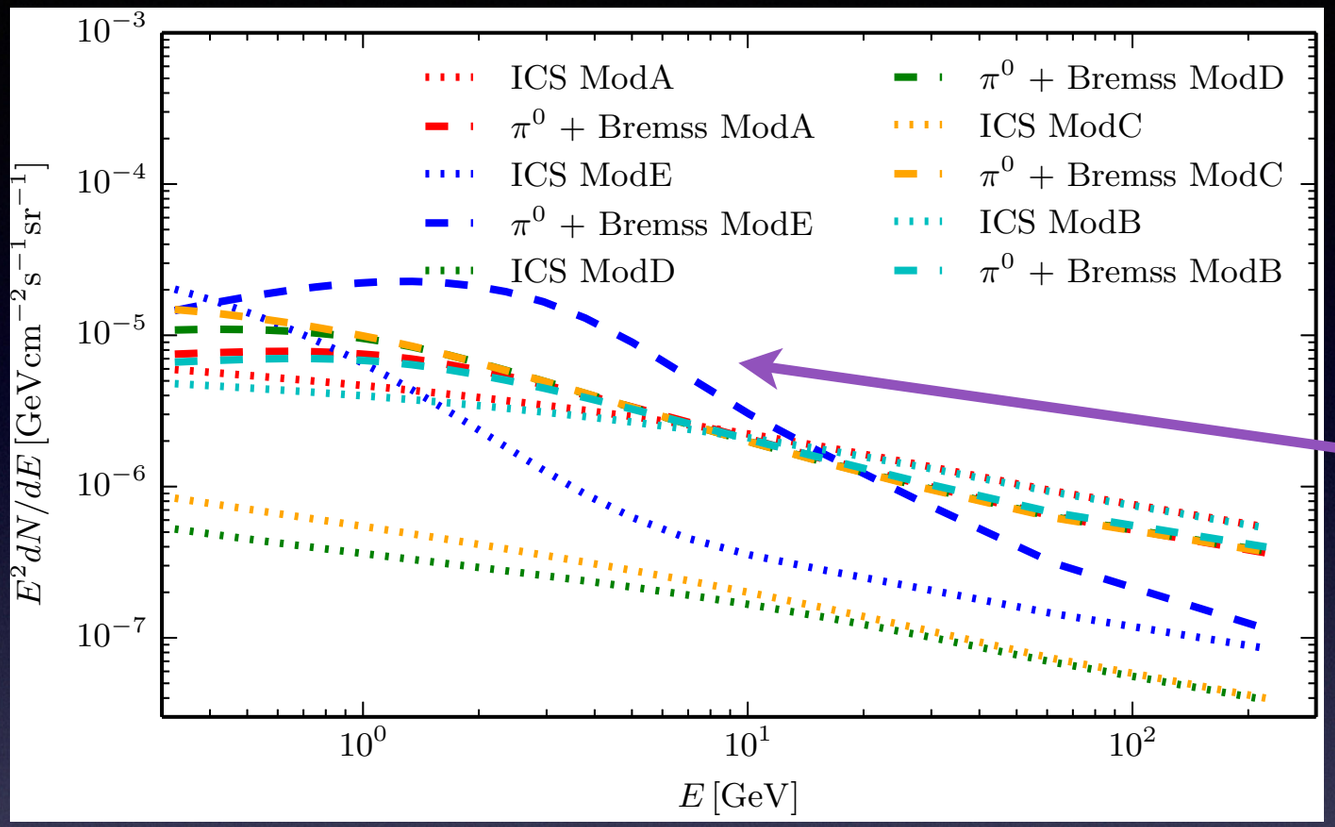

The exact astrophysics model assumptions can affect both the gamma-ray background spectrum and its morphology on the galactic sky.

Calore, **IC**, Weniger, JCAP 2015

IC, Zhong, McDermott, Surdutovich, PRD 2022

60 degrees in latitude

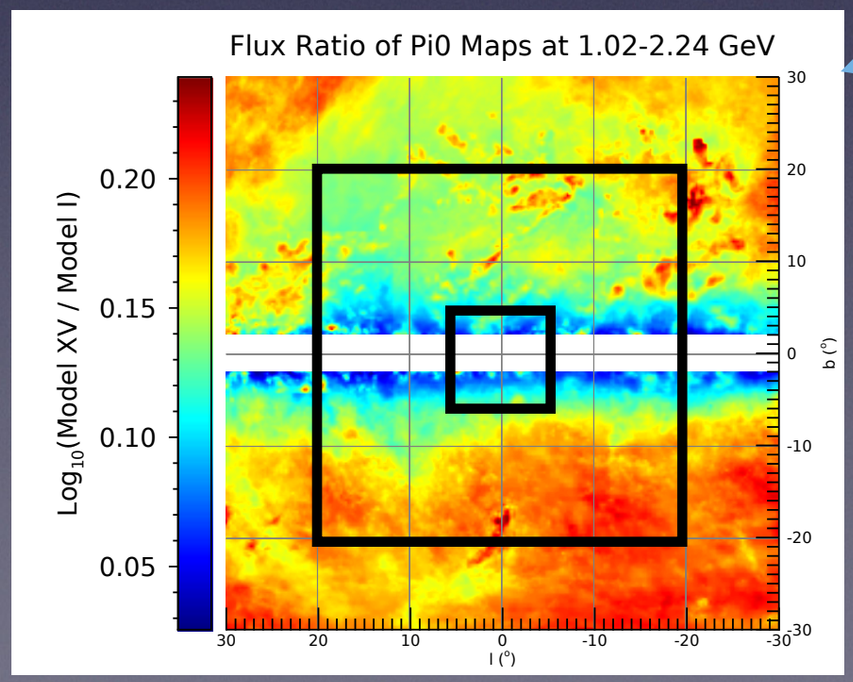

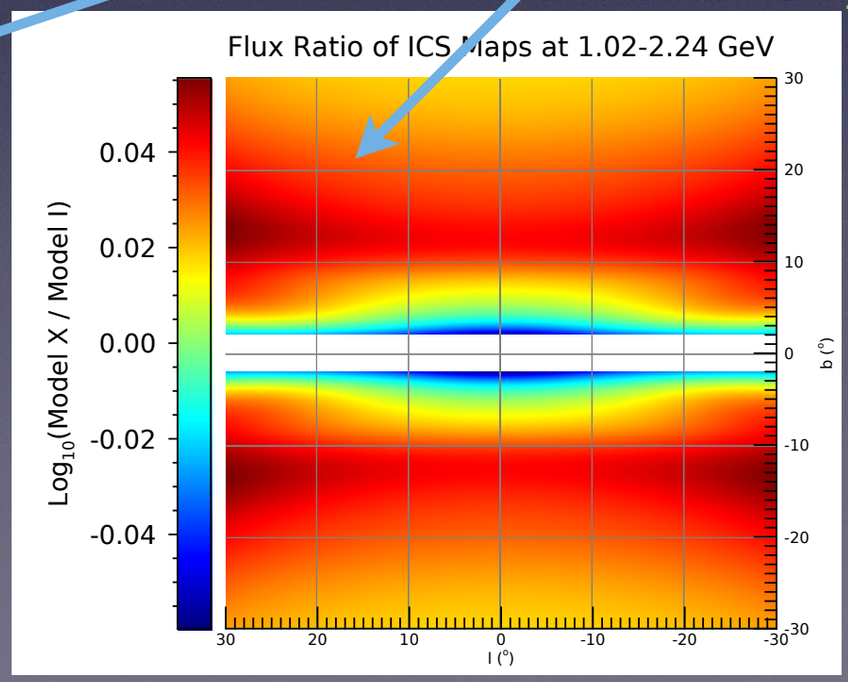

Accounting for the galactic diffuse emission uncertainties

We use models, accounting for uncertainties related to the diffusion of CRs, the presence of convective winds, diffusive re-acceleration, energy losses, CR injection sources, gas and other interstellar medium properties. To account for new observations in 2020-2021 we created and tested 45K high resolution templates.

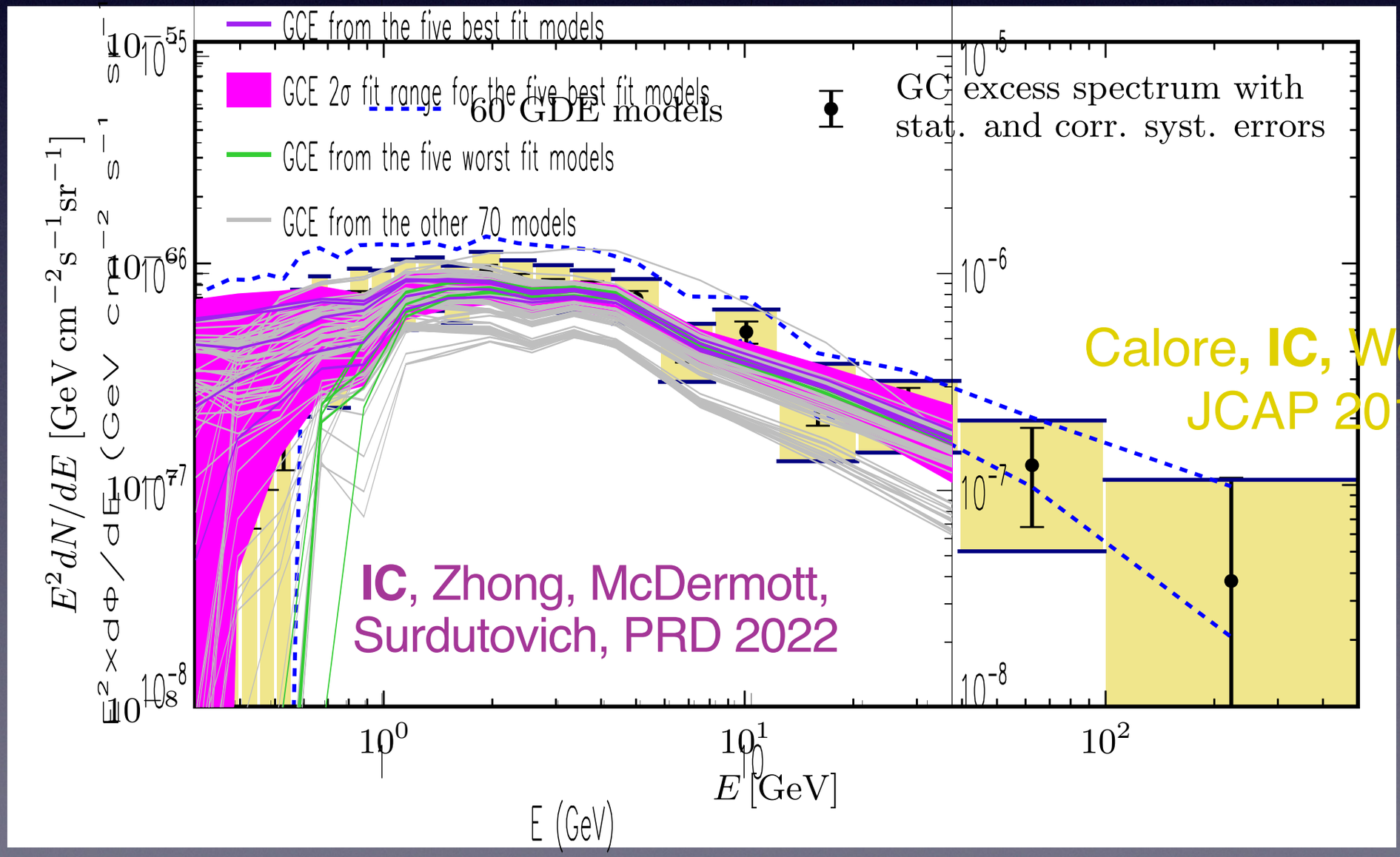

IC, Zhong, McDermott, Surdutovich, PRD 2022

Maps, Astrophysical Models and Correlated Errors publicly available via Zenodo

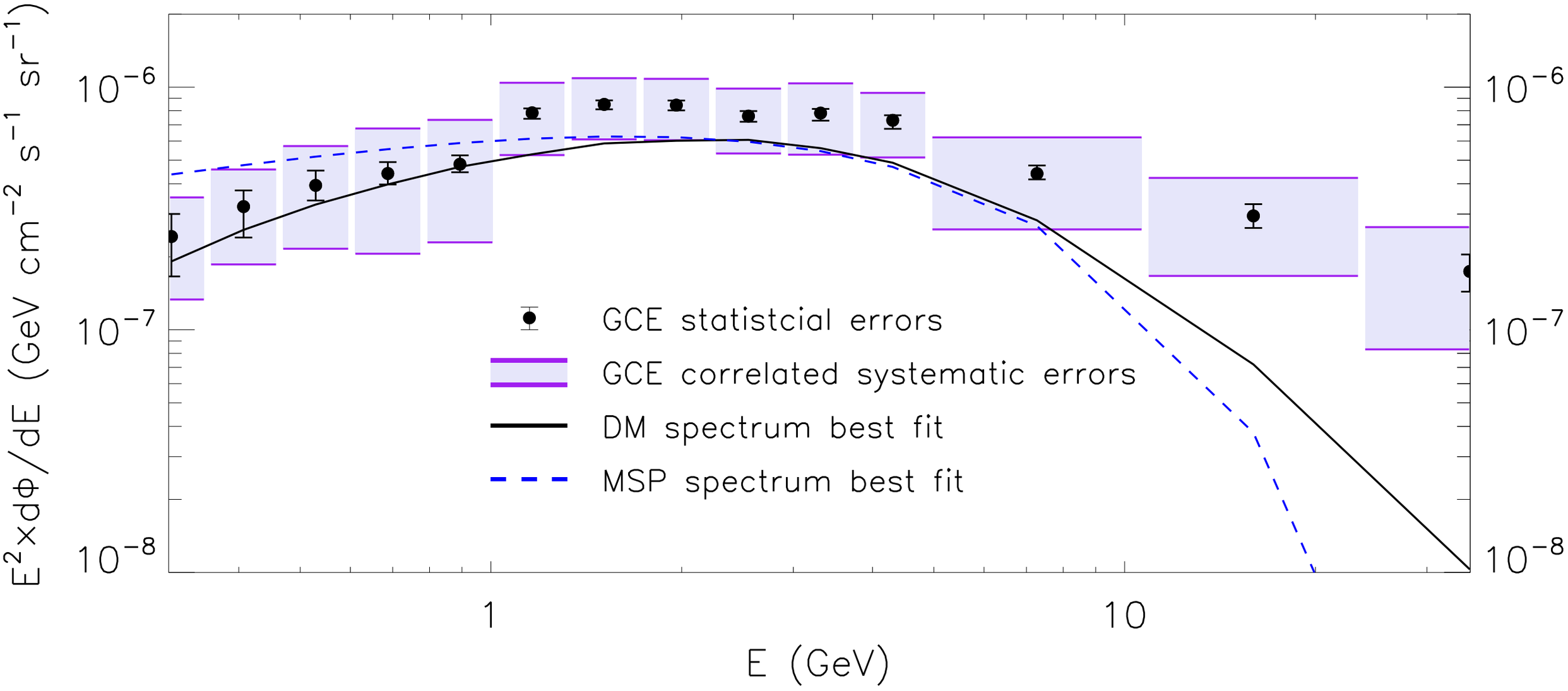

TABLE V. The first four principal components of the systematic uncertainty contribution to the covariance matrix, defined as in Eq. (16), in units of 10^{-7} GeV cm^{-2} s^{-1} sr^{-1}.

PC$_i$	Φ_1	Φ_2	Φ_3	Φ_4	Φ_5	Φ_6	Φ_7	Φ_8	Φ_9	Φ_{10}	Φ_{11}	Φ_{12}	Φ_{13}	Φ_{14}
PC$_1$	2.52	2.37	2.47	2.43	2.19	2.35	2.08	1.83	1.65	1.69	1.38	1.09	0.67	0.34
PC$_2$	−1.70	−1.07	−0.16	0.14	0.54	0.42	0.40	0.31	0.58	0.41	0.56	0.48	0.41	0.33
PC$_3$	0.27	0.06	−0.53	−0.22	−0.21	−0.18	−0.08	0.25	0.04	0.45	0.23	0.24	0.20	0.24
PC$_4$	0.20	−0.15	0.15	−0.14	0.06	−0.04	−0.04	−0.27	0.08	−0.25	0.11	0.25	0.27	0.17

The profile for the GCE. Does it look like a DM signal?

IC, Zhong, McDermott, Surdutovich, PRD 2022

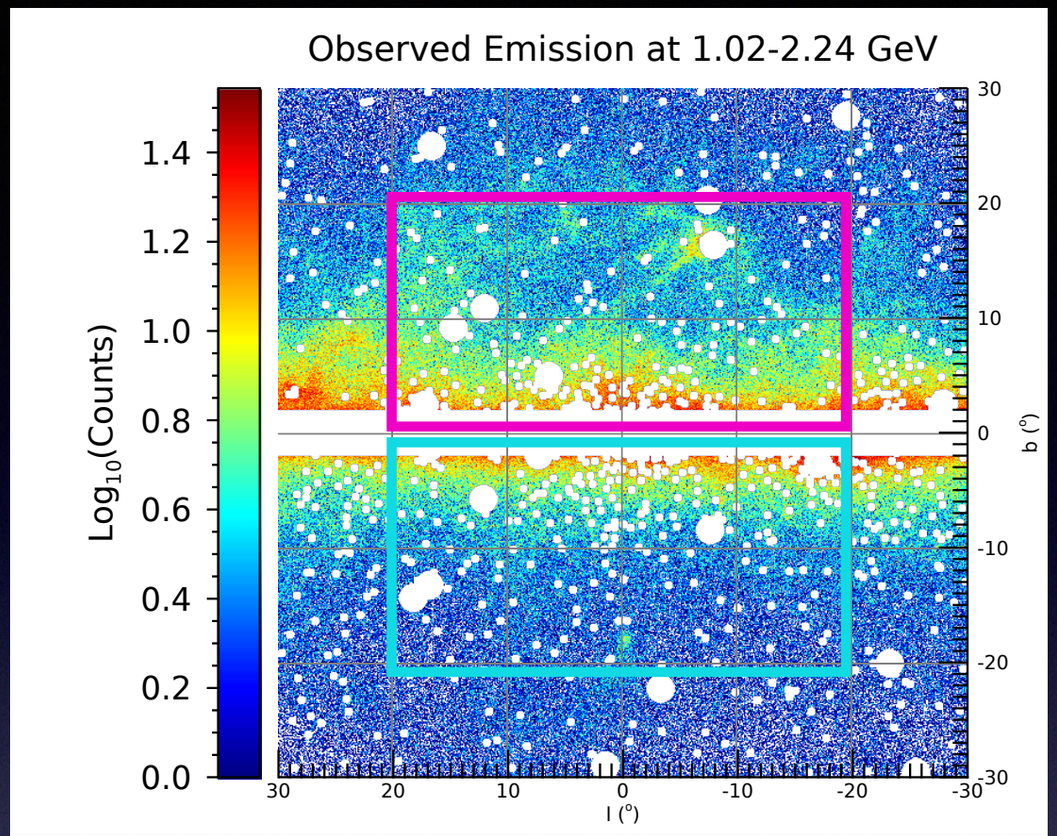

North

South

Roughly consistent between southern and northern galactic hemisphere as expected from dark matter

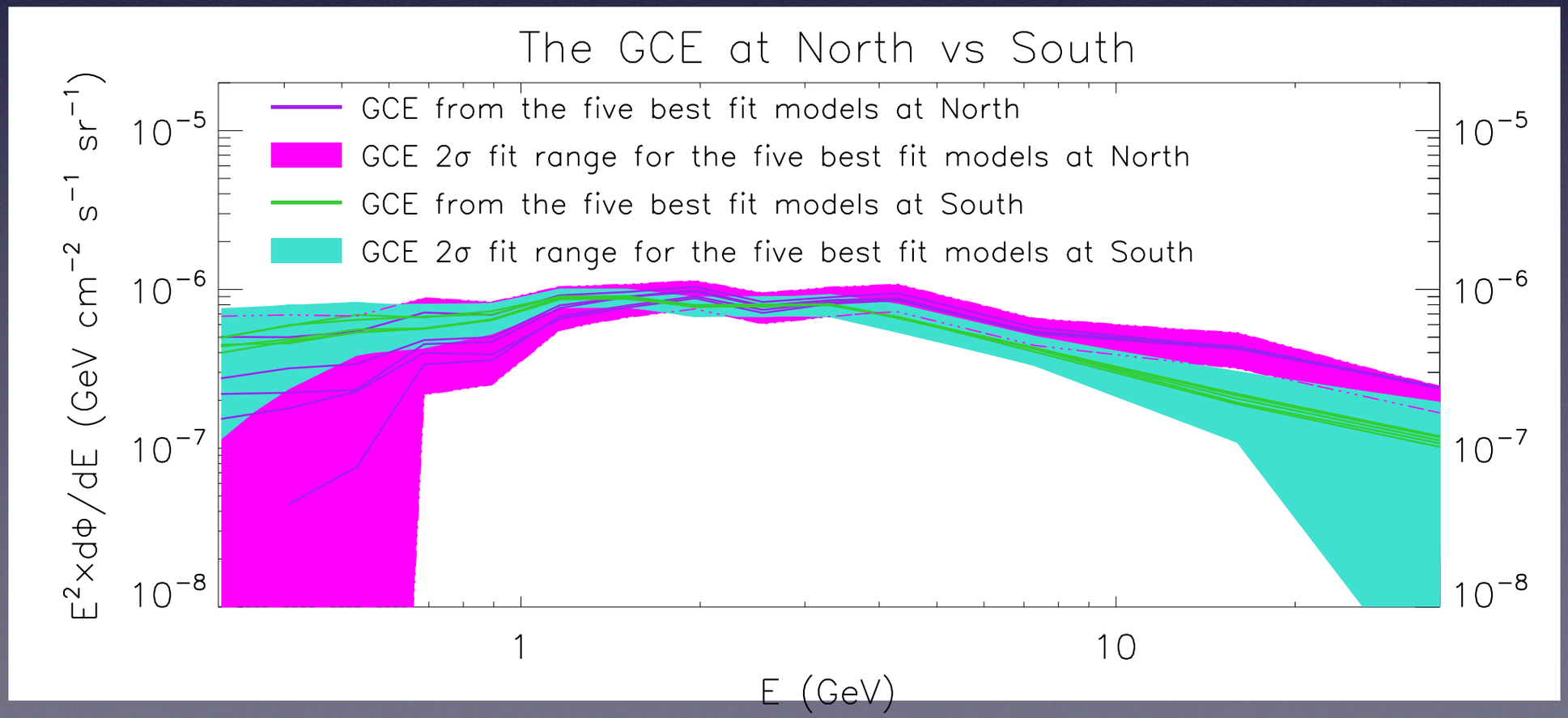

If this is a DM annihilation signal what do we learn about the particle physics?

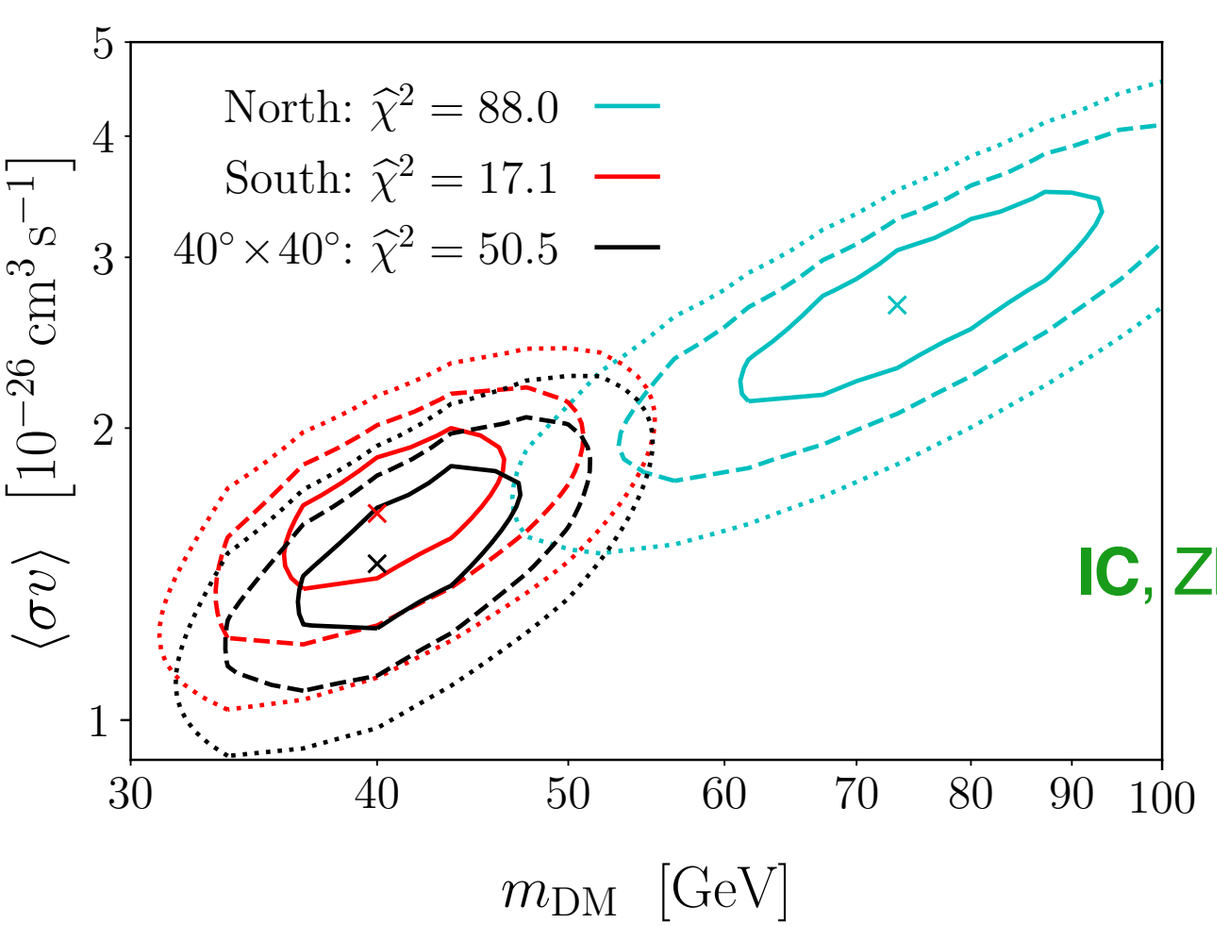

The mass range preferred very much within the WIMP range.

IC, Zhong, McDermott, Surdutovich, PRD 2022

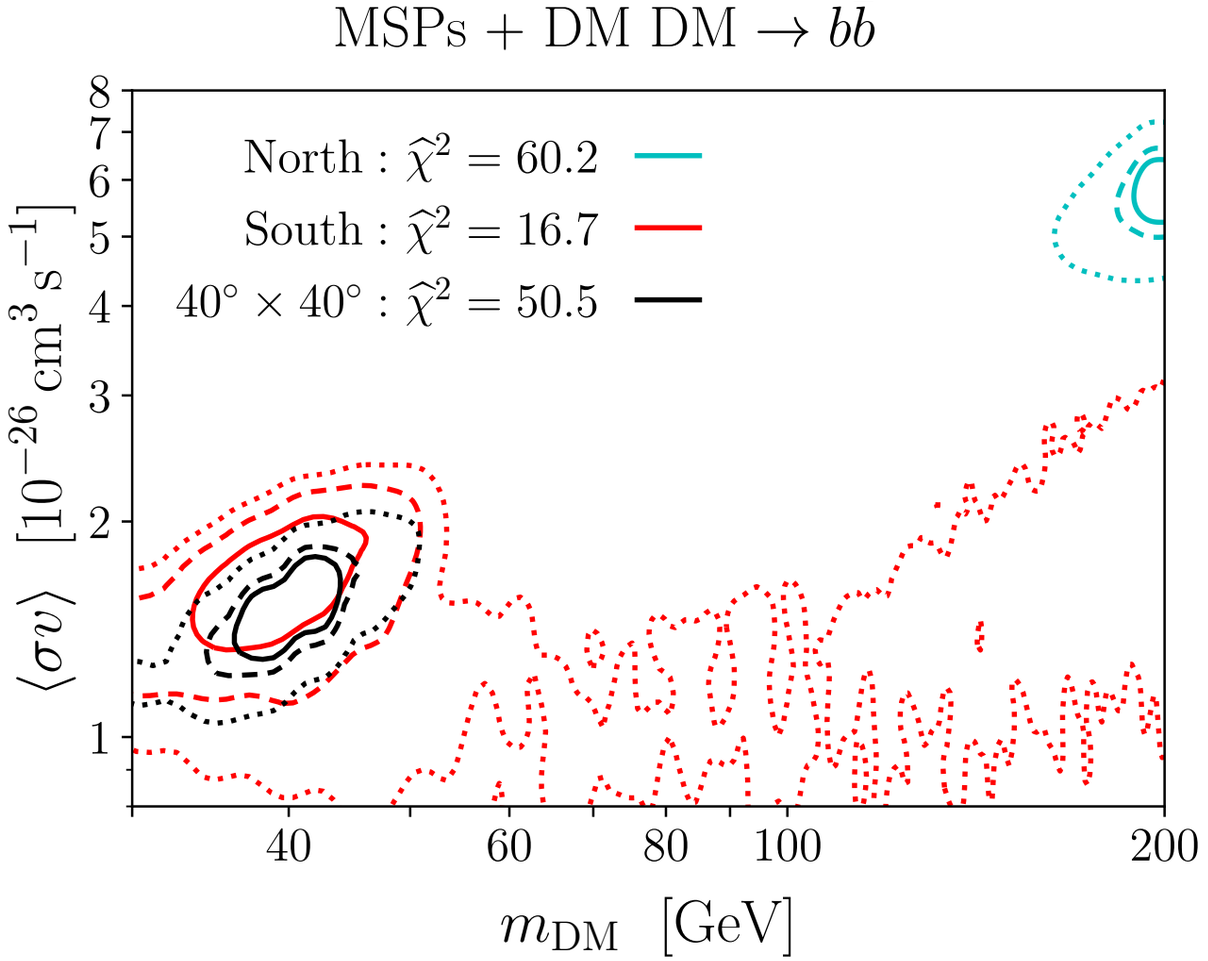

Adding an MSP component affects the fits on the more “dirty” (more galactic gas) Northern Hemisphere, but the Southern Hemisphere and the overall Inner Galaxy fit are fairly unaffected.

The profile for the GCE. Does it look like a DM signal?

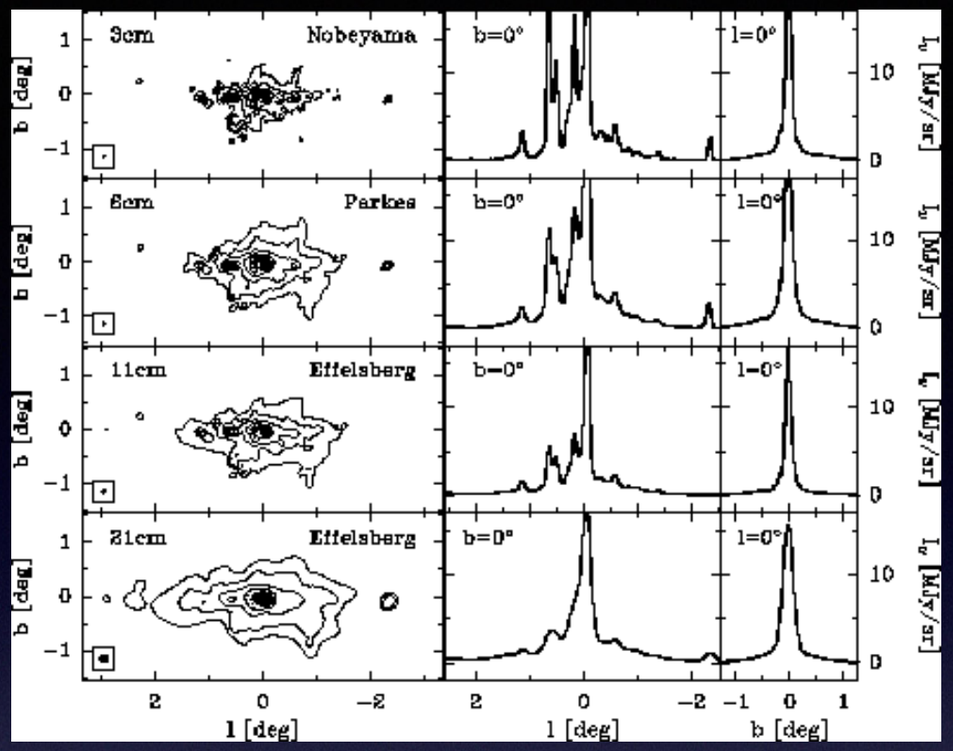

Nuclear Bulge @ Radio

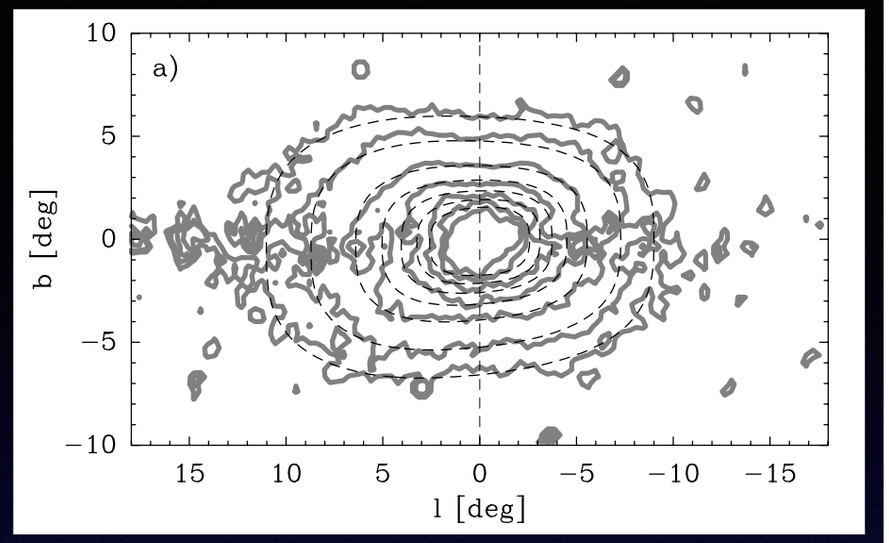

Boxy Bulge @ 2-5 μm

Launhardt et al. A&A 2002

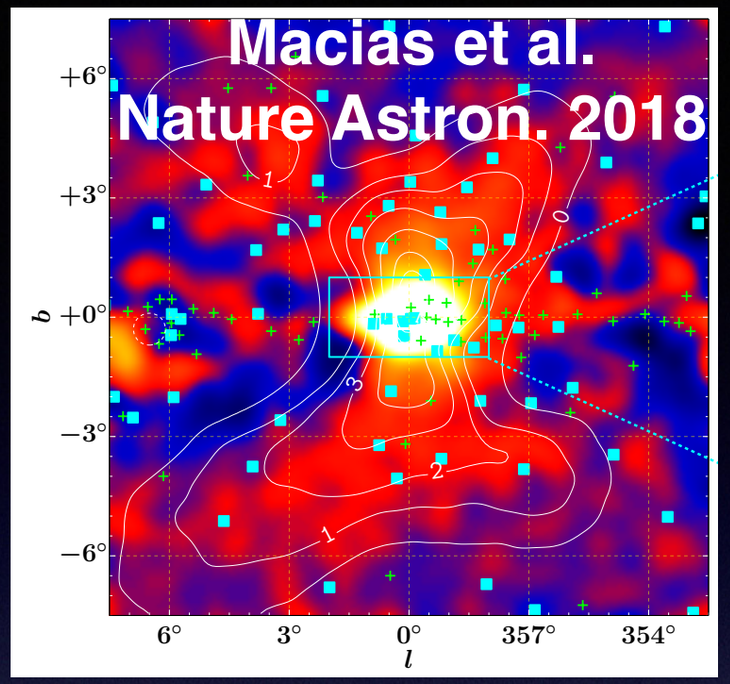

X-shaped Bulge @ "low" gamma-rays

IC, Zhong, McDermott, Surdutovich, PRD 2022

Statistical Preference

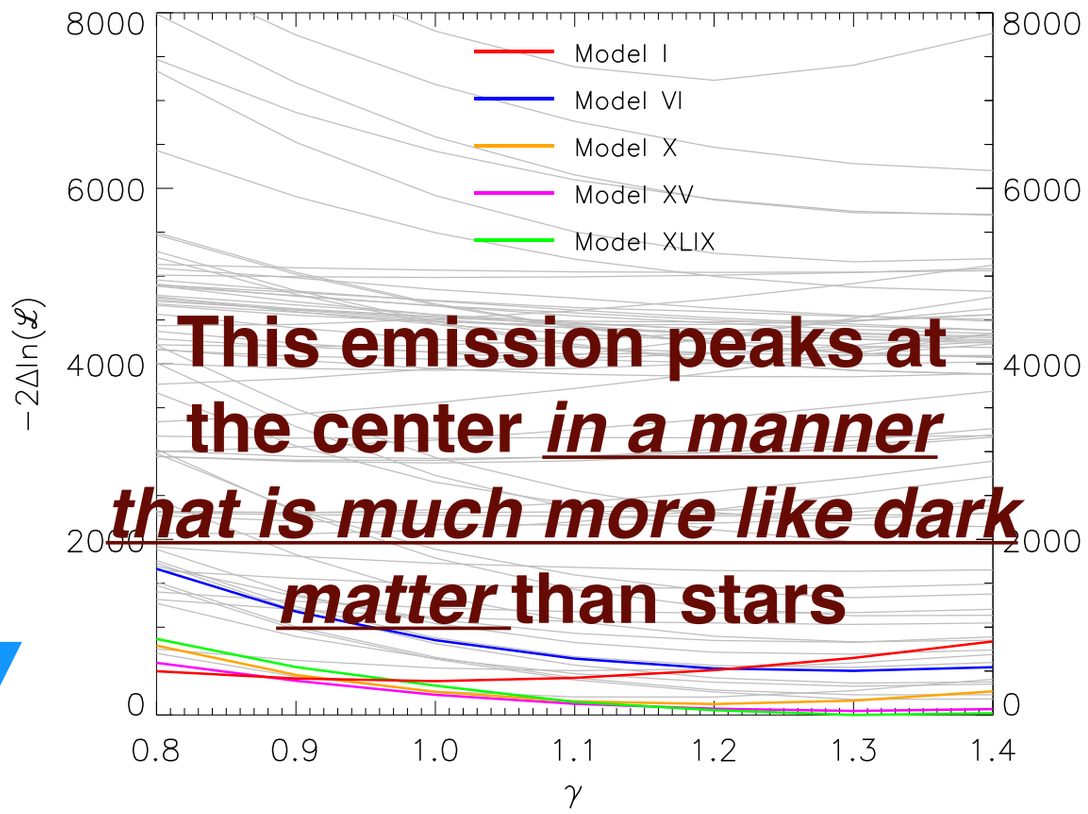

This emission peaks at the center *in a manner that is much more like dark matter* than stars

Bartels et al. 2018

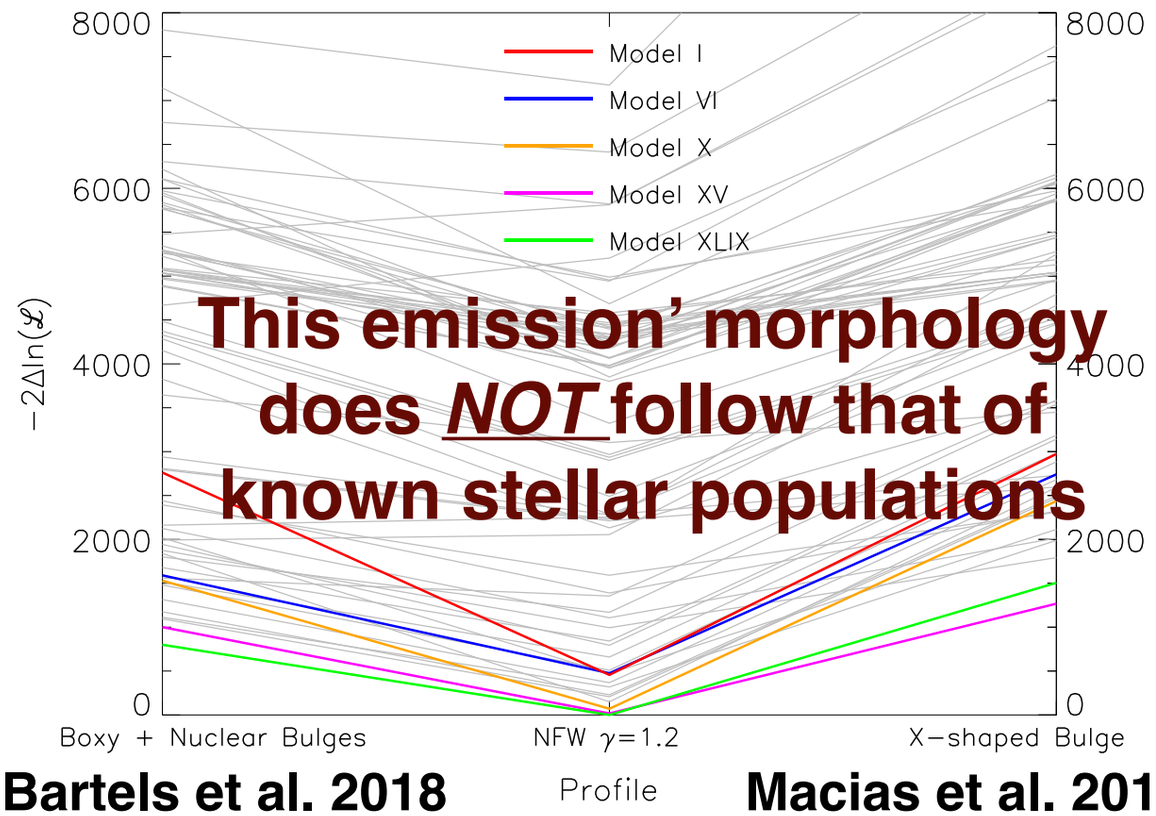

This emission' morphology does *NOT* follow that of known stellar populations

Macias et al. 2018

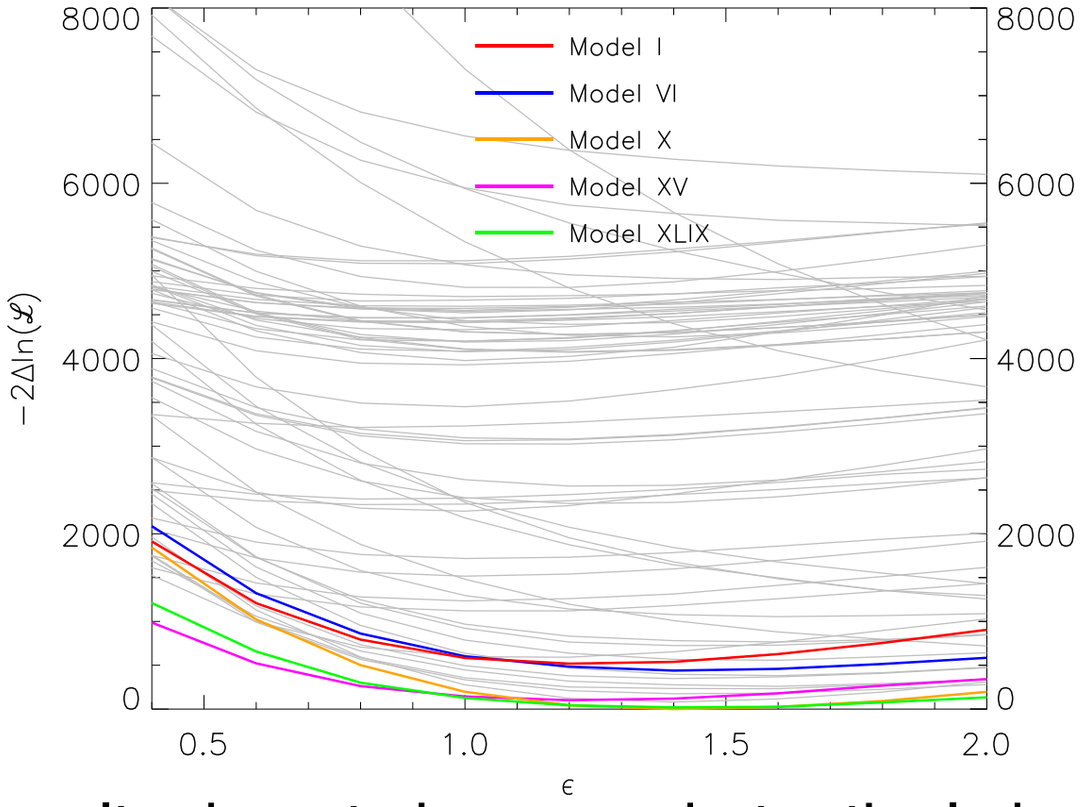

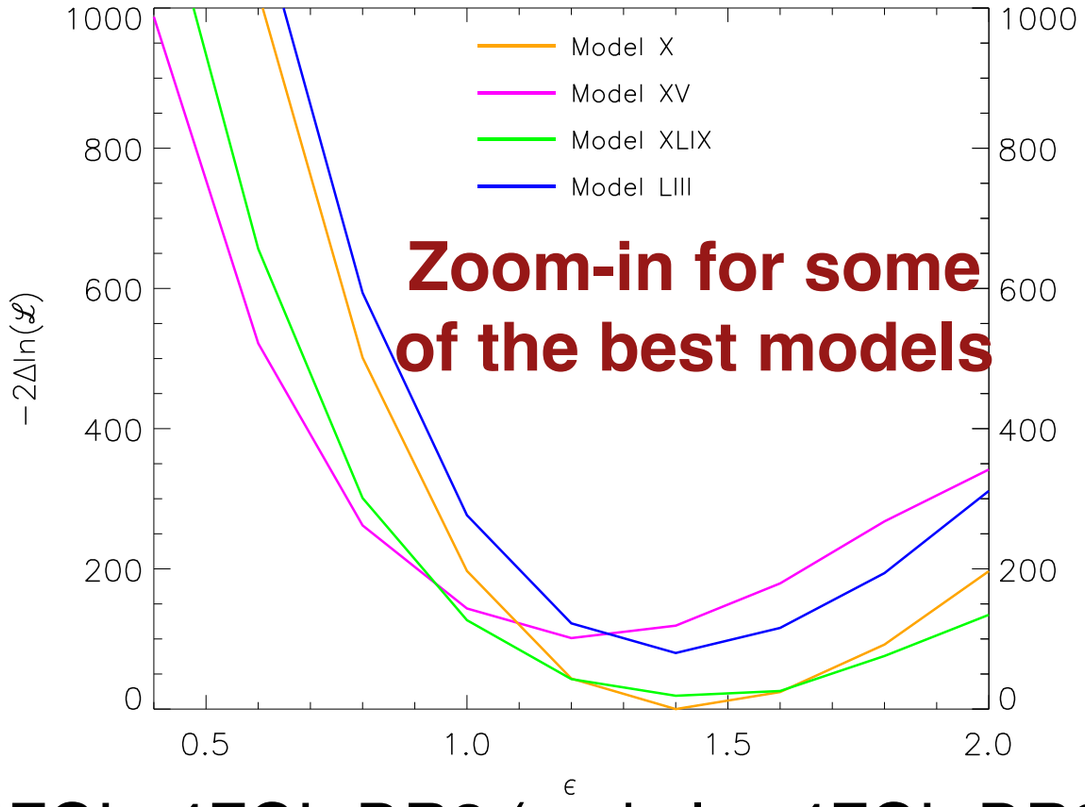

Results do not change substantively between 4FGL, 4FGL-DR2 (and also 4FGL-DR3) point source catalogues

IC, Zhong, McDermott, Surdutovich, PRD 2022

Even when we allow for an additional stellar bulge component (probing MSPs) component, we still get preference for a dominant cuspy NFW-like profile

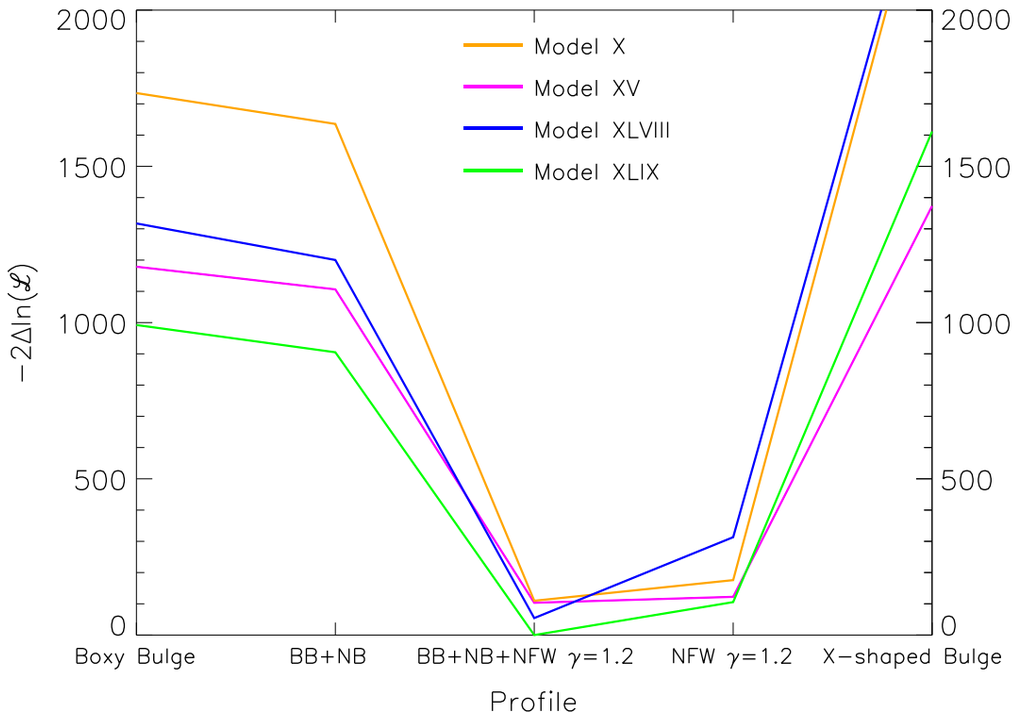

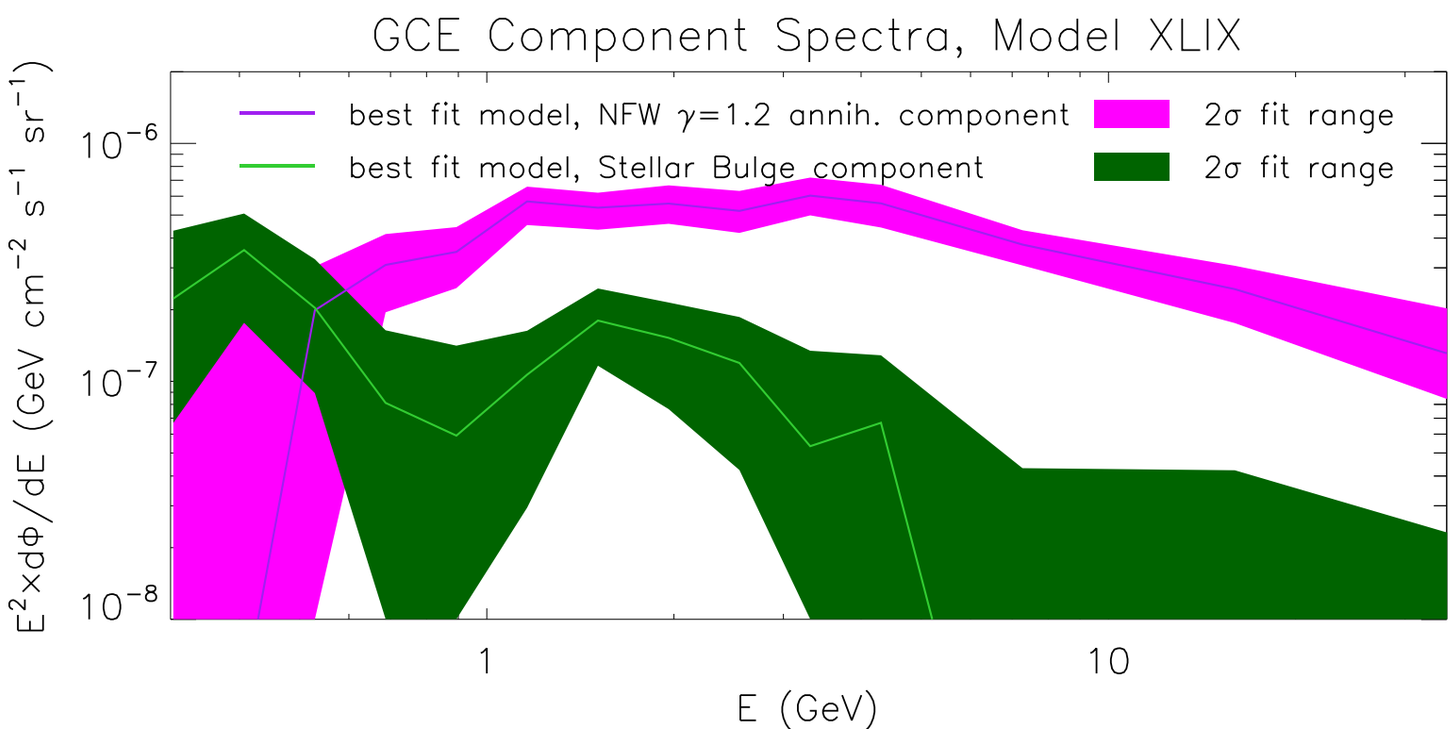

The background assumptions on the galactic diffuse emission affect the derived conclusions on the GCE.

McDermott, Zhong, **IC** MNRAS Letters 2023

Comparing astrophysically motived templates (IC et al. 2022) vs ring-based templates (Pohl et al. 2022).

Table 1. Comparison of models of the GCE. The first six results, generated in this work, rely on the ring-based method of Pohl et al. (2022) to describe astrophysical emission. The final three results utilize best fit template model XLIX from Cholis et al. (2022).

Excess Model	Bgd. Templates	$-2\Delta\ln\mathcal{L}$	$\Delta\ln\mathcal{B}$
No Excess	ring-based	0	0
X-Shaped Bulge	ring-based	+30	−190
Dark Matter	ring-based	−237	+12
Boxy & X-Shaped Bulges	ring-based	−634	+178
Boxy Bulge	ring-based	−724	+228
Boxy Bulge “plus”	ring-based	−765	+311
Boxy Bulge “plus” & DM	ring-based	−817	+316
No Excess	astrophysical	−4539	+2933
Boxy Bulge	astrophysical	−6398	+3814
Boxy Bulge “plus”	astrophysical	−6477	+3853
Dark Matter	astrophysical	−7288	+4268
Boxy Bulge “plus” & DM	astrophysical	−7401	+4298

The statistically best models give preference for a more spherical GCE morphology

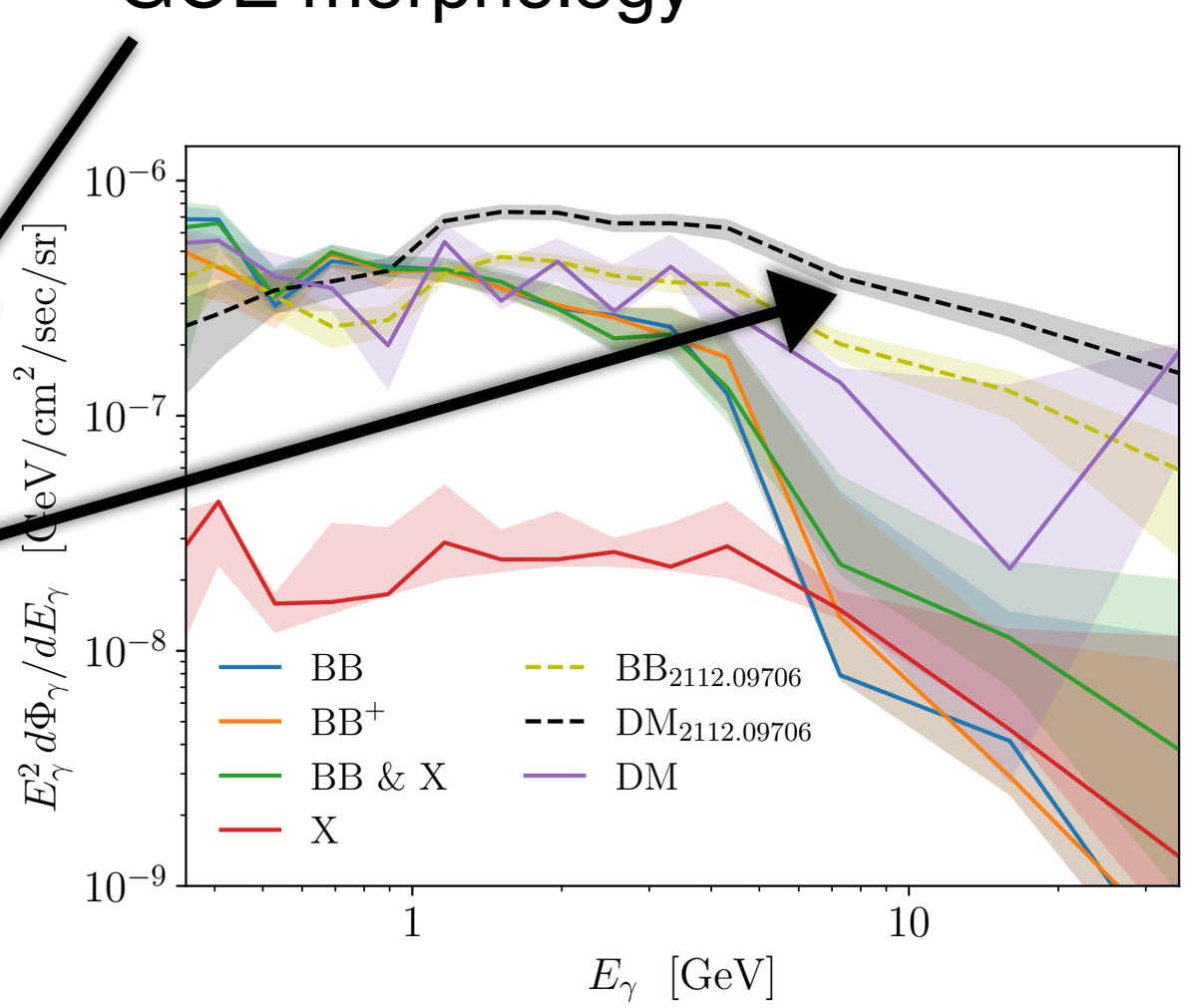

And also a preference for a harder GCE spectrum at higher energies (and also a smoother spectrum).

Mask effects i.e. accounting for point sources : Zhong, **IC** 2024 PRD

Further Tests on the GCE morphology with Alternative Masks, including using wavelets to identify hot-spots:

4FGL-DR1, 2 or 3 + all of the disk

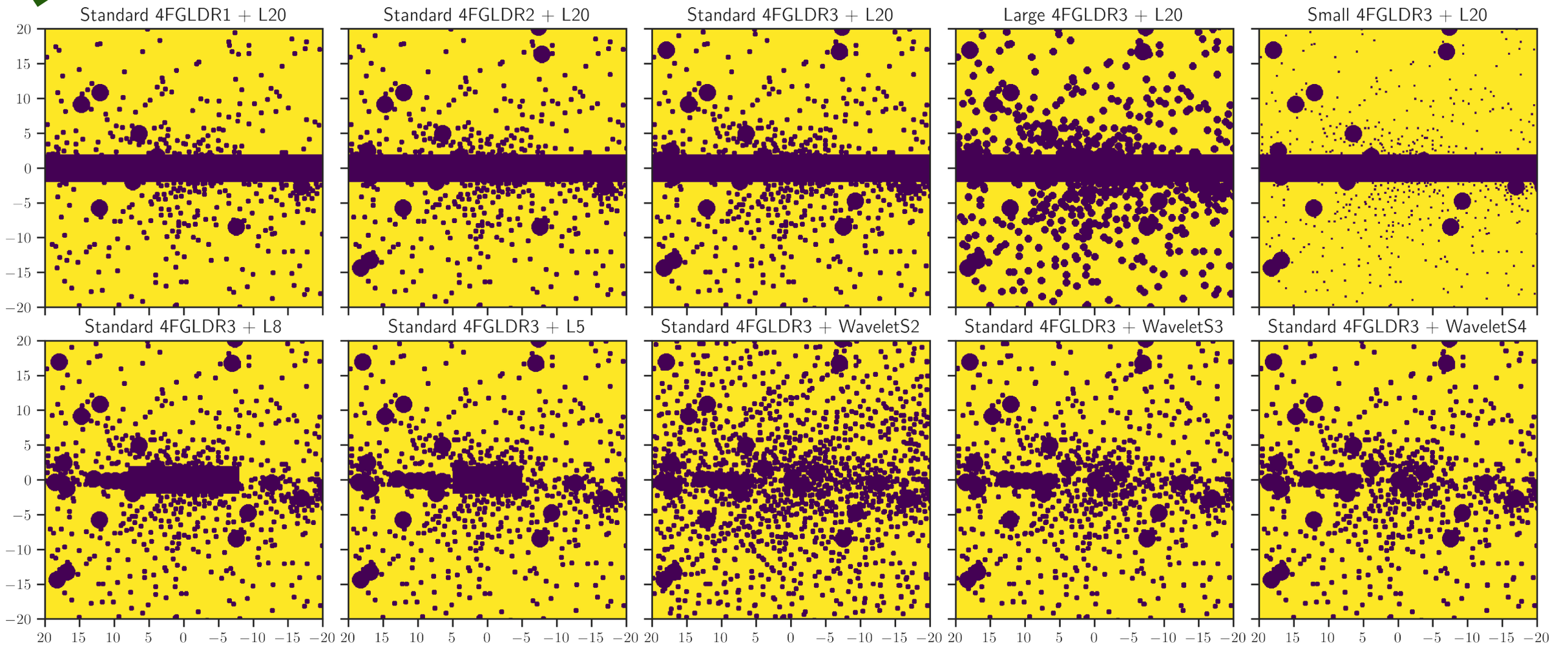

4FGL-DR3 + part of the disk

4FGL-DR3 + Wavelet-based

Zhong, **IC** 2024 PRD

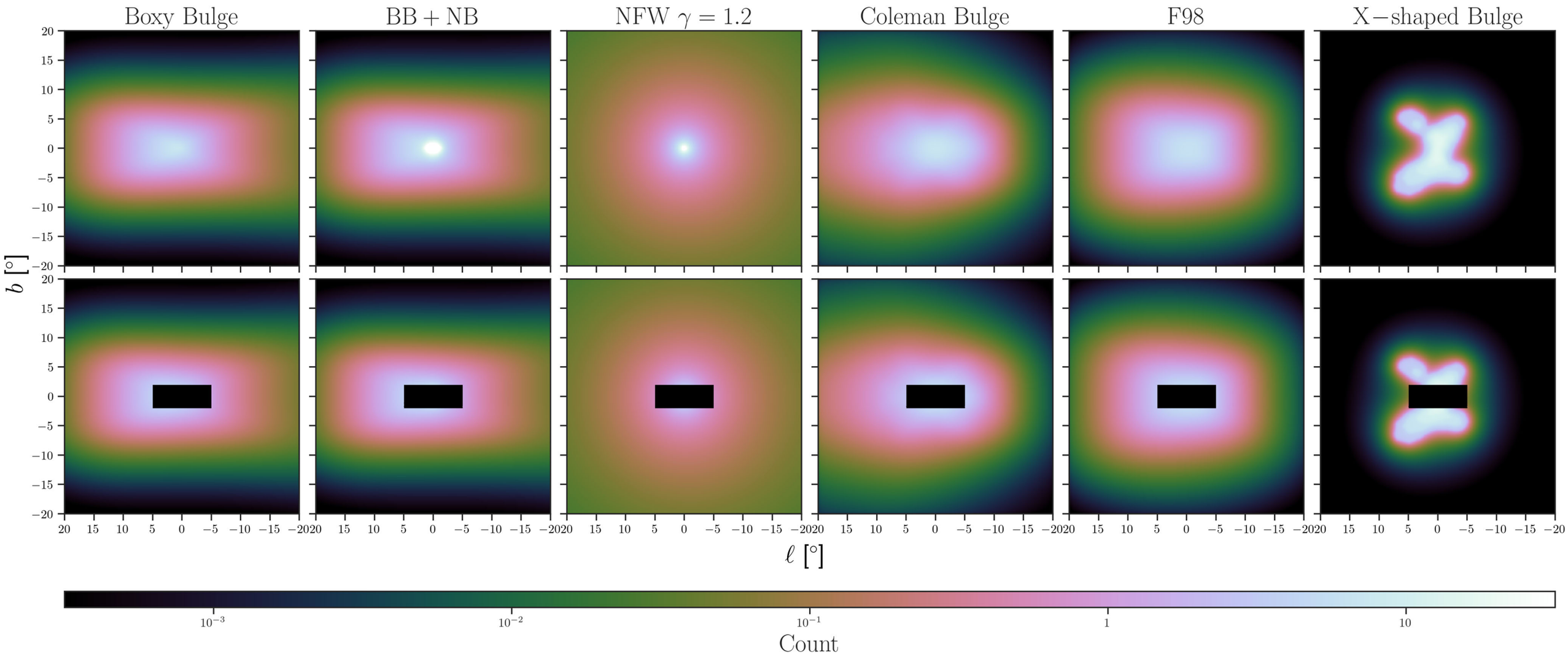

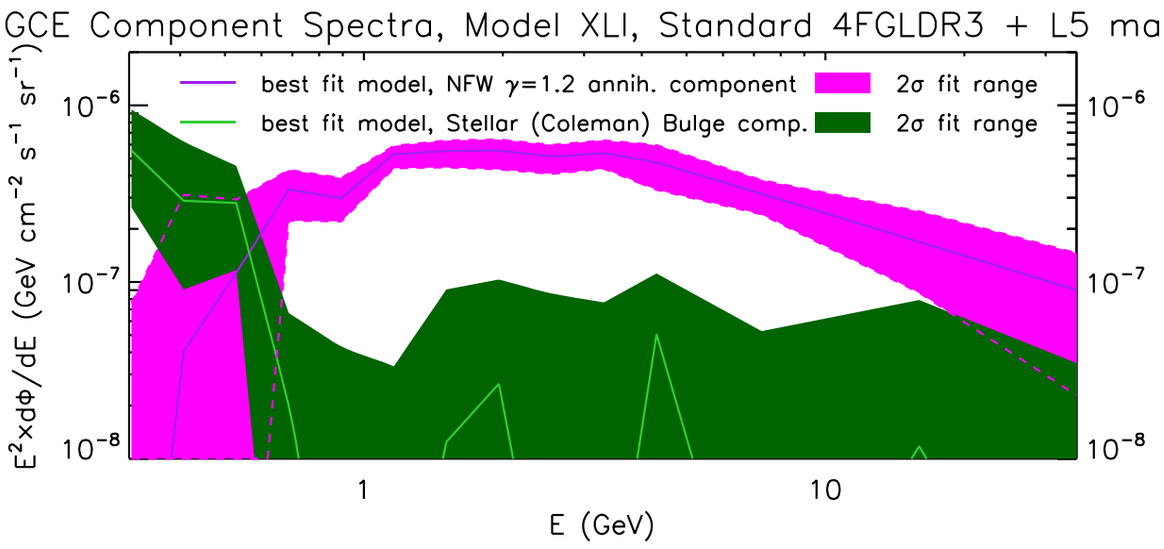

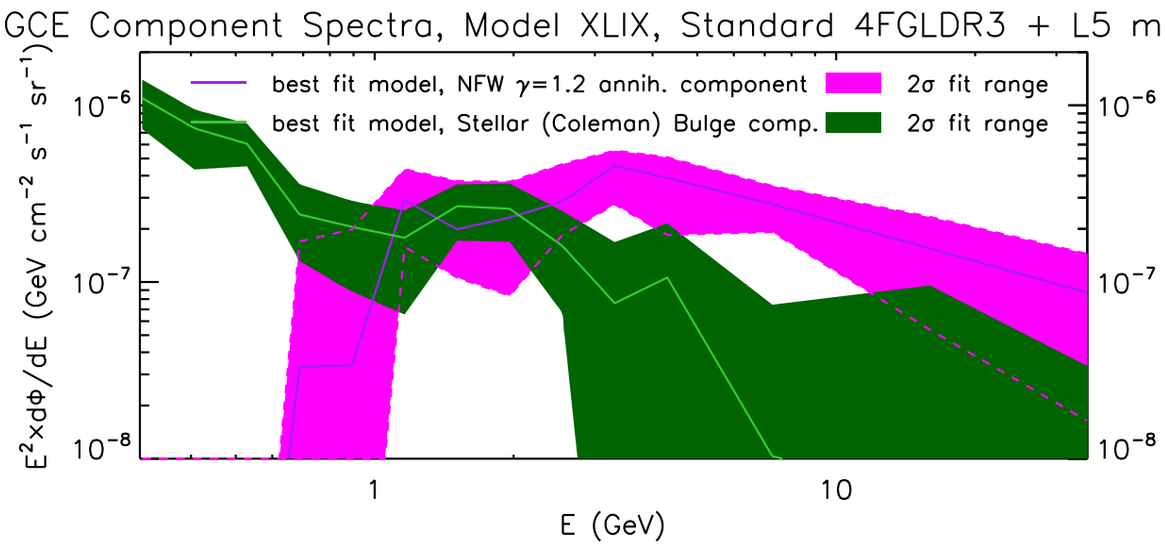

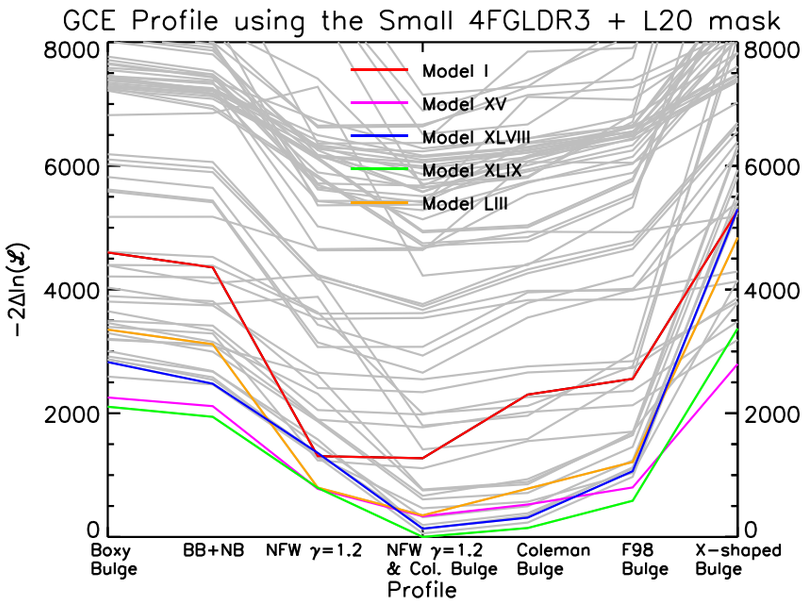

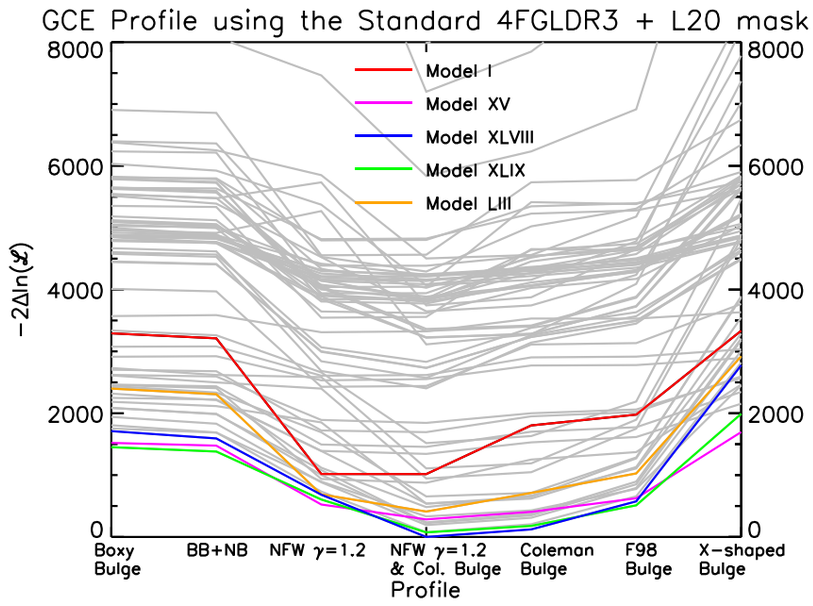

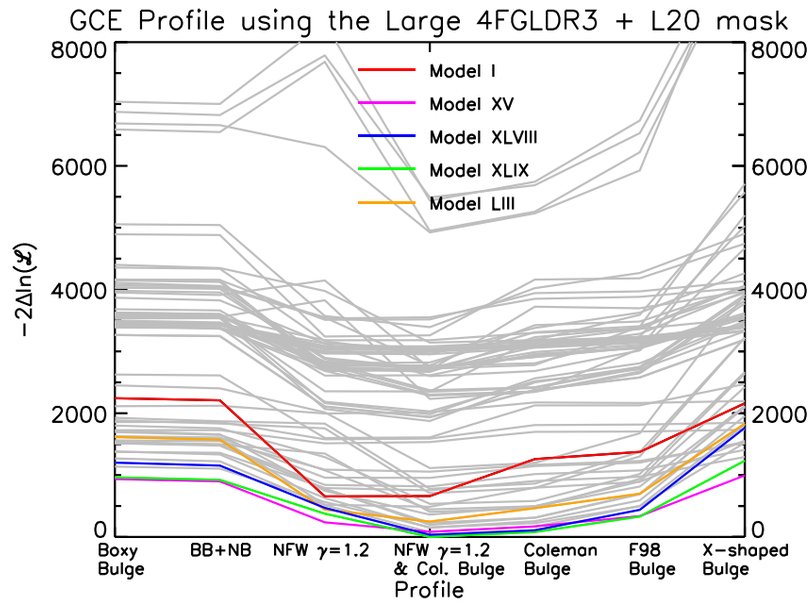

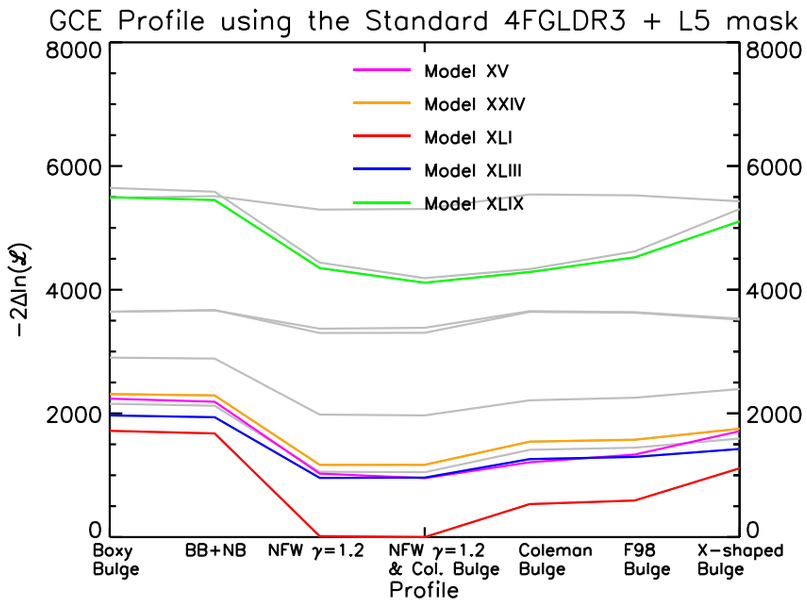

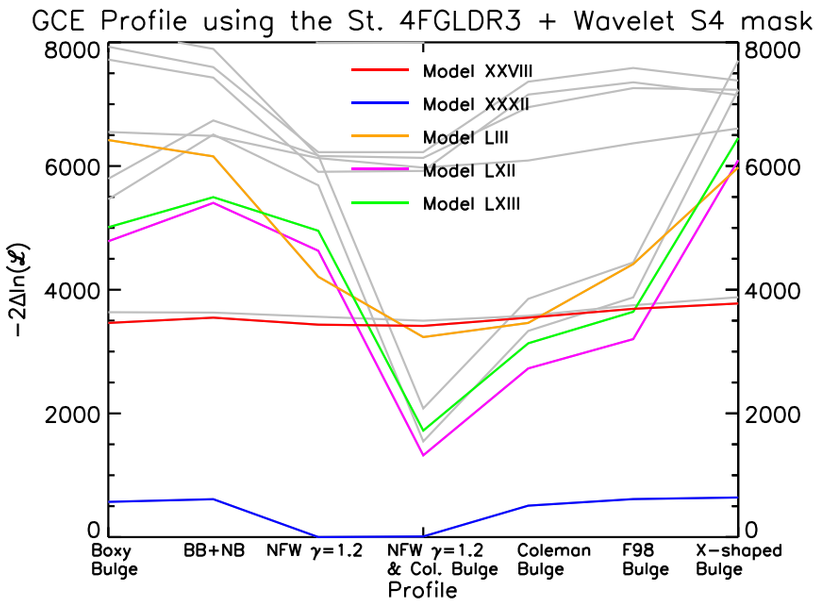

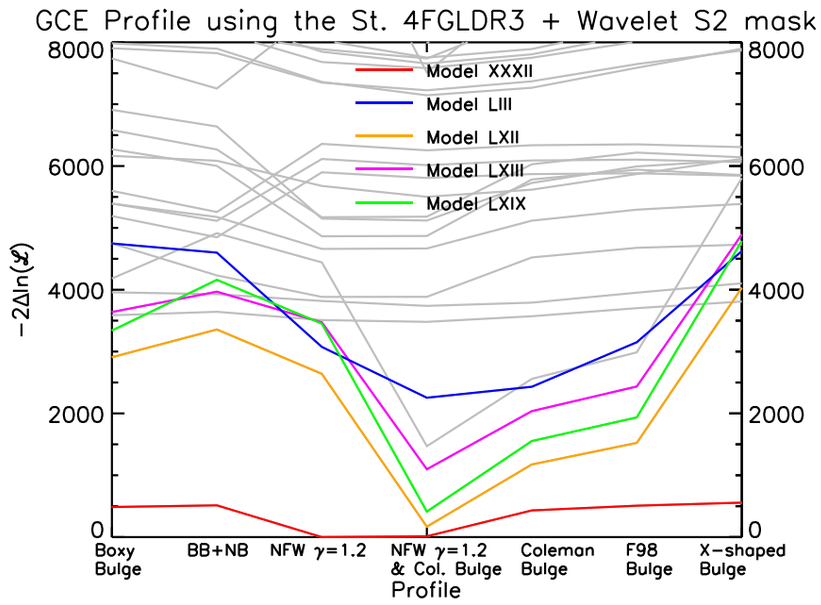

Accounting for all possible combinations of background models and point sources masks we found a systematic preference for DM-like morphology with a subdominant component of an MSP-like morphology

Triaxial & rotated dark matter profiles

Recent studies of Galactic surveys, such as Gaia, and the H3 survey (Arizona) have revealed that the Milky Way's gravitational potential comes from a matter distribution that is triaxial and rotated with respect to the Galactic center-Sun axis.

Han et al. Astron. J. 2022

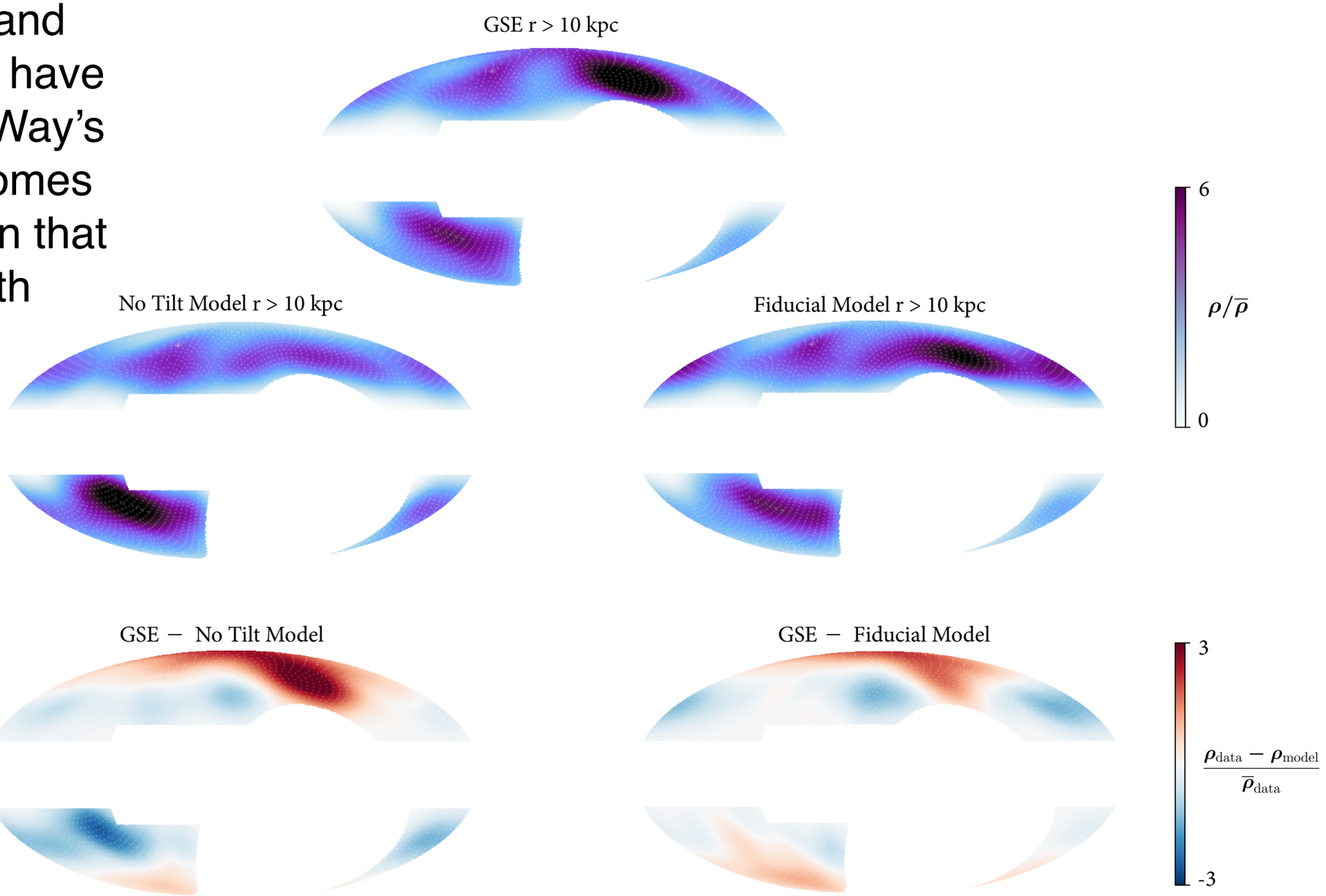

Figure 8. On-sky stellar density of the data and of the models projected onto data space. The top panel shows the density of GSE, and middle left (right) shows the density of a non-tilted (fiducial) model. Densities are normalized by the mean density in each panel. The bottom left (right) panel shows the residuals of the data subtracted by the non-tilted (fiducial) model, normalized by the mean density of the data. The fiducial model is a tilted, triaxial ellipsoid, and the non-tilted model is created by fixing all other parameters of the fiducial model and setting the rotation angles (both pitch and yaw) to zero. All panels are smoothed with a 20° Gaussian kernel. The faint white dots mark H3 tiles. The top and middle panels include the significant effect of the H3 selection function. However, the model residuals in the bottom panels are insensitive to the selection function.

Hu, **IC,** Zhong arXiv:2602.20252

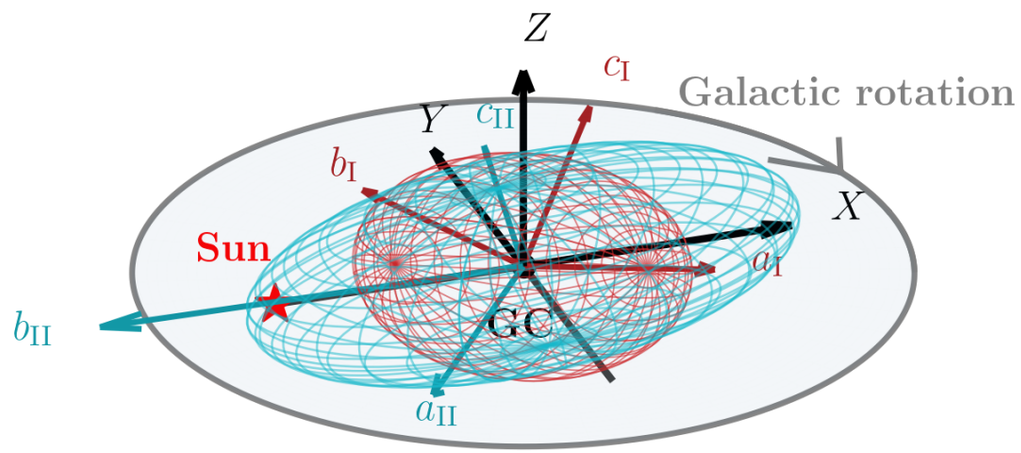

Figure 1. 3D view of the tilted triaxial halo of BM I (red) and BM II (cyan). a_i, b_i, c_i $(i = \mathrm{I}, \mathrm{II})$ represent the directions of major, intermediate, and minor axes of the halos, respectively.

Table I. Parameters for the tilted halo benchmarks used in this work.

BM	Yaw (ϕ)	Pitch (θ)	$p \equiv b/a$	$q \equiv c/a$	Ref.
I	24°	25°	0.81	0.73	[85]
II	97°	56°	0.95	0.65	[88]
Flipped I	−24°	25°	0.81	0.73	–

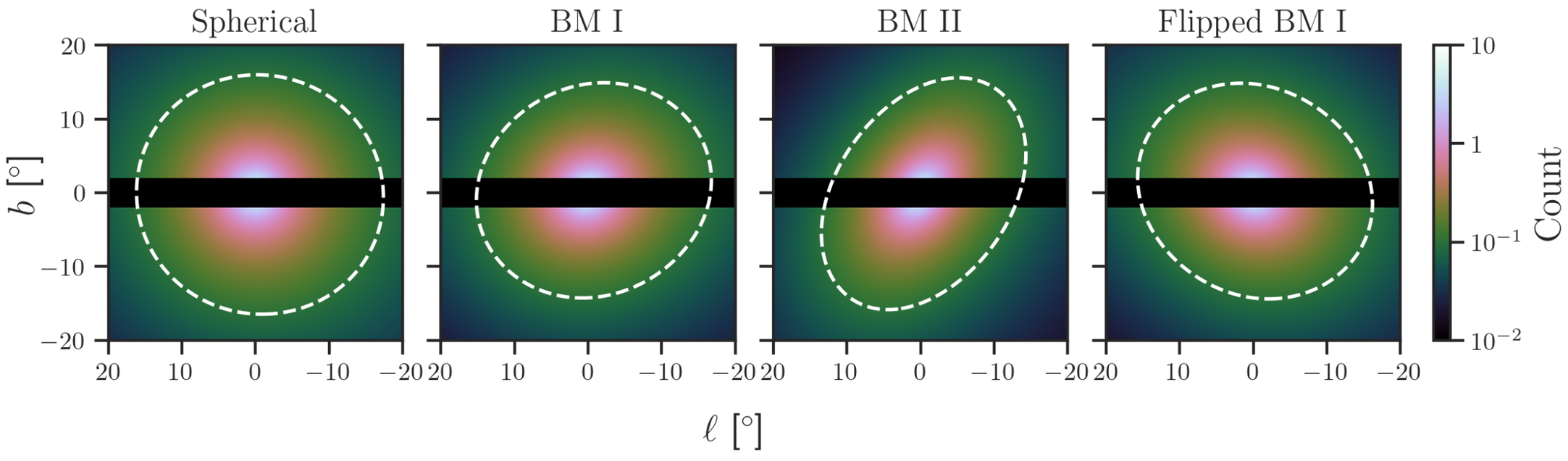

Figure 2. GCE count maps for a spherical dark matter halo (left), tilted halo BM I (middle left), tilted halo BM II (middle right), and the flipped BM I (right). For all models, we assume a cuspiness of $\gamma = 1.2$, take the energy range of $1.02 - 1.32$ GeV, and mask the disk region with $|b| < 2°$. The white dashed lines show contours of equal count to guide the eye.

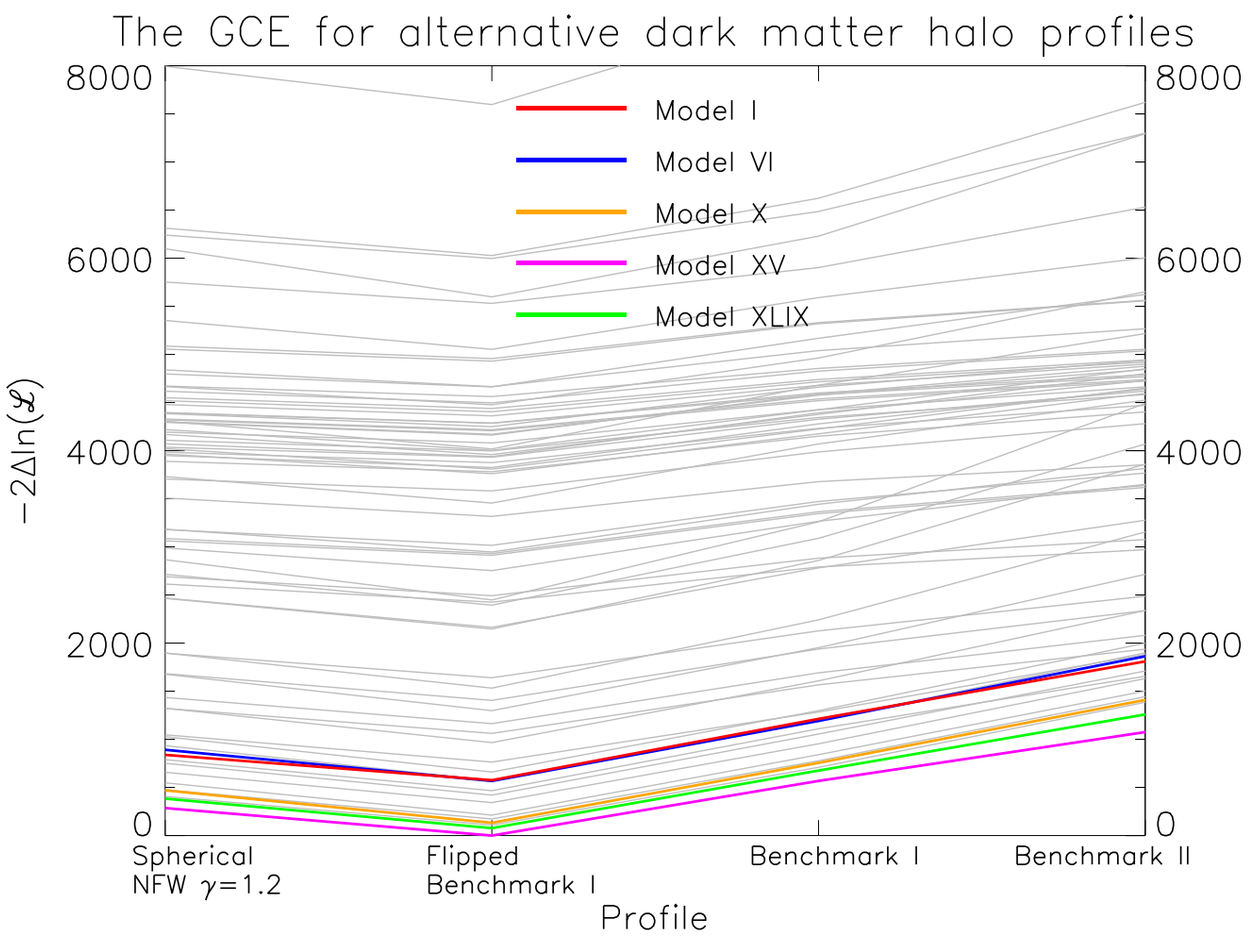

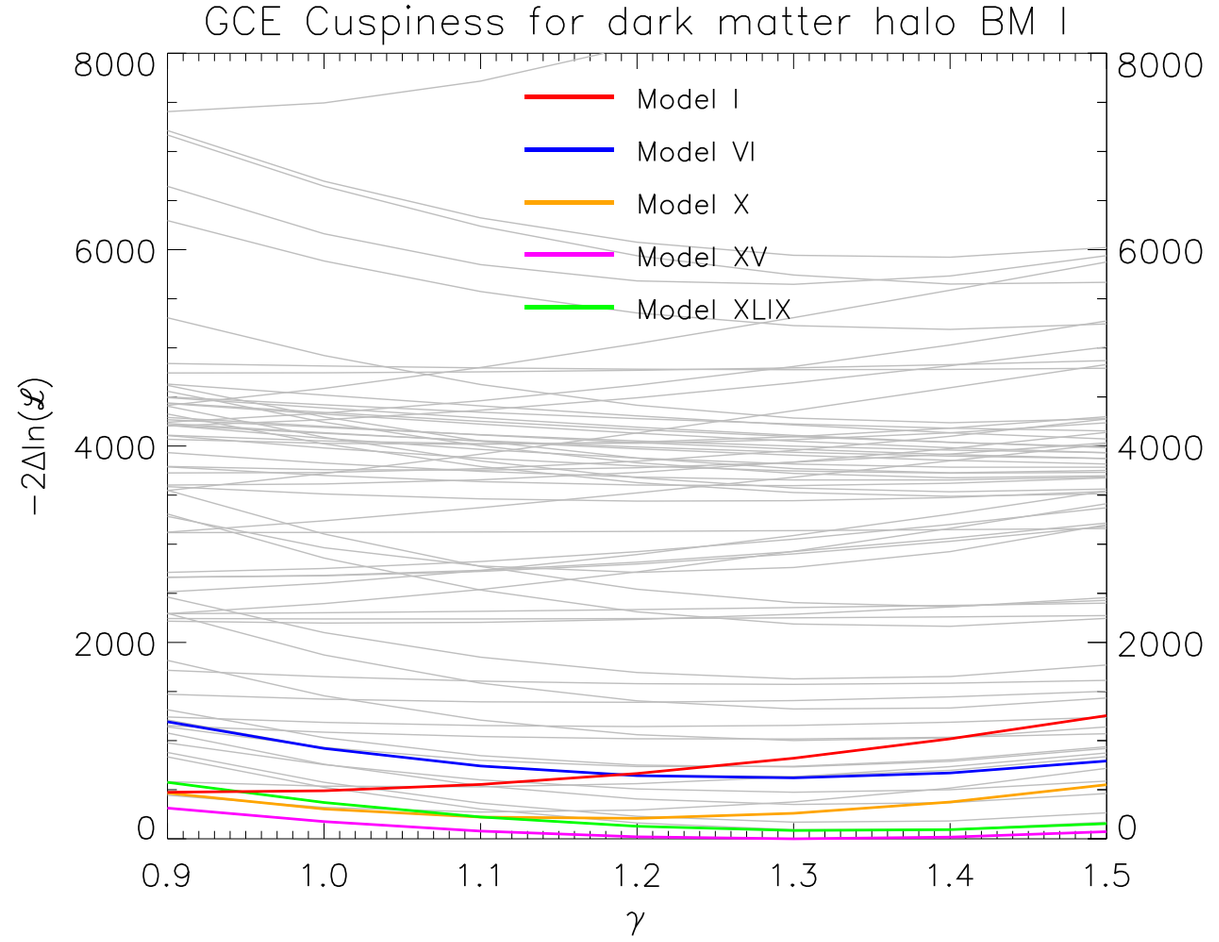

The gamma ray observations are sensitive to the morphological assumptions on the dark matter distribution.

We find some preference for a triaxial & rotated profile in a pattern that would suggest that the DM profile in the inner kilo-parsecs is aligned with the galactic bar and bulge more than the outer stellar halo. The cuspiness of the GCE is still best for gamma~1.2-1.3 (as has been from past results).

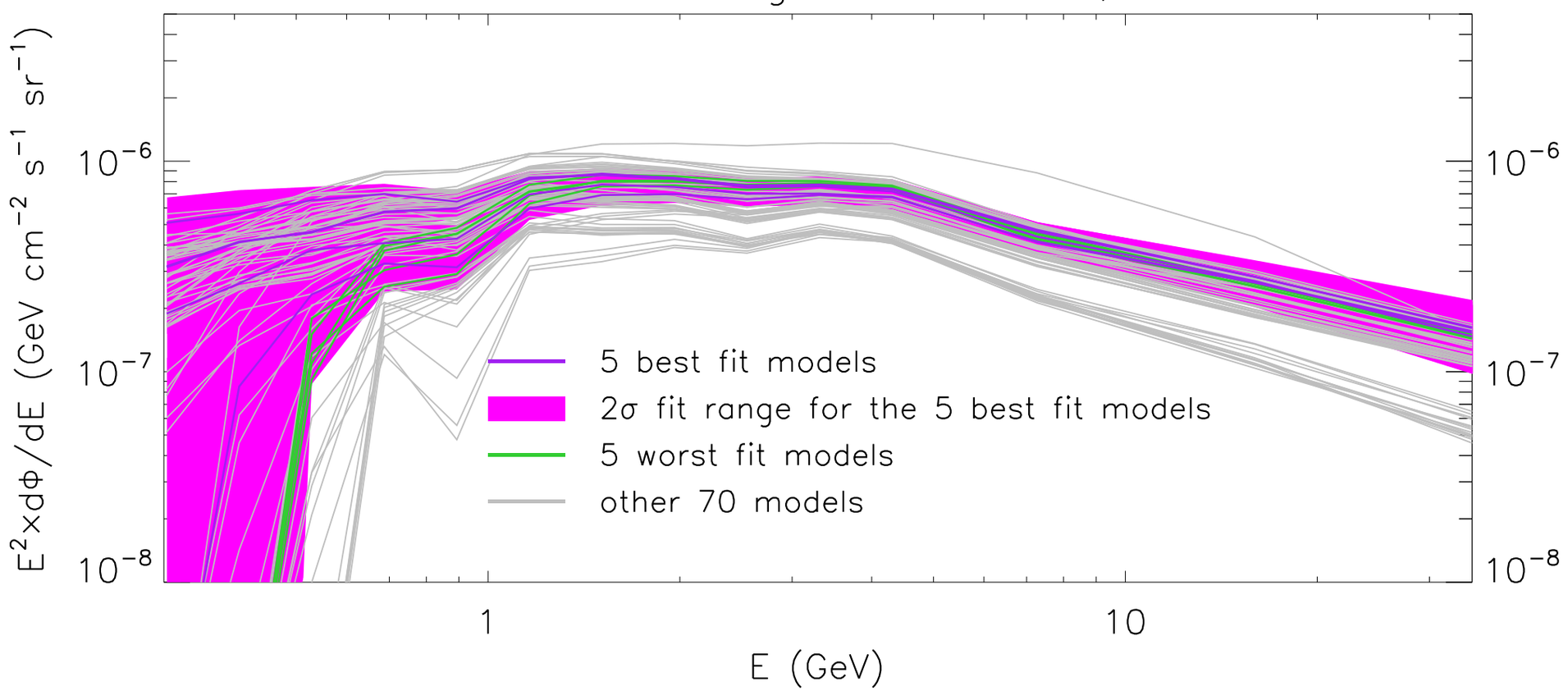

The GCE spectrum even for the triaxial DM profile is basically the same as past analysis of the inner galaxy. The GCE spectrum is quite stable to the exact assumptions on the DM profile cuspiness or assumptions on its triaxial 3D distribution and further rotations with respect to our line of sight.

Hu, **IC,** Zhong arXiv:2602.20252

Is there a second 20 GeV excess at high latitudes?

20 GeV halo-like excess of the Galactic diffuse emission and implications for dark matter annihilation

JCAP **11**, 080 (2025), arXiv:2507.07209

Tomonori Totani[a,b]

[a]Department of Astronomy, School of Science, The University of Tokyo, Bunkyo-ku, Tokyo 113-0033, Japan

Abstract. Fifteen years of the *Fermi* Large Area Telescope (LAT) data in the halo region of the Milky Way (MW) are analyzed to search for gamma rays from dark matter annihilation. Gamma-ray maps within the region of interest ($|l| \leq 60°$, $10° \leq |b| \leq 60°$) are modeled using point sources, the GALPROP models of cosmic-ray interactions, isotropic background, and

...

Various systematic uncertainties are investigated, but the 20 GeV peak remains significant. In particular, the halo excess with a similar spectrum is detected even relative to the LAT standard background model, which contains non-template patches adjusted to match the observed map. The halo excess spectrum can be fitted by annihilation with a particle mass $m_\chi \sim 0.5$–0.8 TeV and cross section $\langle \sigma v \rangle \sim (5\text{–}8) \times 10^{-25}$ cm^3 s^{-1} for the $b\bar{b}$ channel. This cross section is larger than the upper limits from dwarf galaxies and the canonical thermal relic value, but considering various uncertainties, especially the density profile of the MW halo, the dark matter interpretation of the 20 GeV "Fermi halo" remains feasible. The prospects for verification through future observations are briefly discussed.

The claim:

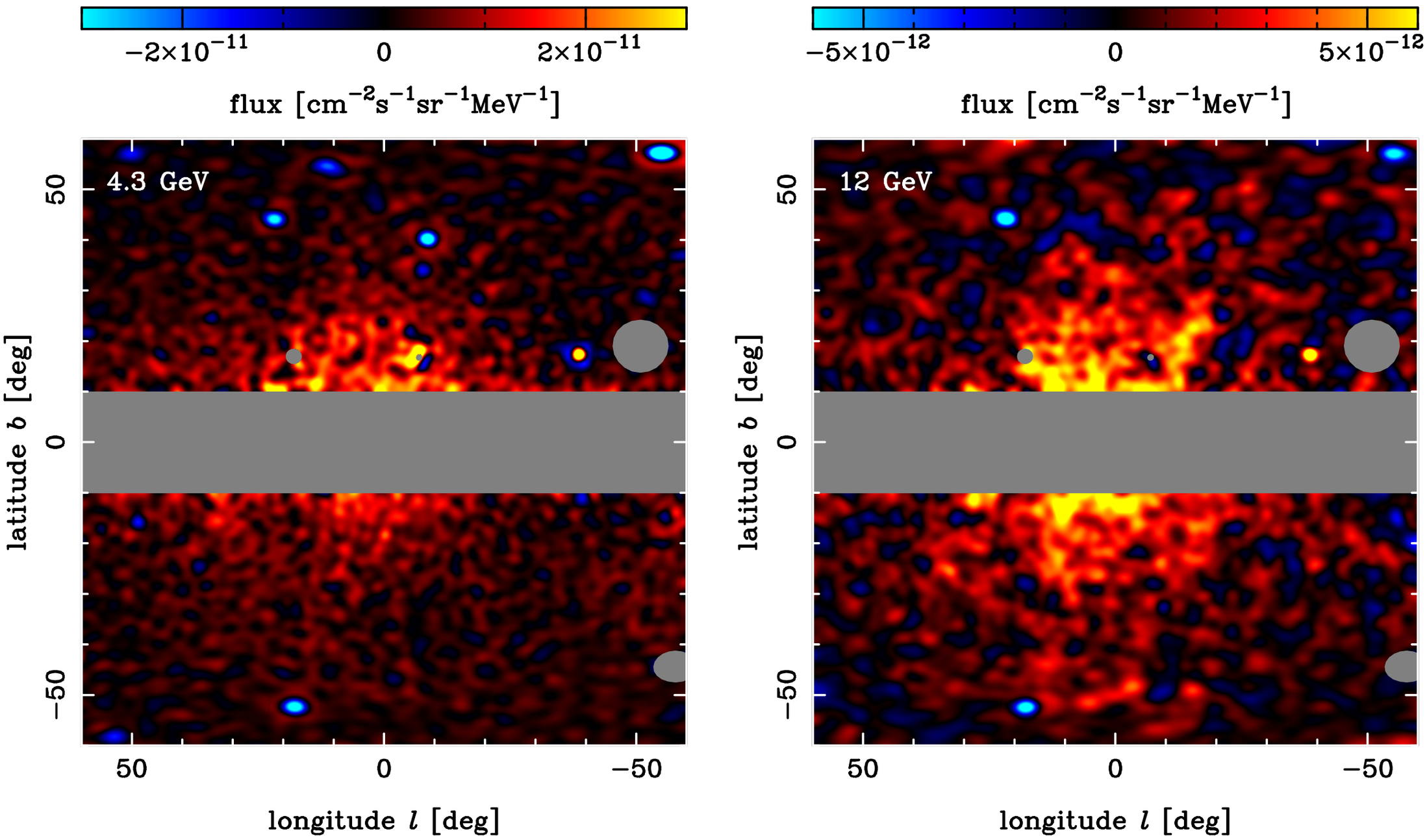

Figure 12. Map images of the halo model plus residual by the fit with the NFW-ρ^2 model at four photon energy bins lower than 21 GeV. The maps are smoothed with a Gaussian of $\sigma = 1°$.

Totani JCAP 2025

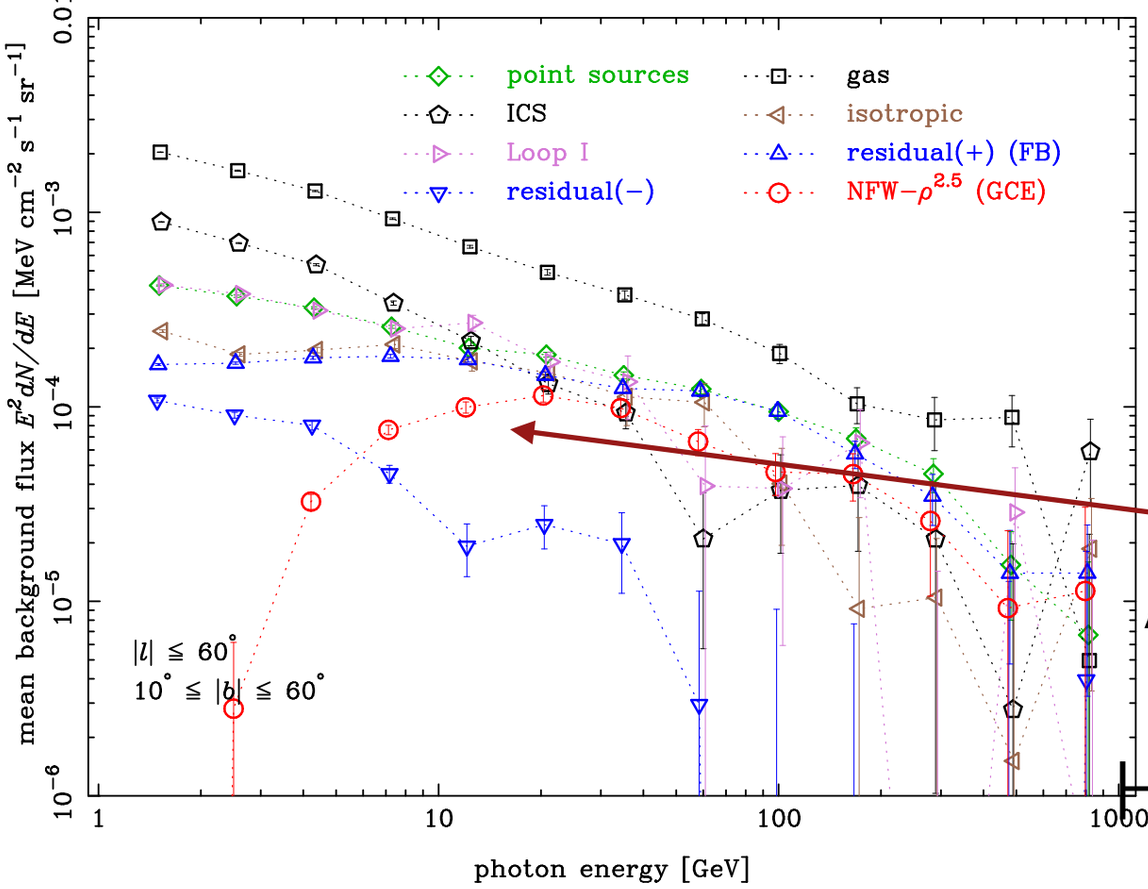

The claim:

A clear excess peaking 20 GeV.
This is a very bright excess…
However (in my opinion) sensitive to modeling assumptions

Figure 5. The same as figure 4, but including the GC GeV excess (GCE) template (NFW-$\rho^{2.5}$).

Totani JCAP 2025

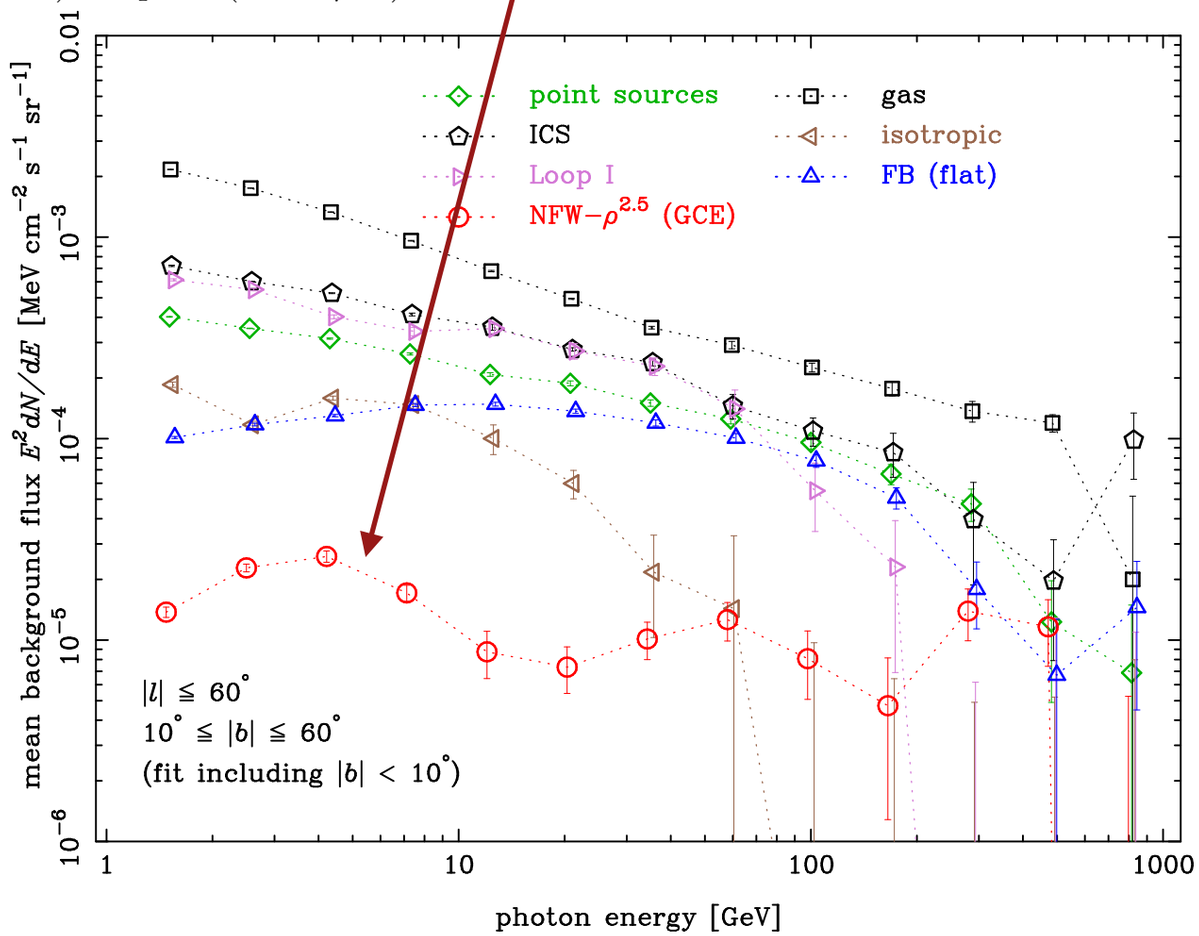

The templates:

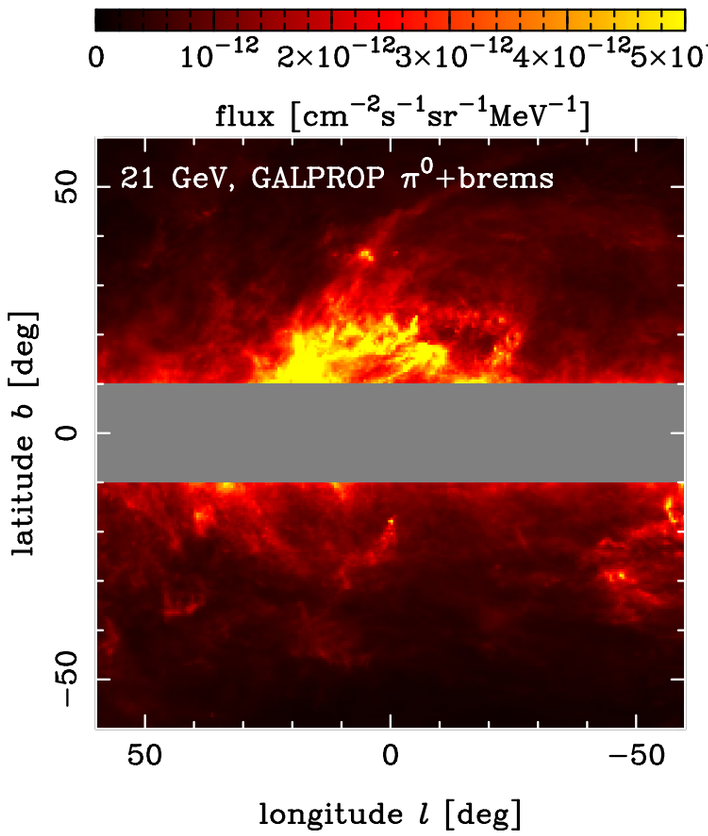

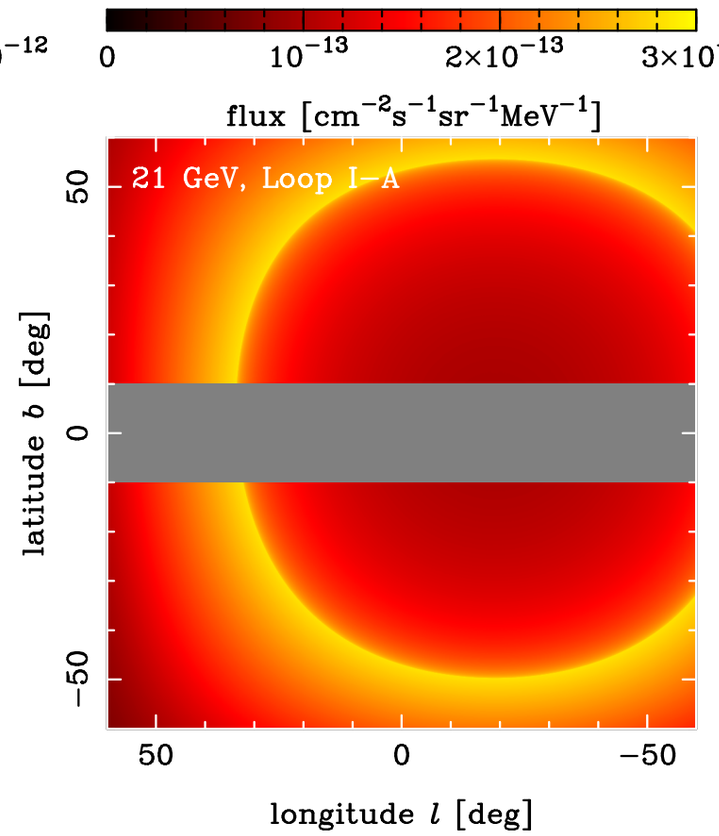

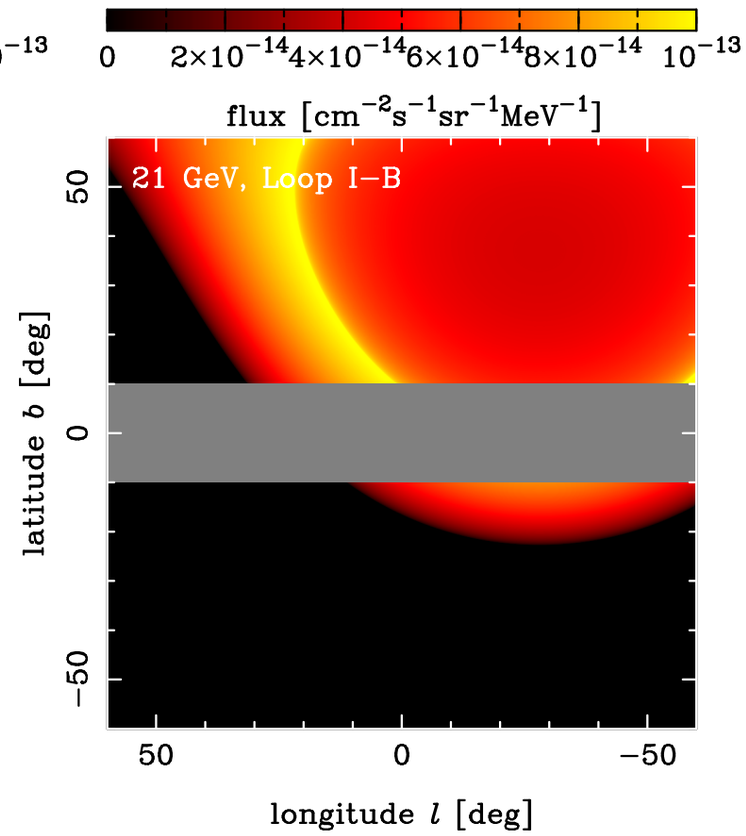

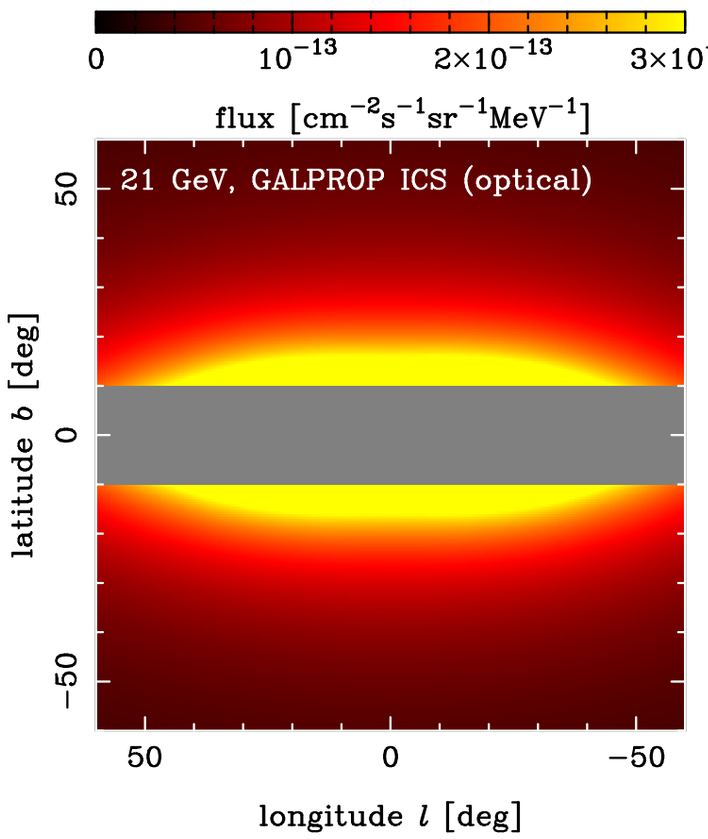

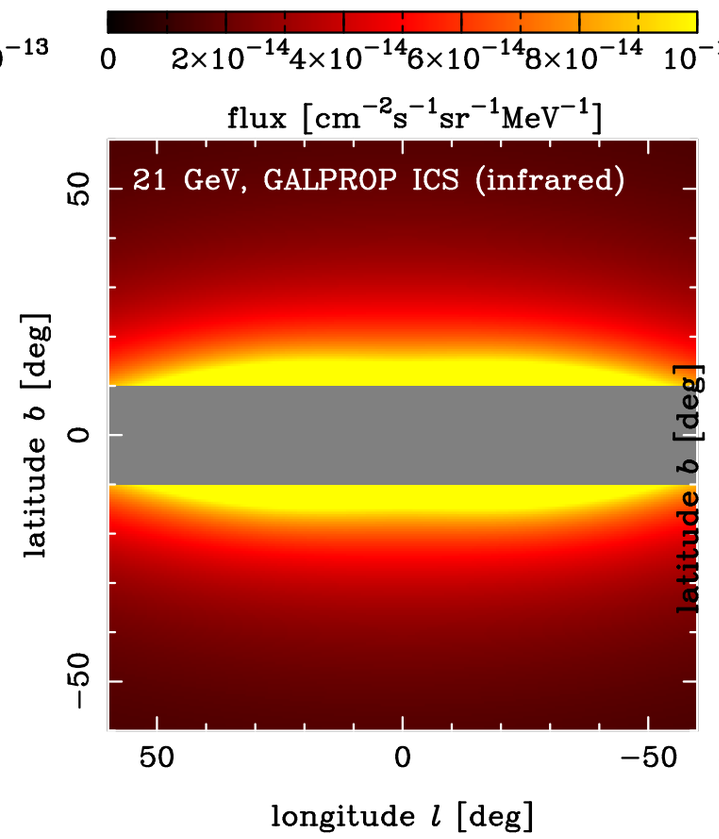

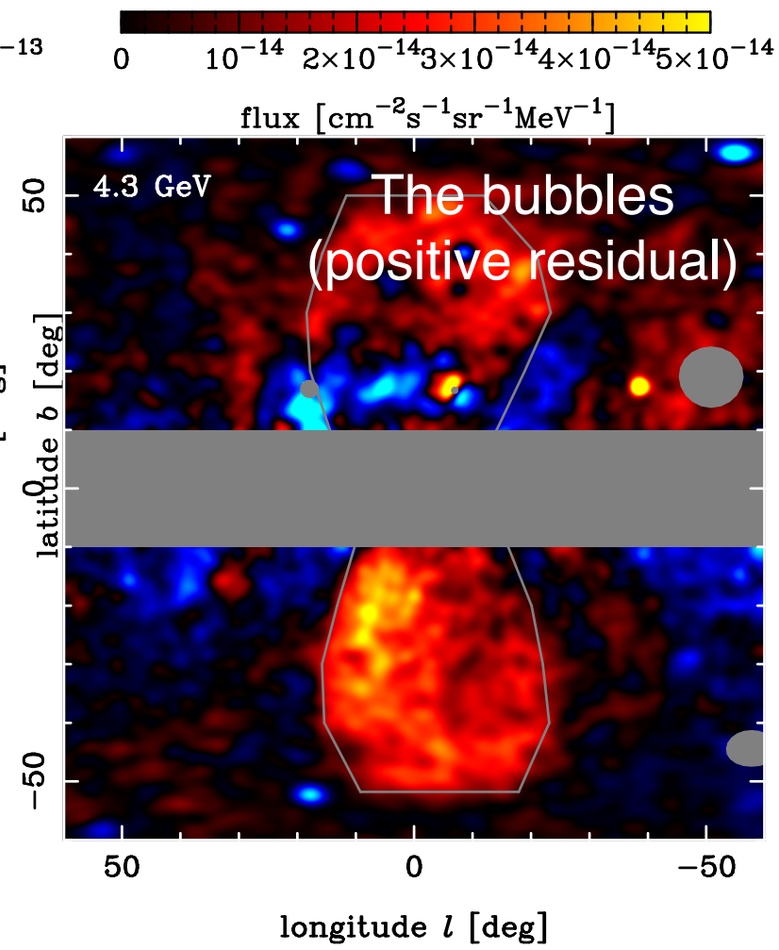

Totani JCAP 2025

Our ongoing work: IC, Hu, Zhong (260X.XXXXX)

First:

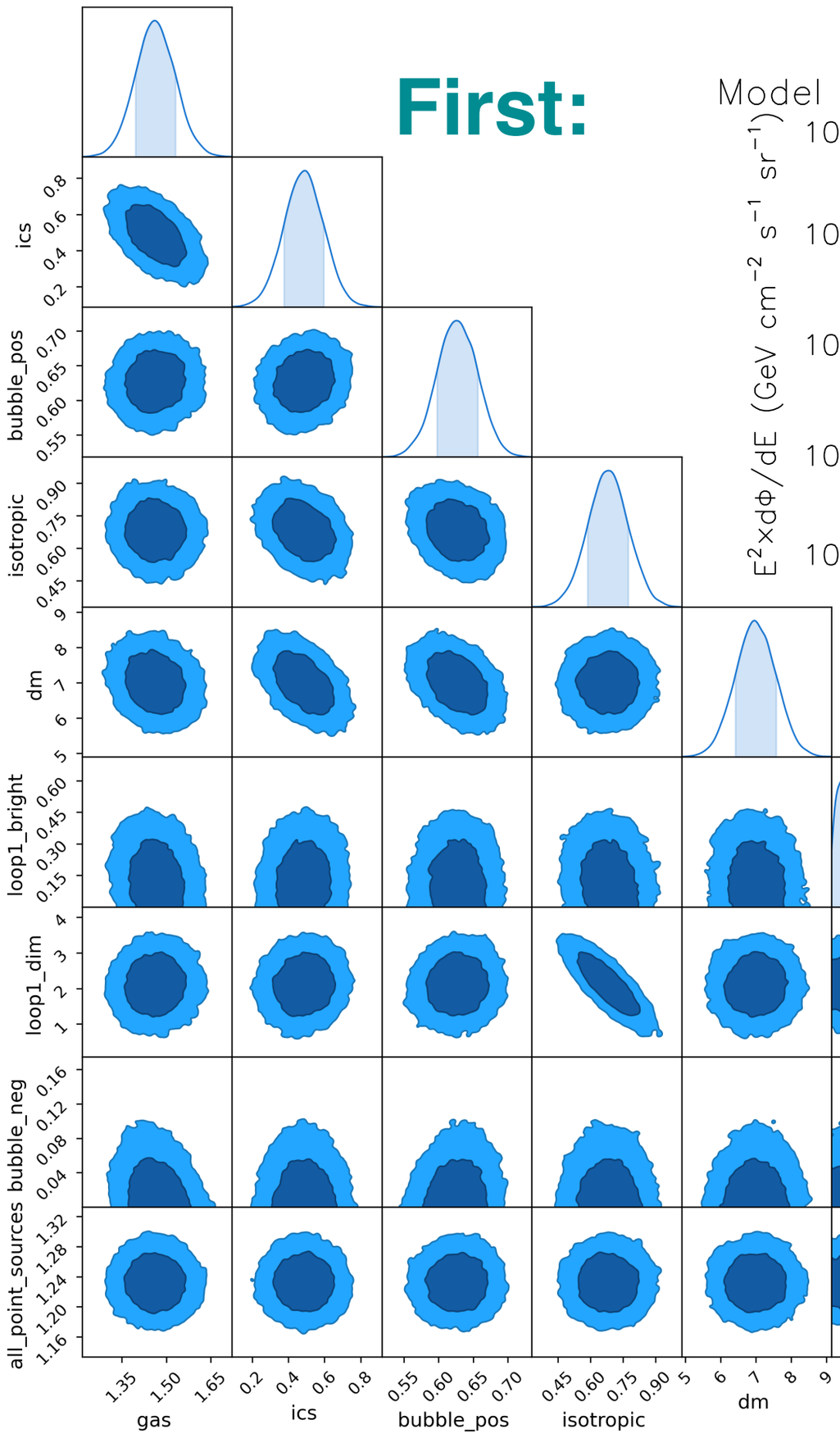

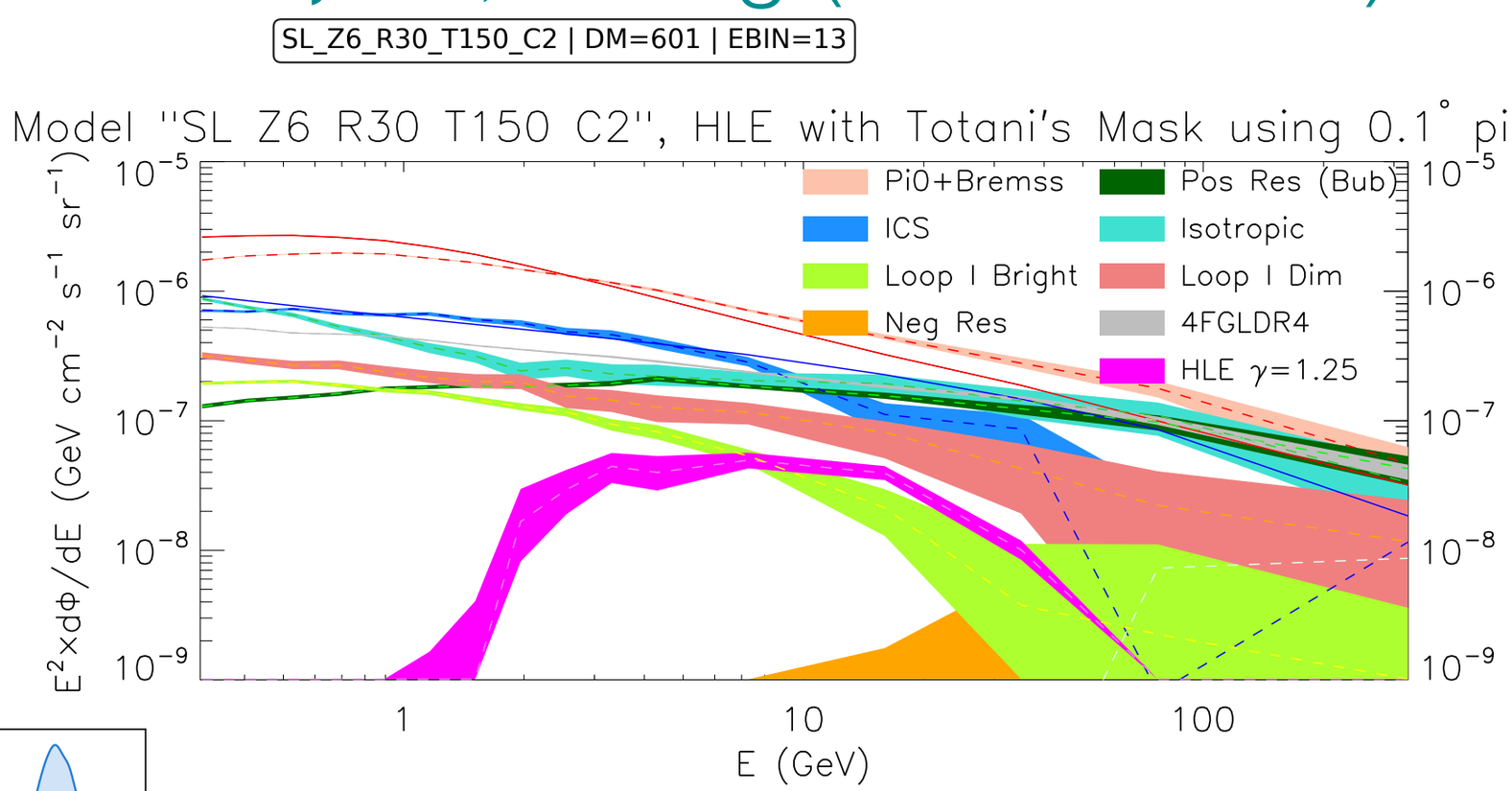

We repeat step by step and find the same results by Totani

And same for a high-res version of this analysis

Then:

i) We break the original region of interest (window in the sky) into many smaller windows of the sky.

ii) We go from the 6 background diffuse emission models (i.e. combinations of templates) to 100. There was a great level of similarity between the original 6 models in Totani.

iii) We try different # of templates in the fit (i.e. 6-9 d.o.f. per energy bin).

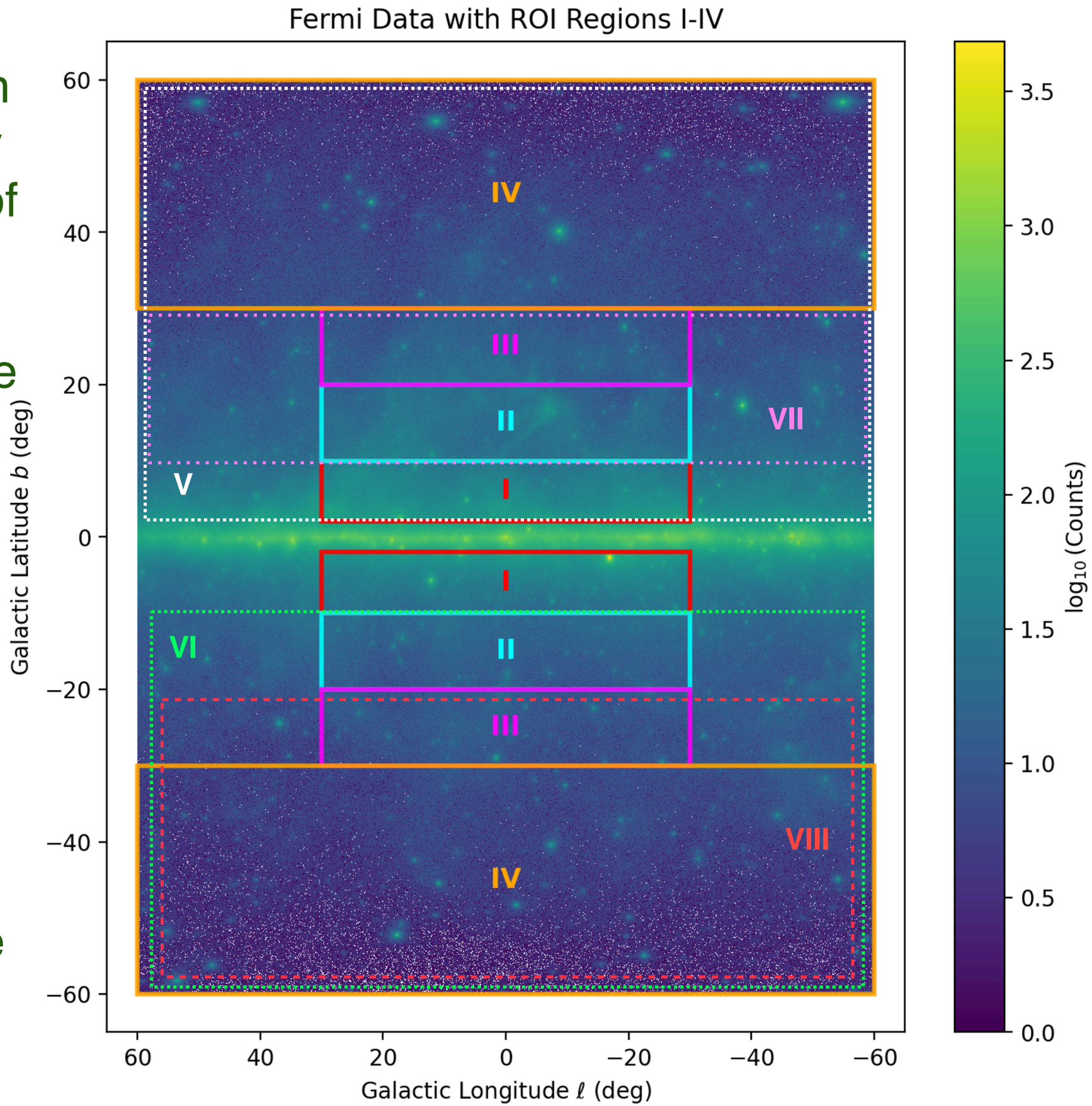

The test: profile for a DM signal,

The flux associated to the excess emission of the GCE was the correct one with the galactic latitude:

Calore, **IC**, McCabe, Weniger, PRD 2015

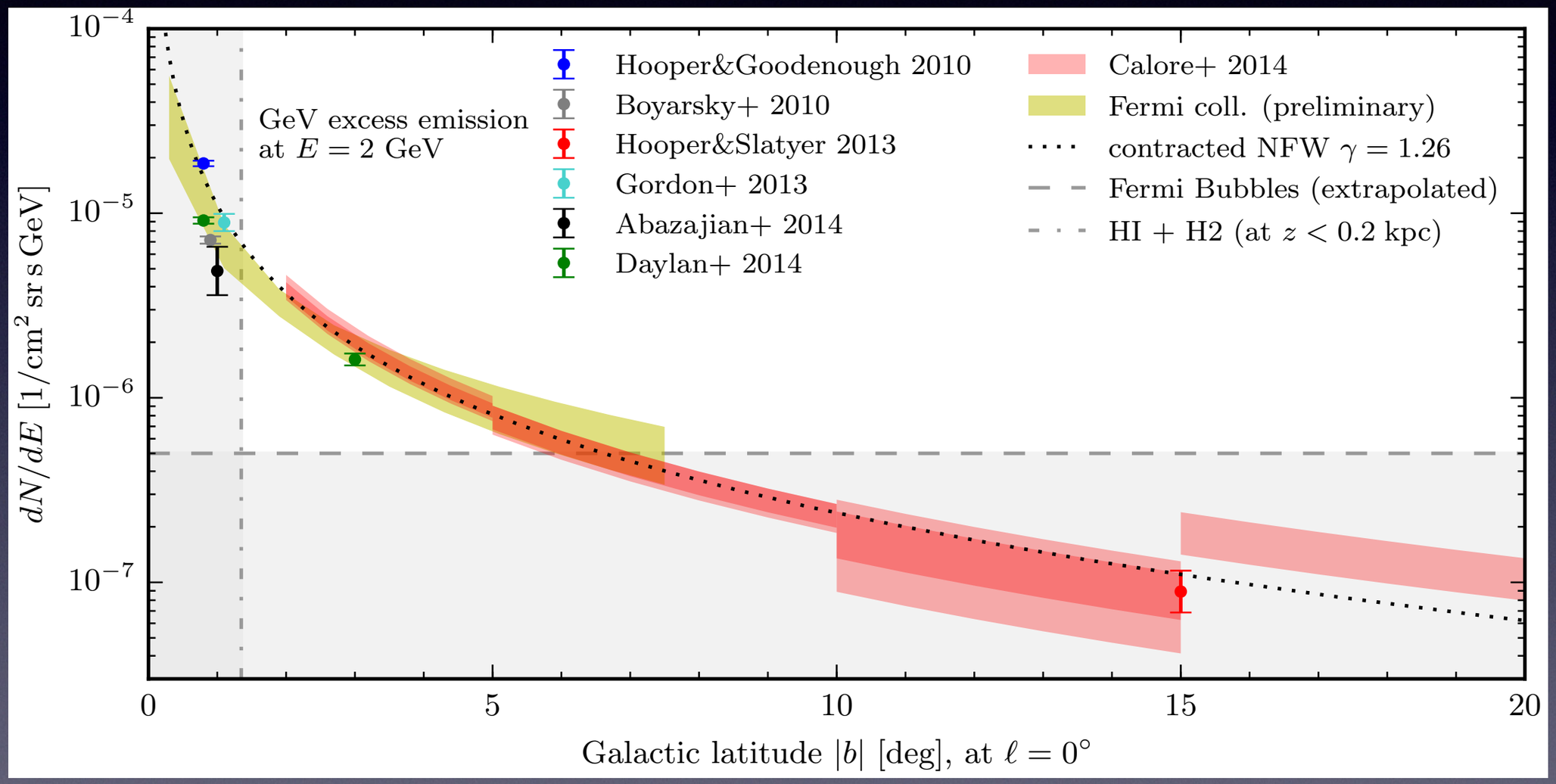

The excess signals from different analyses, agree within a factor of less than 2 in terms of total emission.

The test on the evolution of the amplitude with latitude:

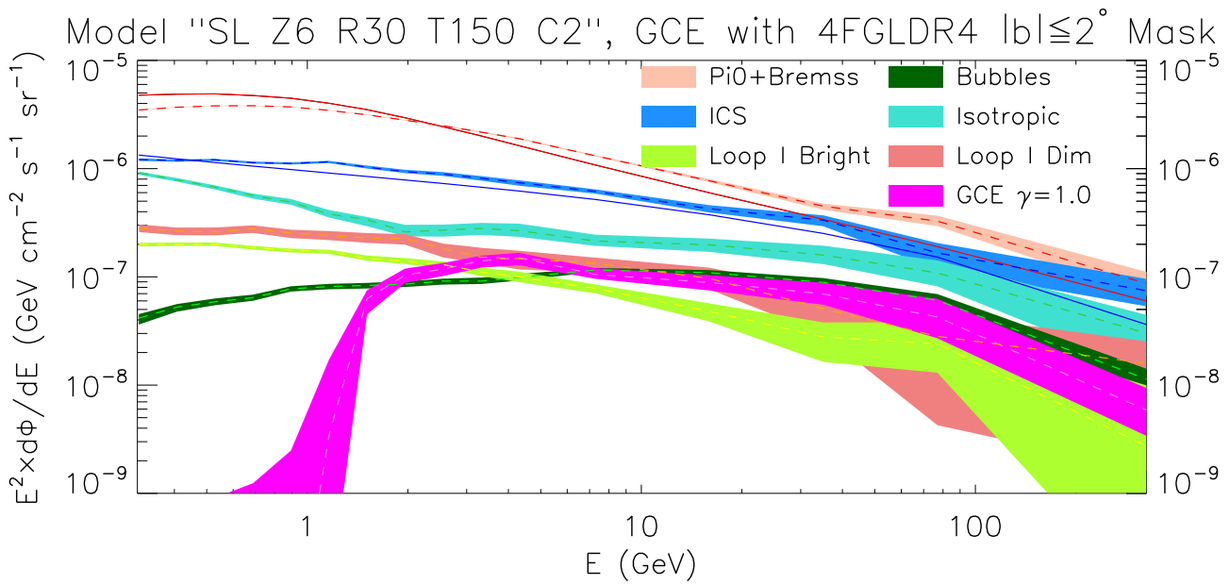

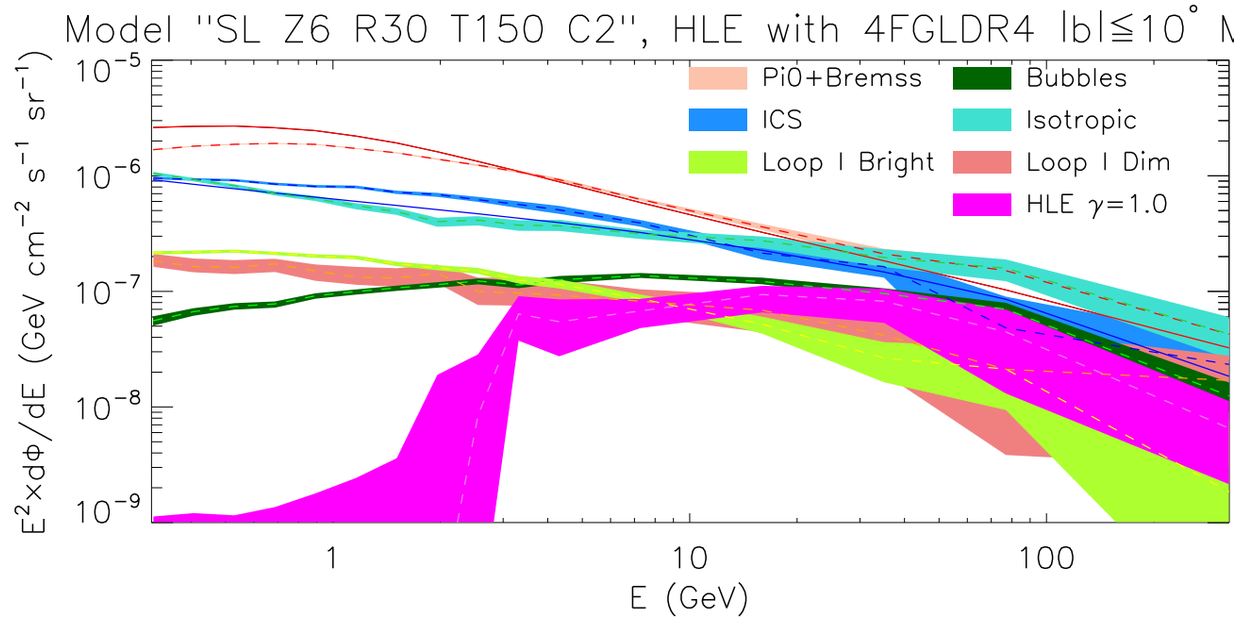

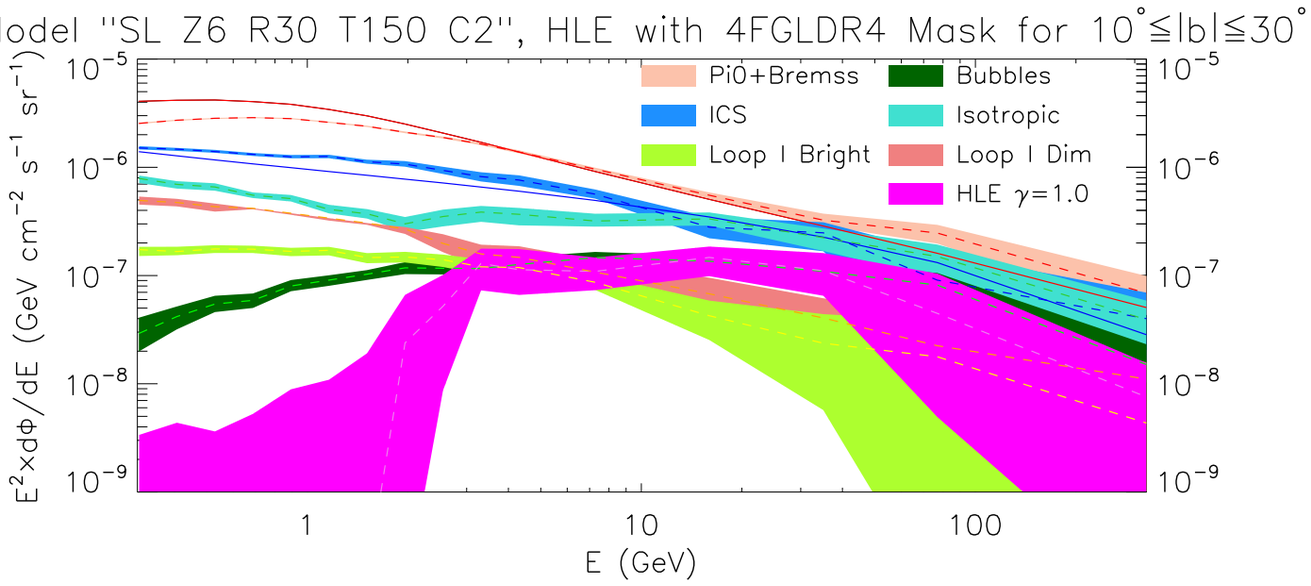

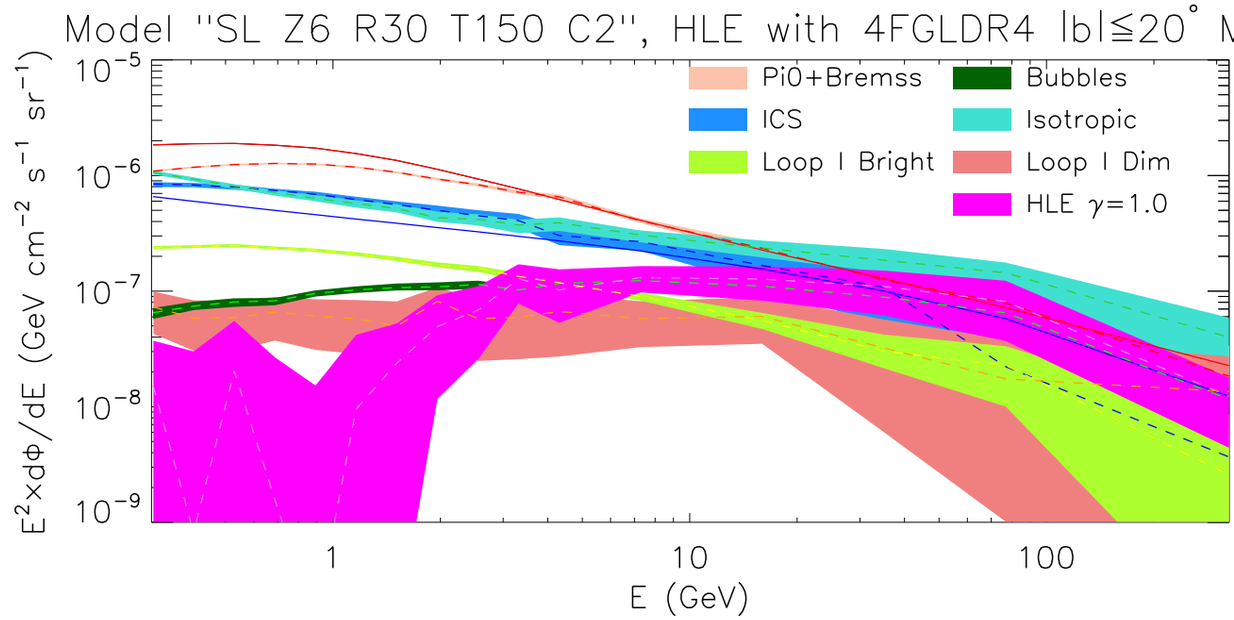

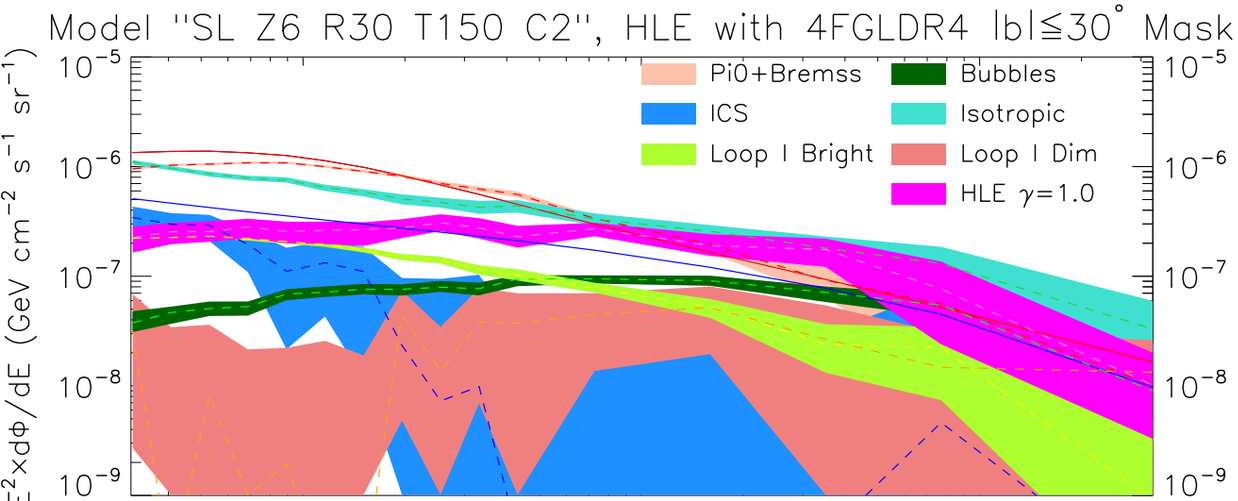

This excess does NOT behave like a DM signal

IC, Hu, Zhong (260X.XXXXX)

This is true across the 100 background diffuse emission models:

This is the GCE:

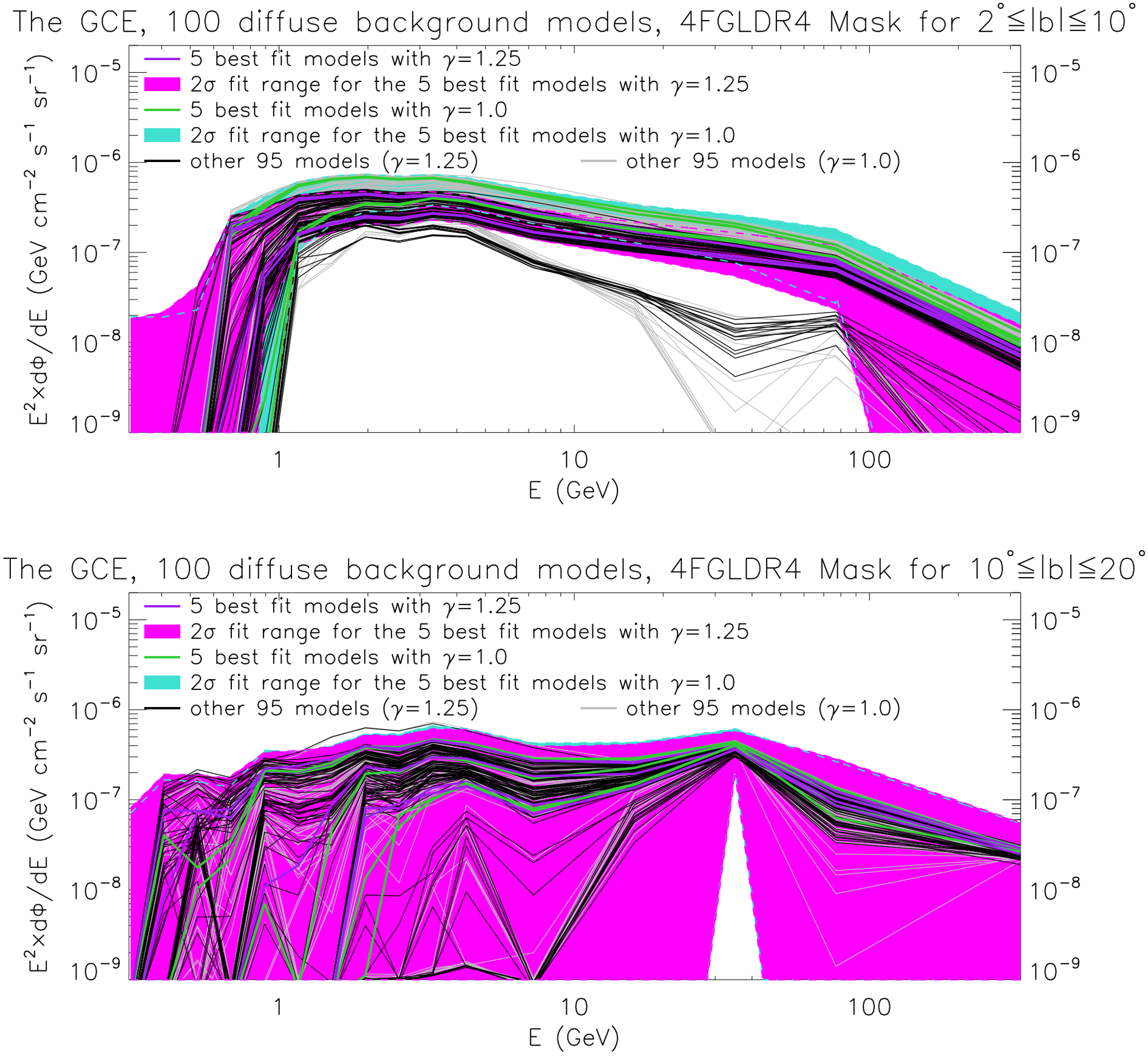

This is true across the 100 background diffuse emission models:

This is the GCE:

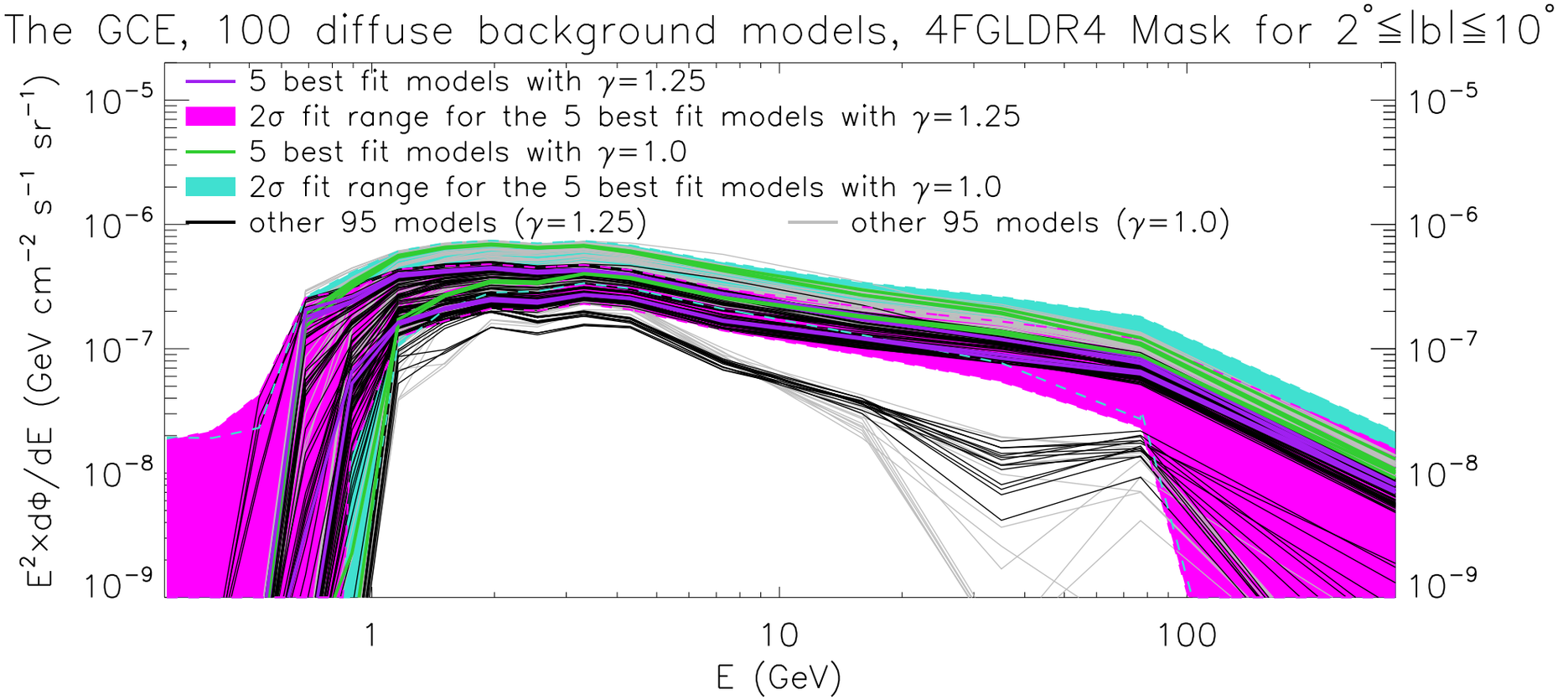

But the HLE is **brighter at high latitudes:**

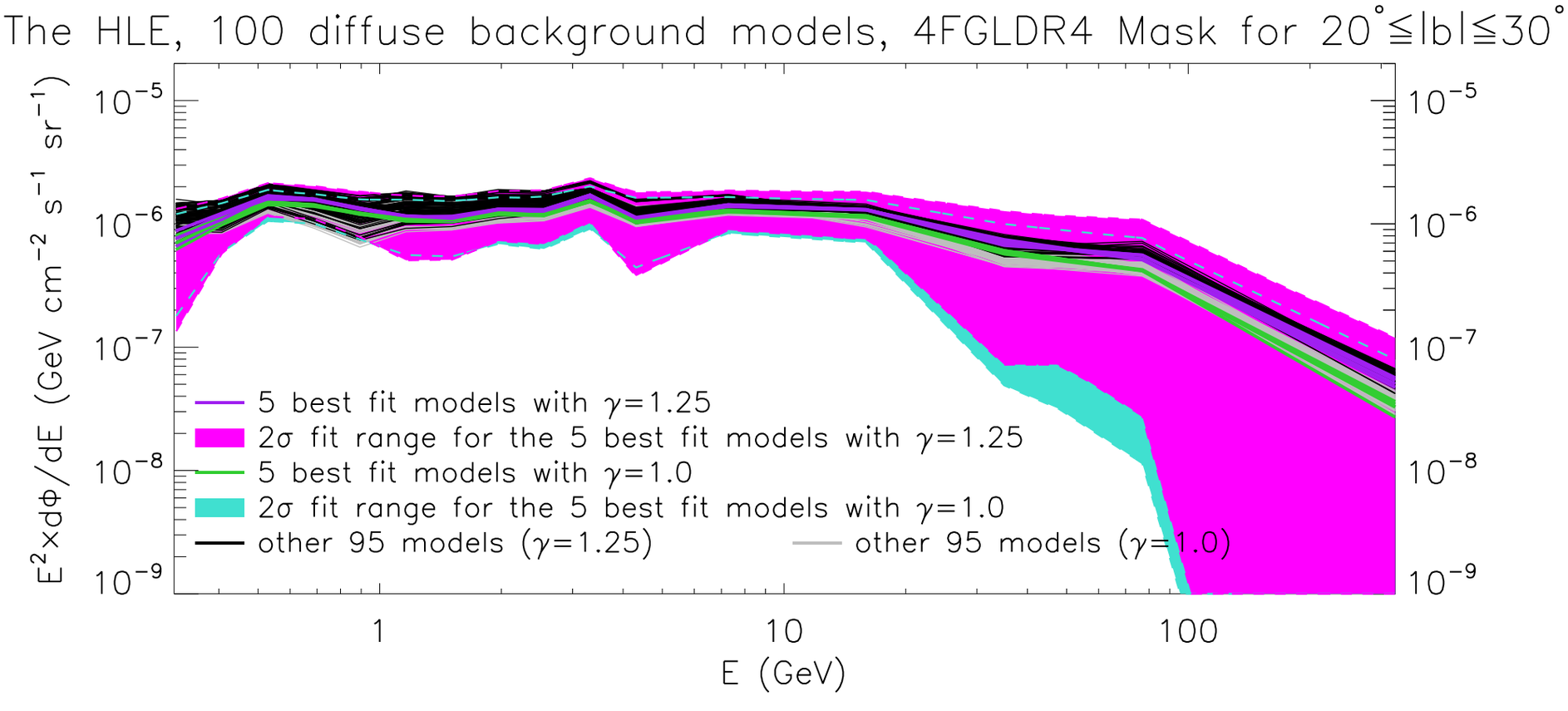

This HLE is probably a component of the Fermi Bubbles and NOT a dark matter signal:

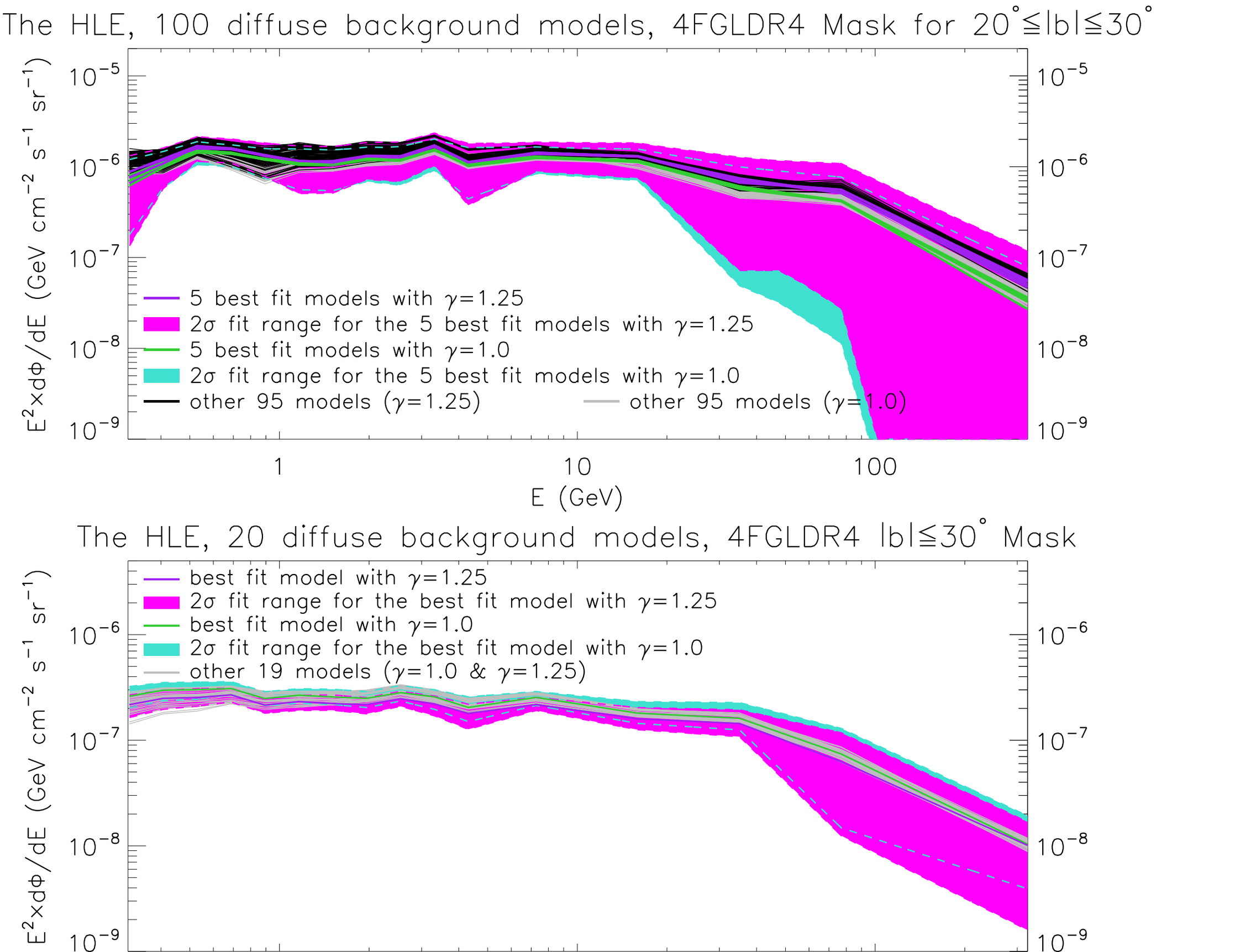

Acknowledgements

My Collaborators: Yi-Ming Zhong (City University of Hong Kong), Leo Hu (City University of Hong Kong),
Sam McDermott (Fermilab)

My Students:
Ian McKinnon (OU—>University of Oklahoma),
Osip Surdutovich (Carleton College—> Ohio State University)

MSGC, NASA No. NNX15AJ20H
MSGC, NASA No. 80NSSC20M0124

Department of Energy, DE-SC0022352

Thank you!

Extra

Combining all Indirect DM searches

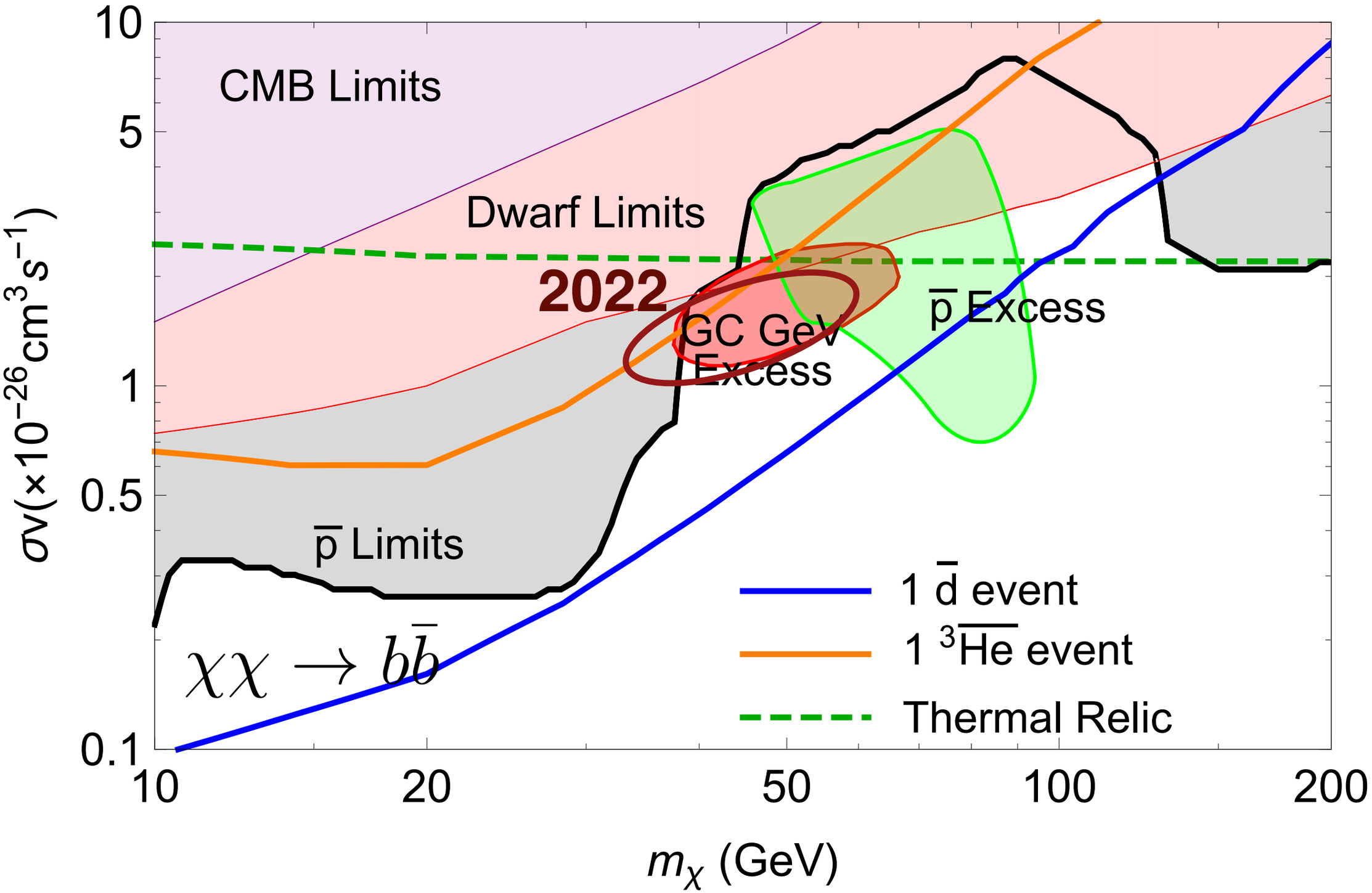

IC, Linden, Hooper PRD 2020

We also find unphysical spectral variations/breaks in the individual flux components associated to the separate rings. This never happens with the modeled astrophysical assumption-based templates.

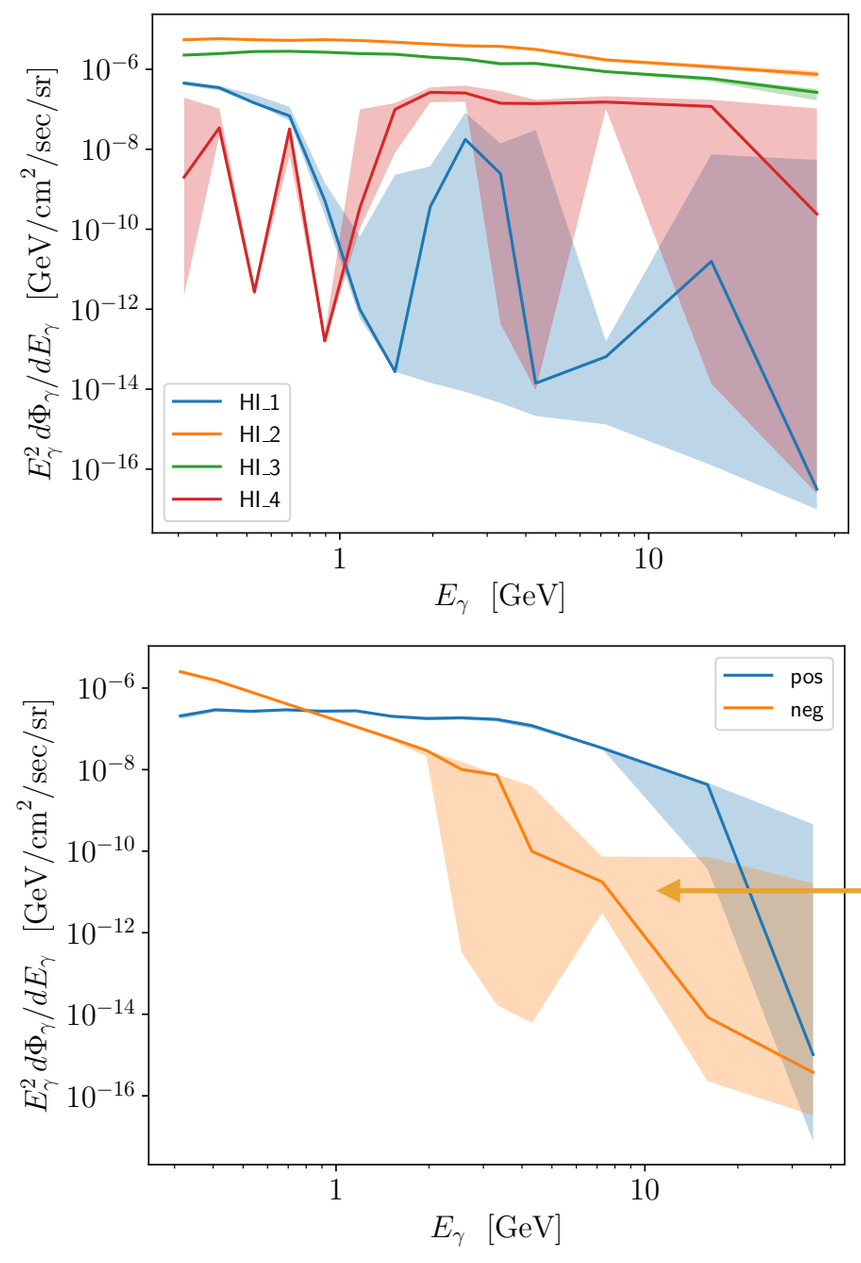

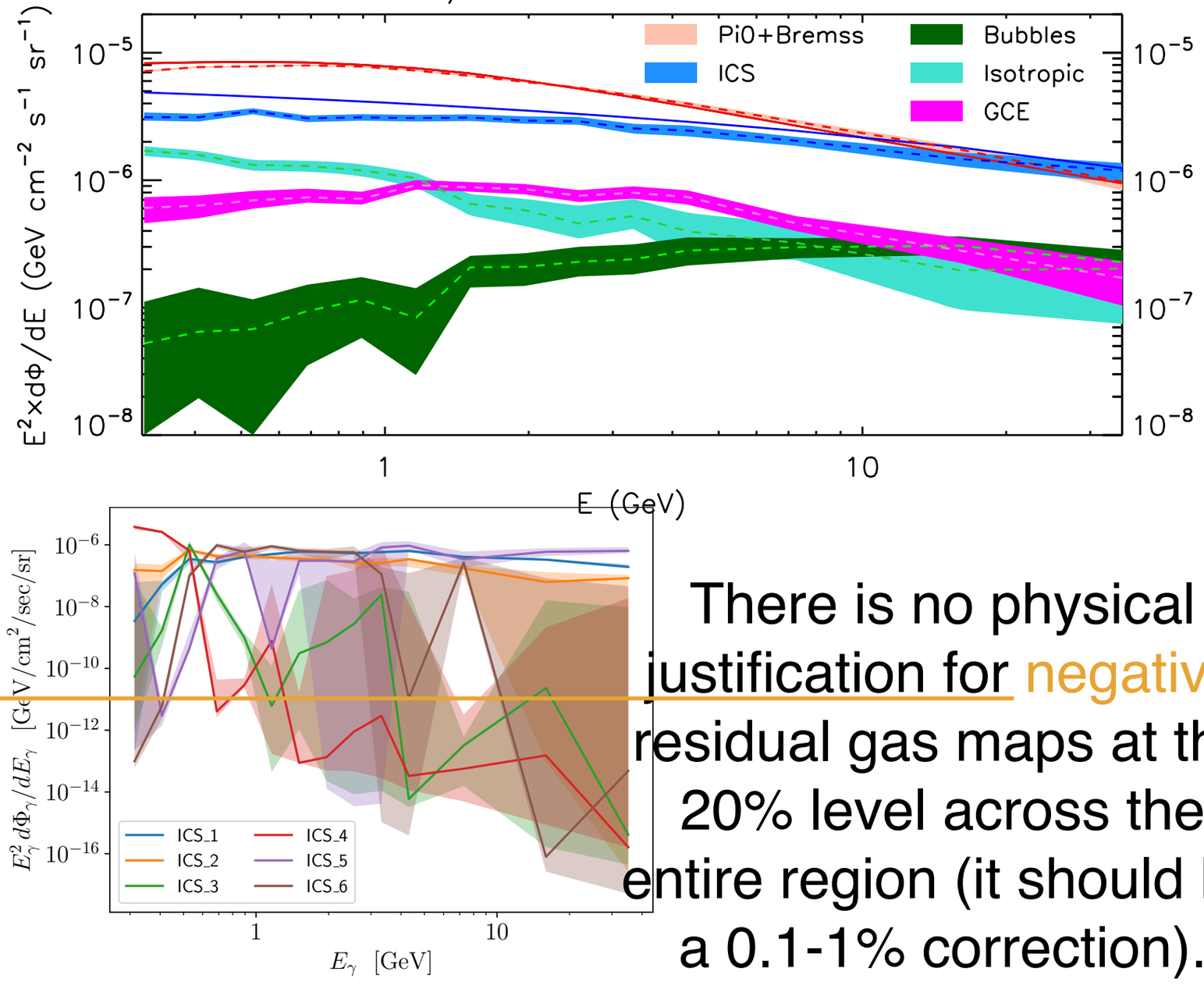

There is no physical justification for negative residual gas maps at the 20% level across the entire region (it should be a 0.1-1% correction).

Figure 2. Best-fit spectra and 95% credible intervals of the flux of the ring-based templates that were fit alongside the boxy bulge excess template. For the negative residual component, we show its absolute value in the lower left panel.

McDermott, Zhong, **IC** MNRAS Letters 2023

A rough sketch of the Milky Way

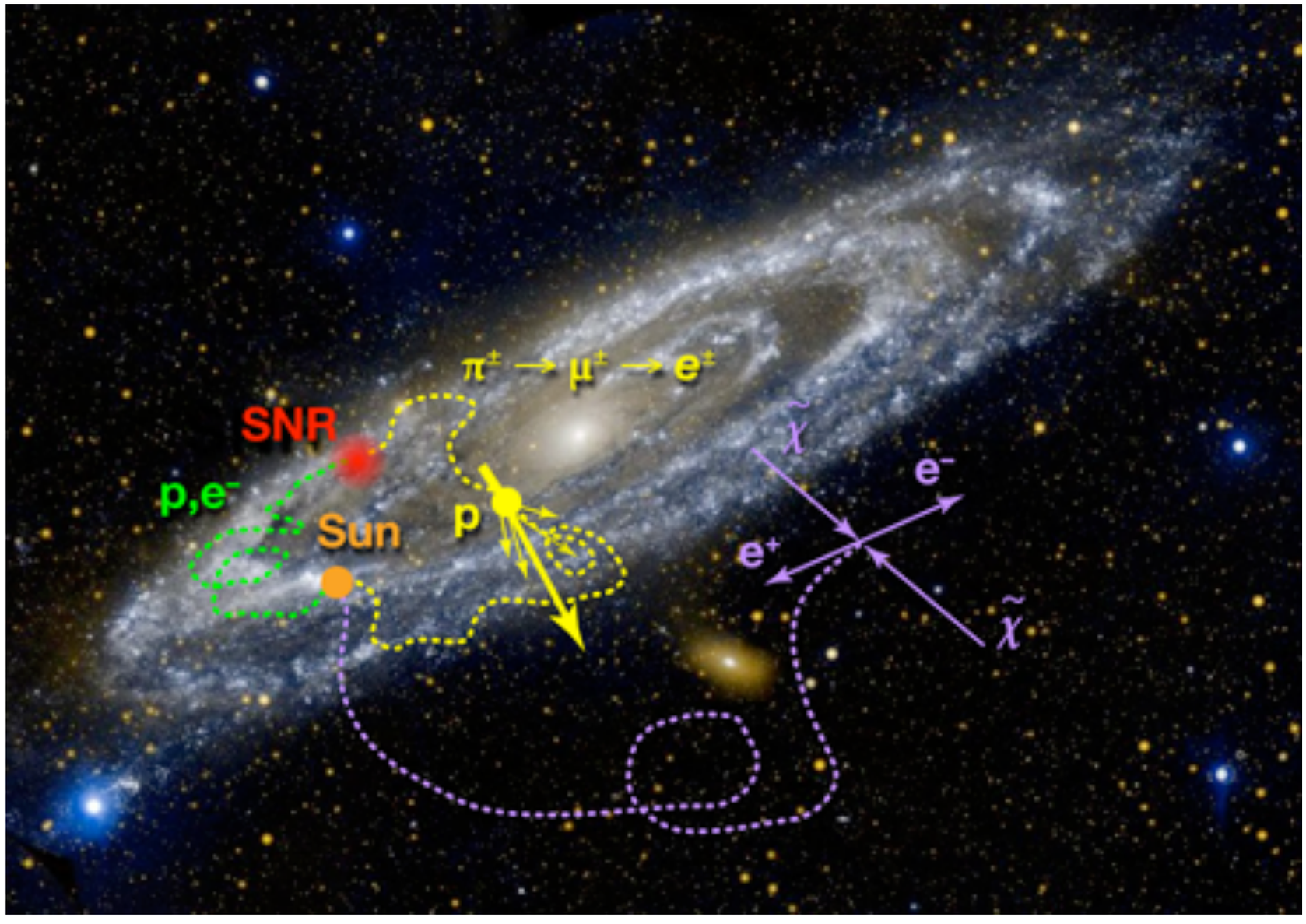

With CR spectral measurements we can understand the properties of the Interstellar Medium (ISM), and probe sources of high energy cosmic rays (CRs) including dark matter that could give a signal in antimatter.

BUT ALSO the UNKOWN, e.g. Looking for DM annihilation signals

For a DM annihilation signal
We want to observe:

$$\frac{d\Phi_\gamma}{dE} = \int\int \frac{\langle\sigma v\rangle}{4\pi} \frac{dN_\gamma}{dE}_{DM} \frac{\rho^2_{DM}(l,\Omega)}{2\,m^2_\chi} dl\,d\Omega$$

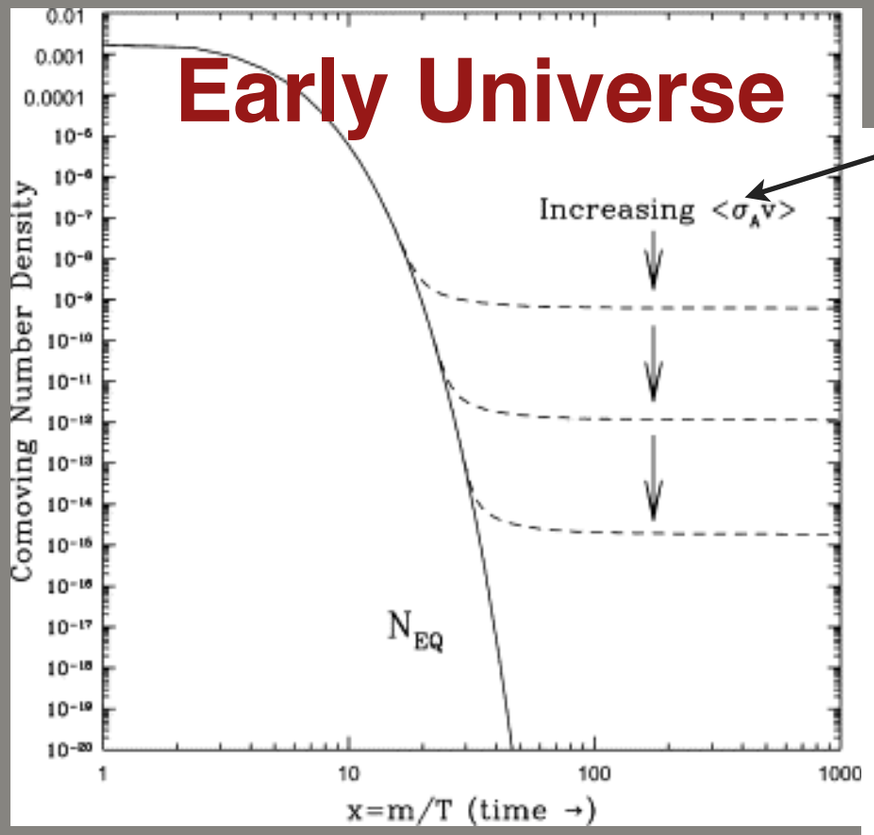

Steigman et al. 2012

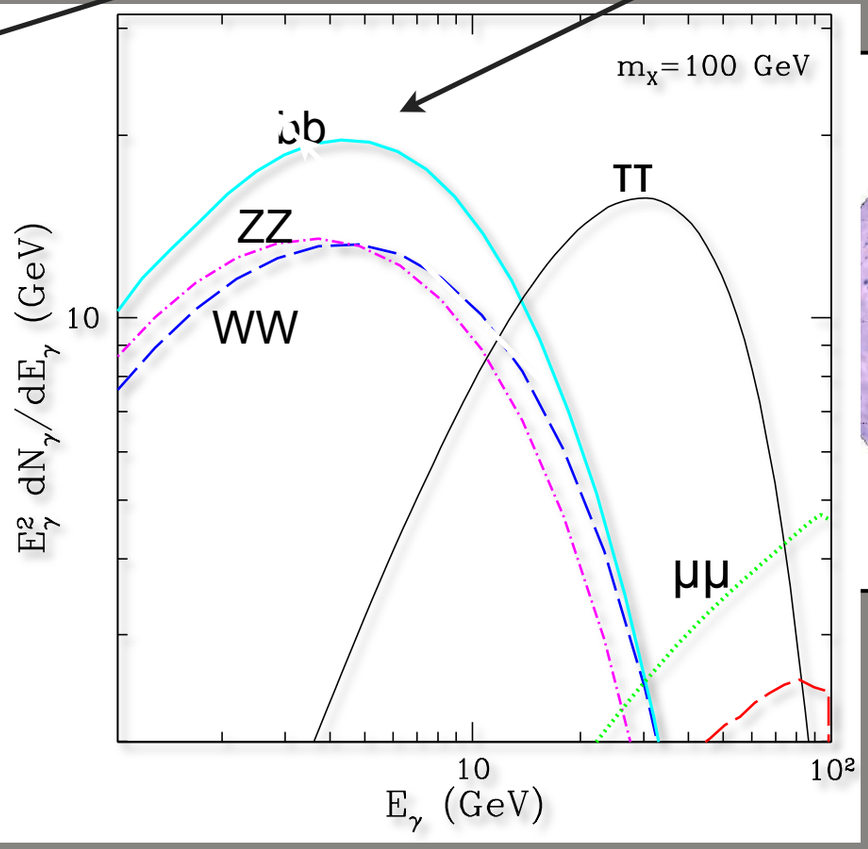

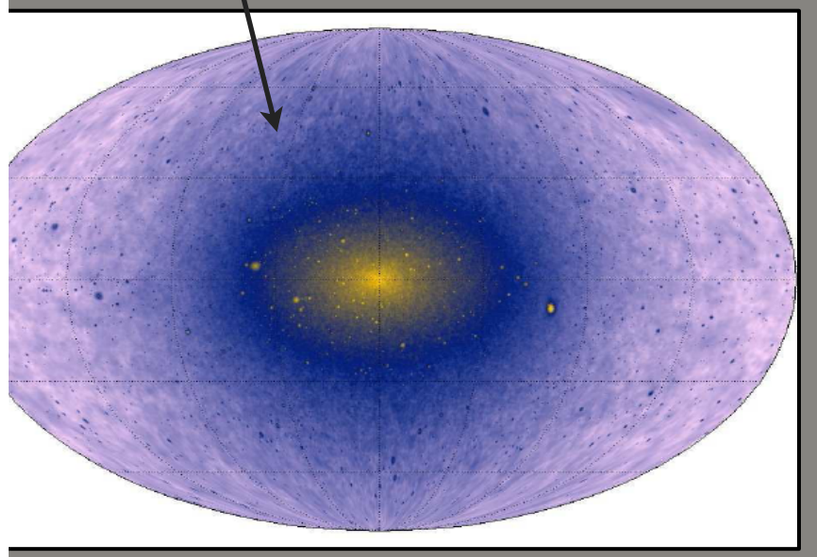

Particle Physics

PYTHIA: Sjostrand et al. 2006 & 2007
HERWIG: Corcella et al. 2001

From Cosmological Simulations what we expect today

Springel et al. 2005,
Kuhlen et al. 2012,
Vera-Ciro et al. 2014

Using templates on Gamma-ray maps —> It's first use led to the discovery of the Fermi(Haze)-Bubbles

Dobler, Finkbeiner, **IC**, Slatyer, Weiner, ApJ, 2010

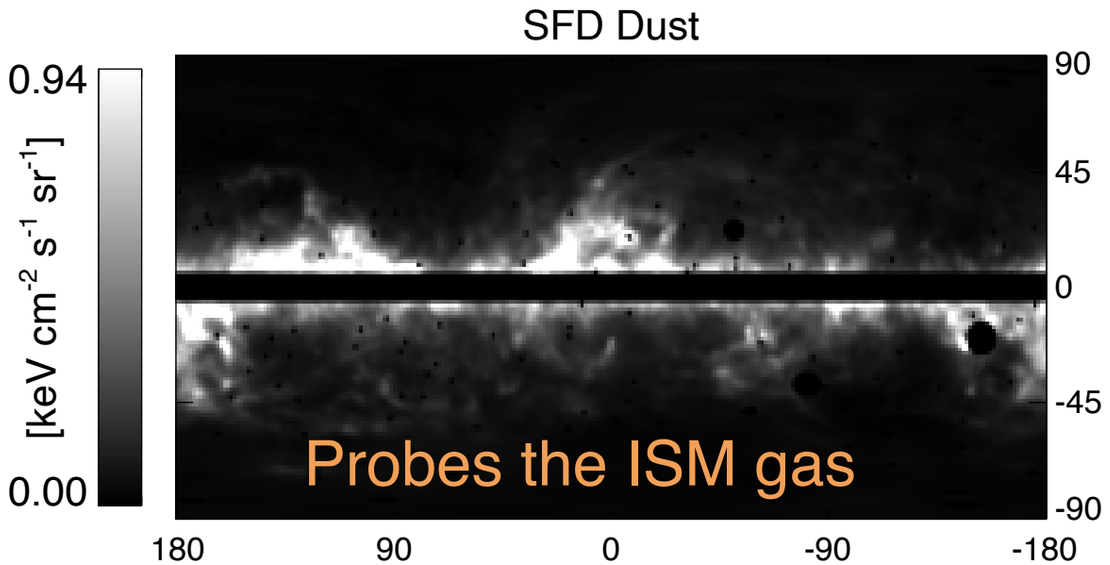

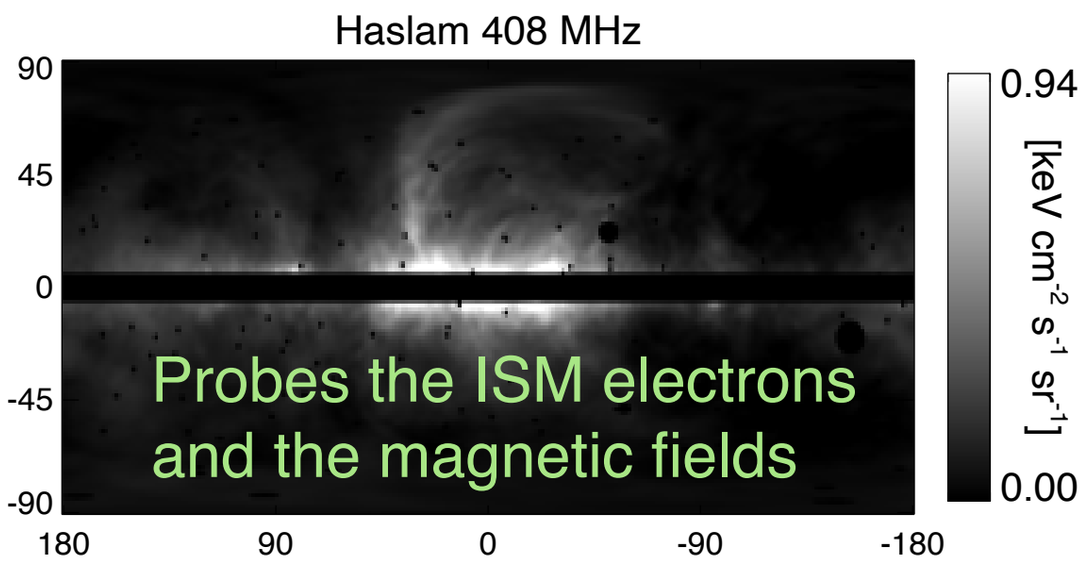

Fermi Bubbles

Su et al. ApJ 724, 1044 (2010)

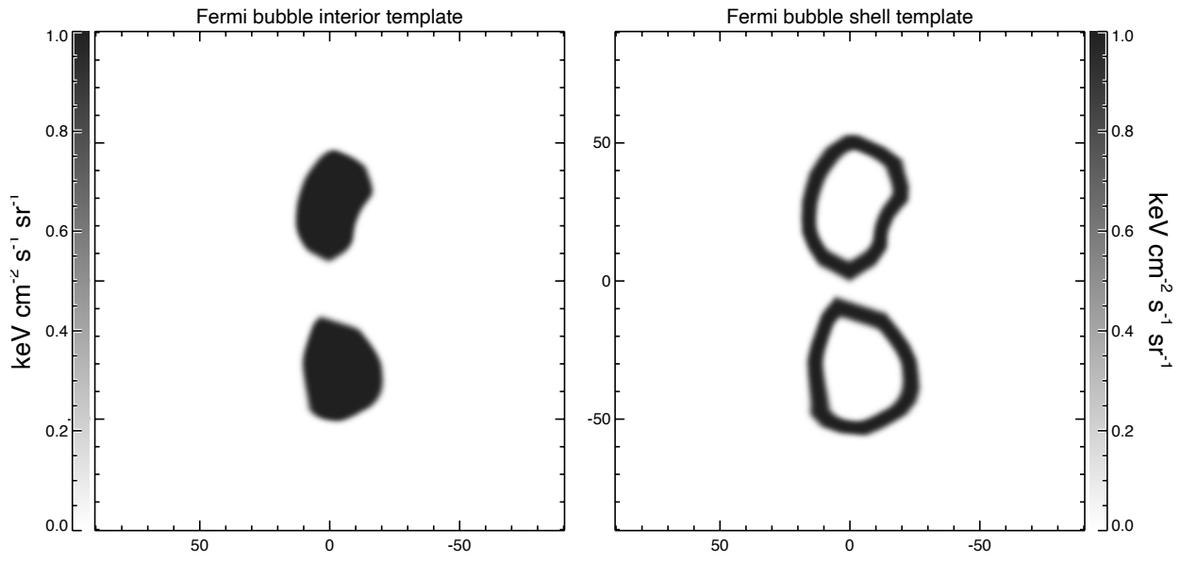

Discovery of edges on the emission.

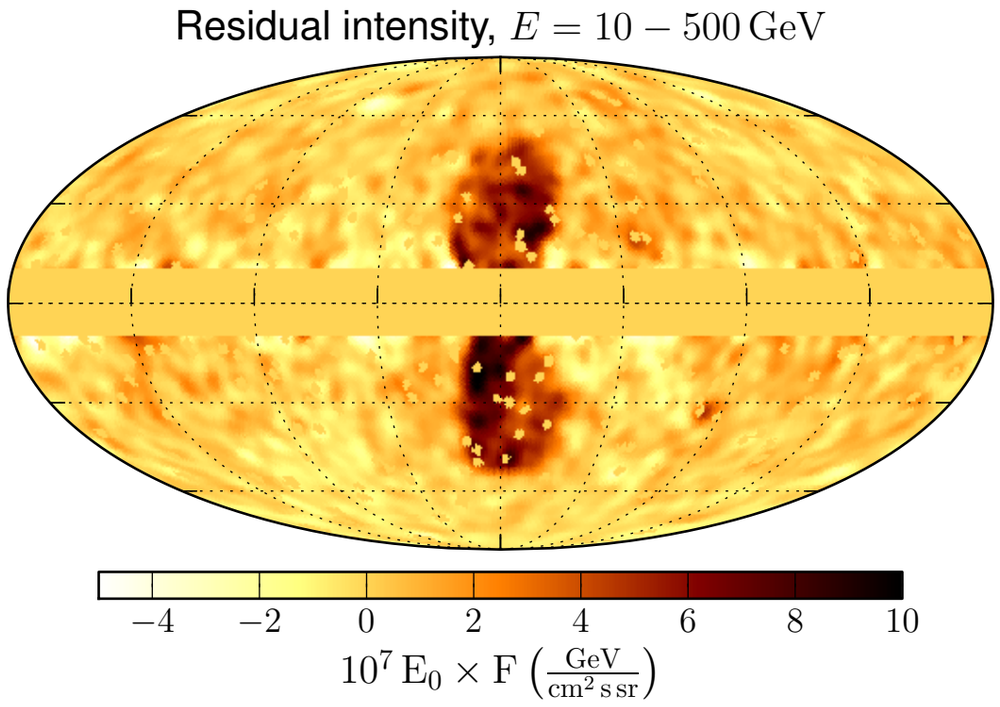

Fermi-LAT Collaboration Result ApJ 2014

Planck* intermediate results. IX. Detection of the Galactic haze with *Planck

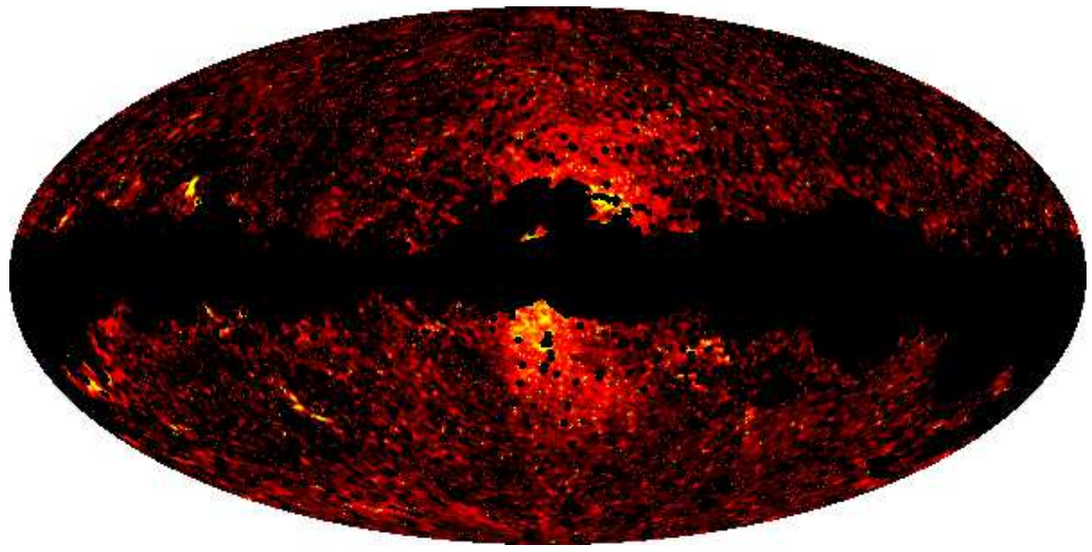

Planck Coll. A&A 2013

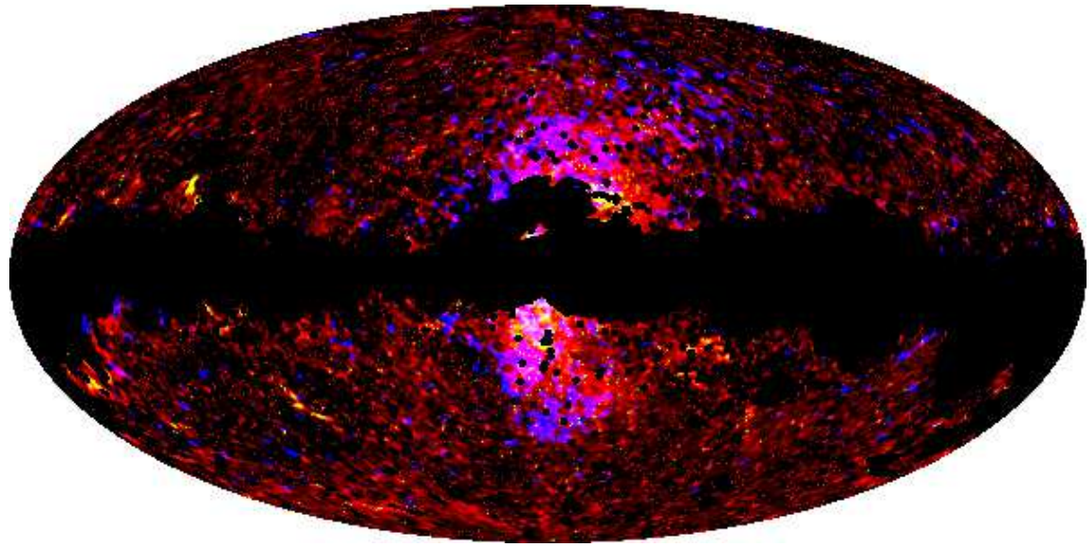

Fig. 9. *Top*: The microwave haze at *Planck* 30 GHz (red, $-12\,\mu\mathrm{K} < \Delta T_{\mathrm{CMB}} < 30\,\mu\mathrm{K}$) and 44 GHz (yellow, $12\,\mu\mathrm{K} < \Delta T_{\mathrm{CMB}} < 40\,\mu\mathrm{K}$). *Bottom*: The same but including the *Fermi* 2-5 GeV haze/bubbles of Dobler et al. (2010) (blue, 1.05 < intensity [keV cm^{-2} s^{-1} sr^{-1}] < 1.25; see their Fig. 11). The spatial correspondence between the two is excellent, particularly at low southern Galactic latitude, suggesting that this is a multi-wavelength view of the same underlying physical mechanism.

Using templates on Gamma-ray maps

Dobler, Finkbeiner, **IC**, Slatyer, Weiner, ApJ, 2010

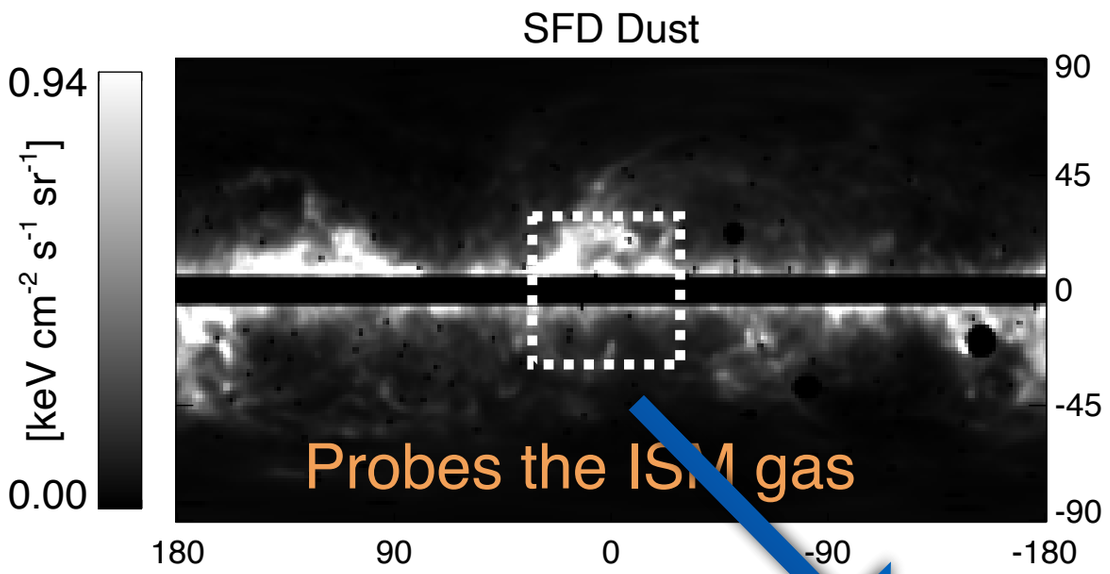

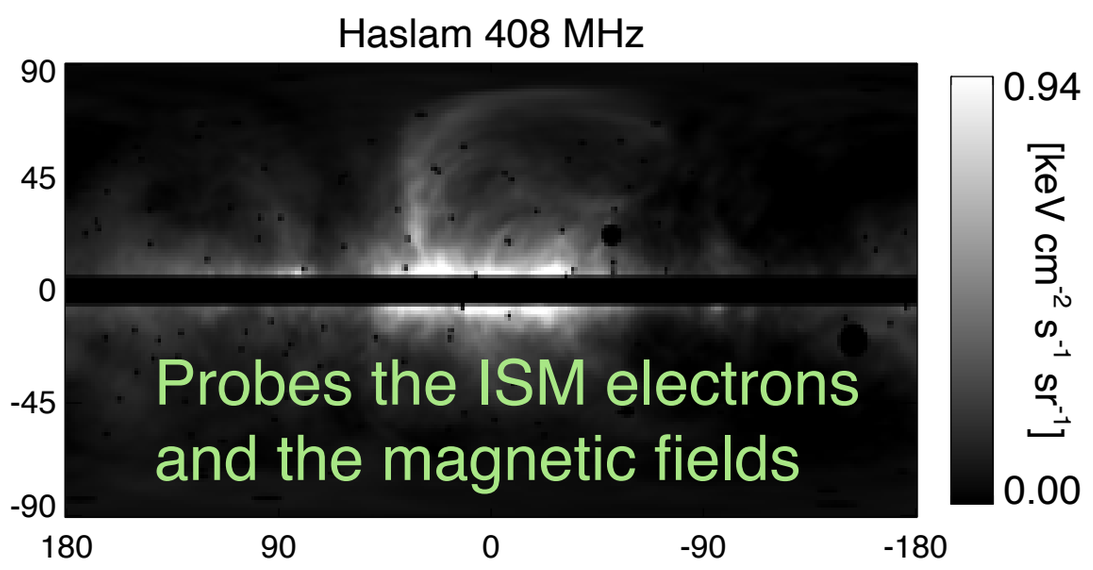

Adding ISM physics, cosmic-ray observations and running an array of Milky Way simulations

…

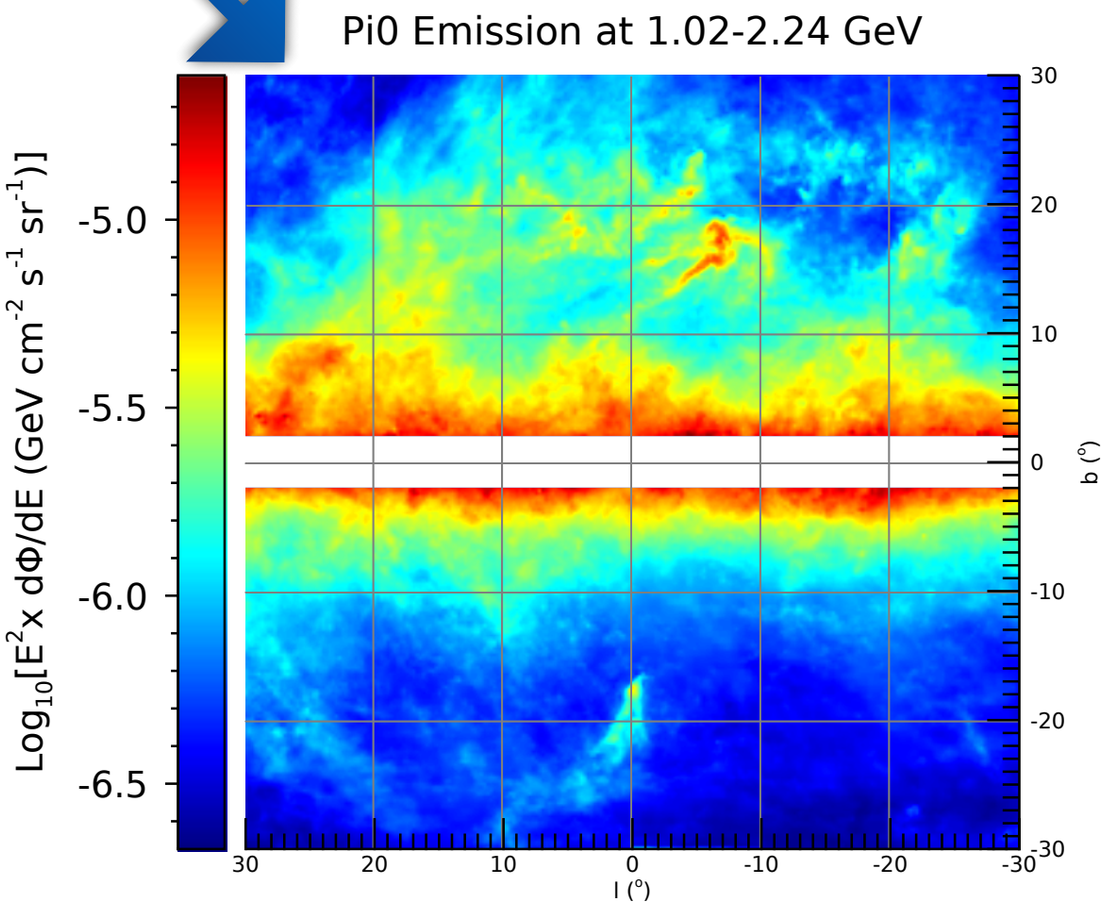

60 degrees in latitude

Accounting for the galactic diffuse emission uncertainties

We use models, accounting for uncertainties related to the diffusion of CRs, the presence of convective winds, diffusive re-acceleration, energy losses, CR injection sources, gas and other interstellar medium properties. From the existing literature and in 2015 we created our own (60) models—> 6660 different Templates!

It turns out that it actually does not affect dramatically the excess spectrum:

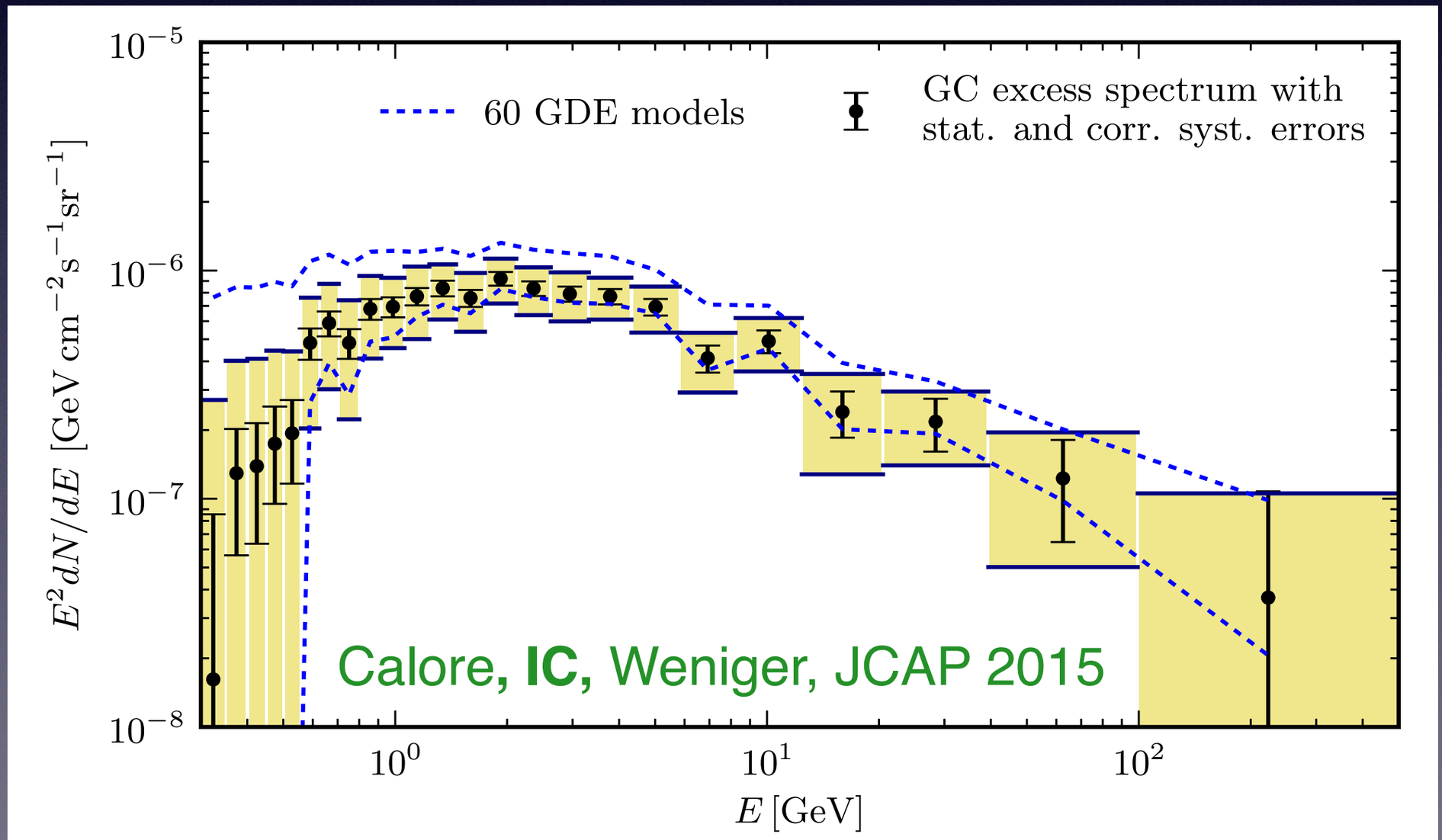

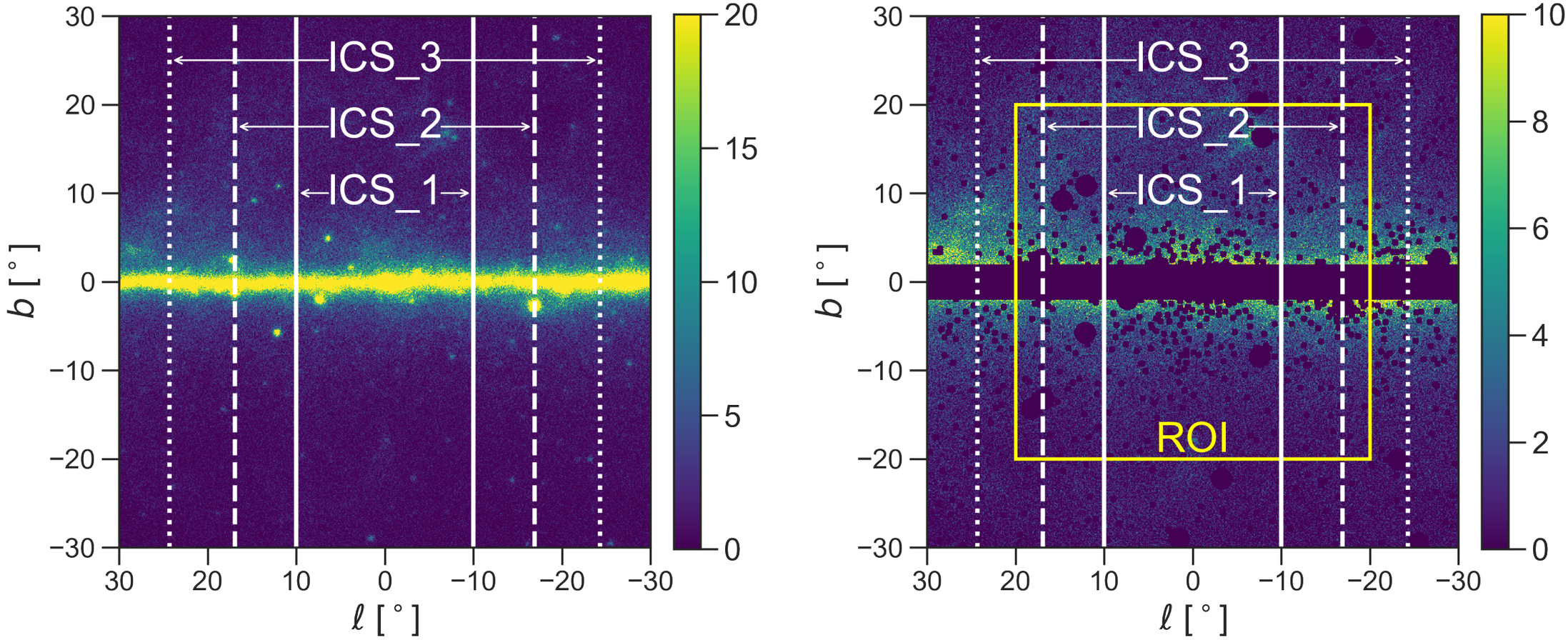

FIG. 2. Photons passing our cuts with energy $1.02\,\mathrm{GeV} < E_\gamma < 1.32\,\mathrm{GeV}$, without (left) and with (right) the mask that we use for our data. For illustration purposes, we show the boundaries of the ICS_1, ICS_2, and ICS_3 rings that vary independently in our fits. In the right panel, we show the region of interest in which we perform our fits.

McDermott, Zhong, **IC** (arXiv:2209.00006)

We also find unphysical spectral variations/breaks in the individual flux components associated to the separate rings.

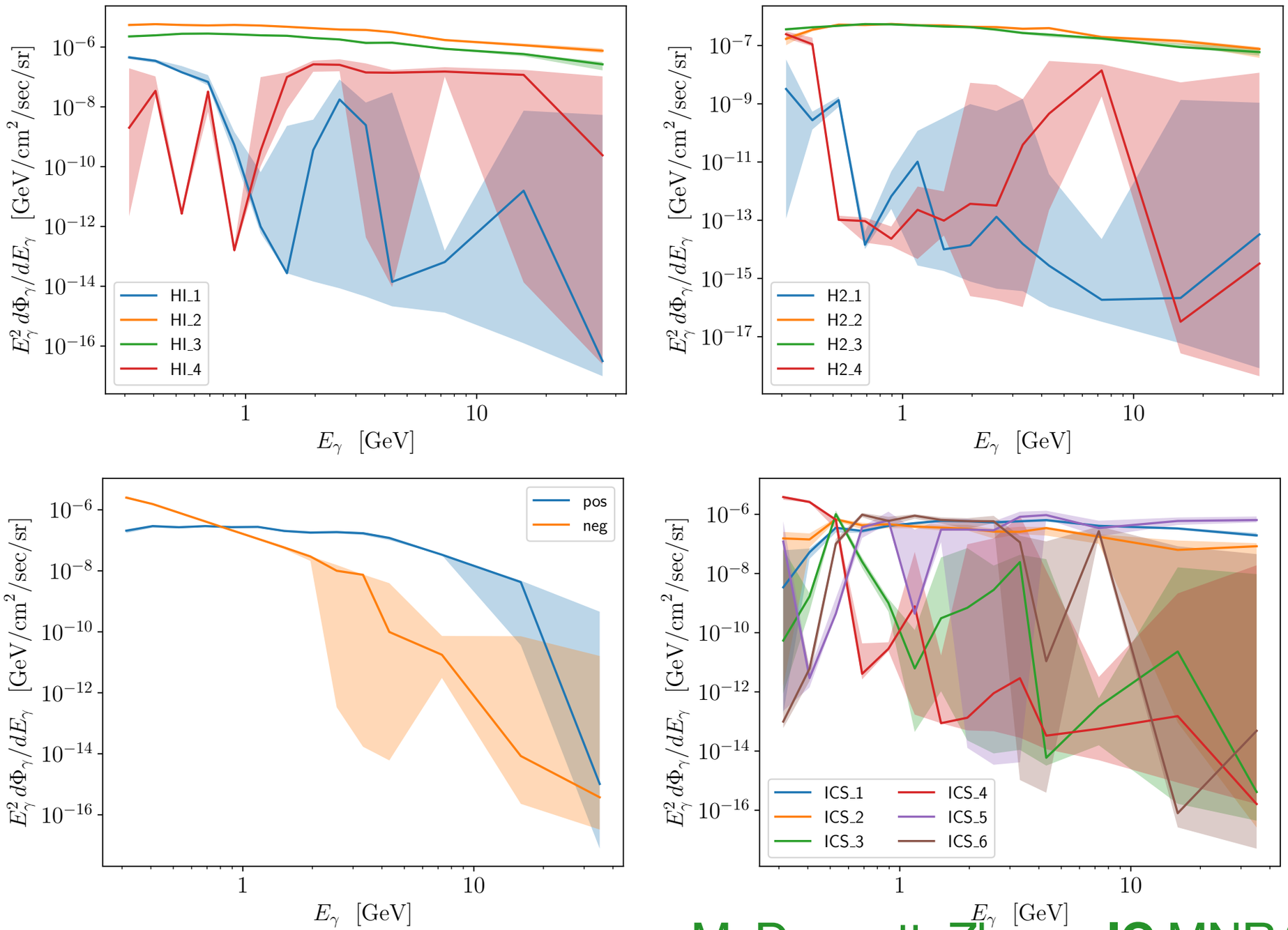

McDermott, Zhong, **IC** MNRAS Letters 2023

Figure 2. Best-fit spectra and 95% credible intervals of the flux of the ring-based templates that were fit alongside the boxy bulge excess template. For the negative residual component, we show its absolute value in the lower left panel.

The background assumptions on the galactic diffuse emission affect the derived conclusions on the GCE.

McDermott, Zhong, **IC** MNRAS Letters 2023

Comparing astrophysically motived templates (IC et al. 2022) vs ring-based templates (Pohl et al. 2022).

Table 1. Comparison of models of the GCE. The first six results, generated in this work, rely on the ring-based method of Pohl et al. (2022) to describe astrophysical emission. The final three results utilize best fit template model XLIX from Cholis et al. (2022).

Excess Model	Bgd. Templates	$-2\Delta\ln\mathcal{L}$	$\Delta\ln\mathcal{B}$
No Excess	ring-based	0	0
X-Shaped Bulge	ring-based	+30	−190
Dark Matter	ring-based	−237	+12
Boxy & X-Shaped Bulges	ring-based	−634	+178
Boxy Bulge	ring-based	−724	+228
Boxy Bulge “plus”	ring-based	−765	+311
Boxy Bulge “plus” & DM	ring-based	−817	+316
No Excess	astrophysical	−4539	+2933
Boxy Bulge	astrophysical	−6398	+3814
Boxy Bulge “plus”	astrophysical	−6477	+3853
Dark Matter	astrophysical	−7288	+4268
Boxy Bulge “plus” & DM	astrophysical	−7401	+4298

The statistically best models give preference for a more spherical GCE morphology

Wide priors fit:

Excess Model	Bgd. Templates	$-2\Delta\ln\mathcal{L}$
No Excess	astrophysical - ring-based	1805
X-Shaped Bulge	astrophysical - ring-based	574
Boxy Bulge	astrophysical - ring-based	-52
Boxy Bulge "plus"	astrophysical - ring-based	-131
Dark Matter	astrophysical - ring-based	-942
DM + Boxy Bulge "plus"	astrophysical - ring-based	-1056

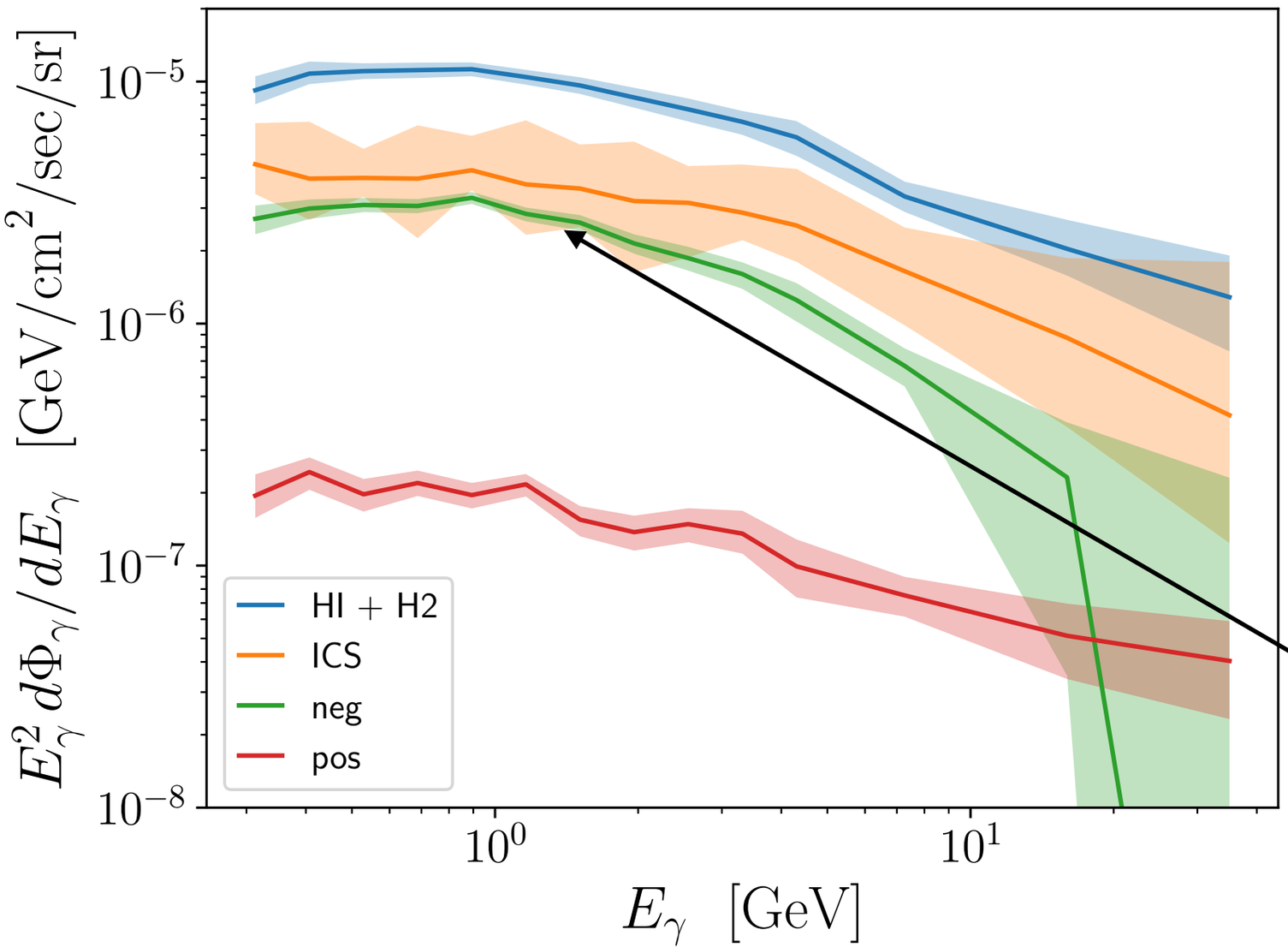

Lower is better

There is no physical justification for negative residual gas maps at the 20% level across the entire region (it should be a 0.1-1% correction).

Ongoing Preliminary:
Further Tests of injected Mock Maps versus what we recover from the fits:

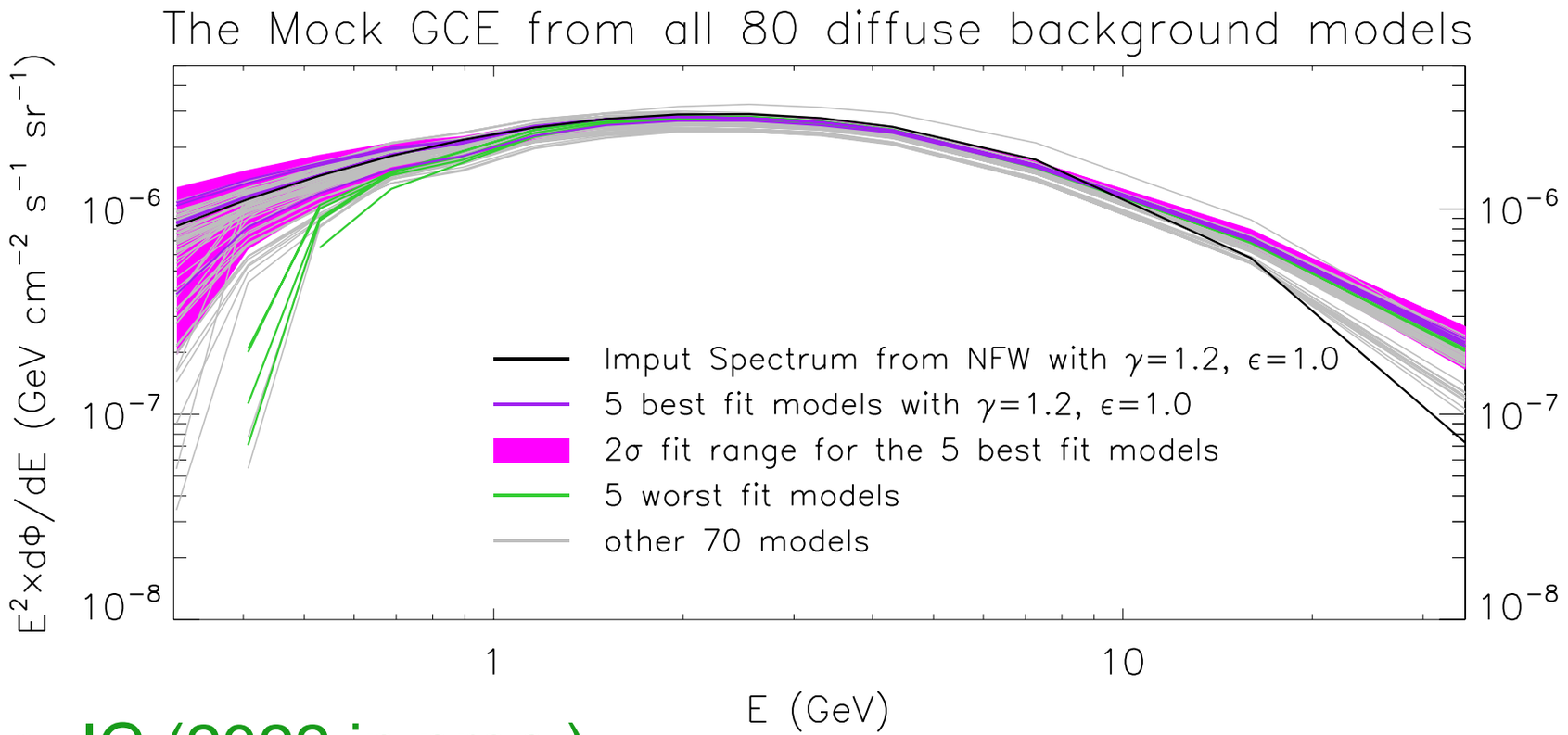

Zhong, IC (2022 in prep.)

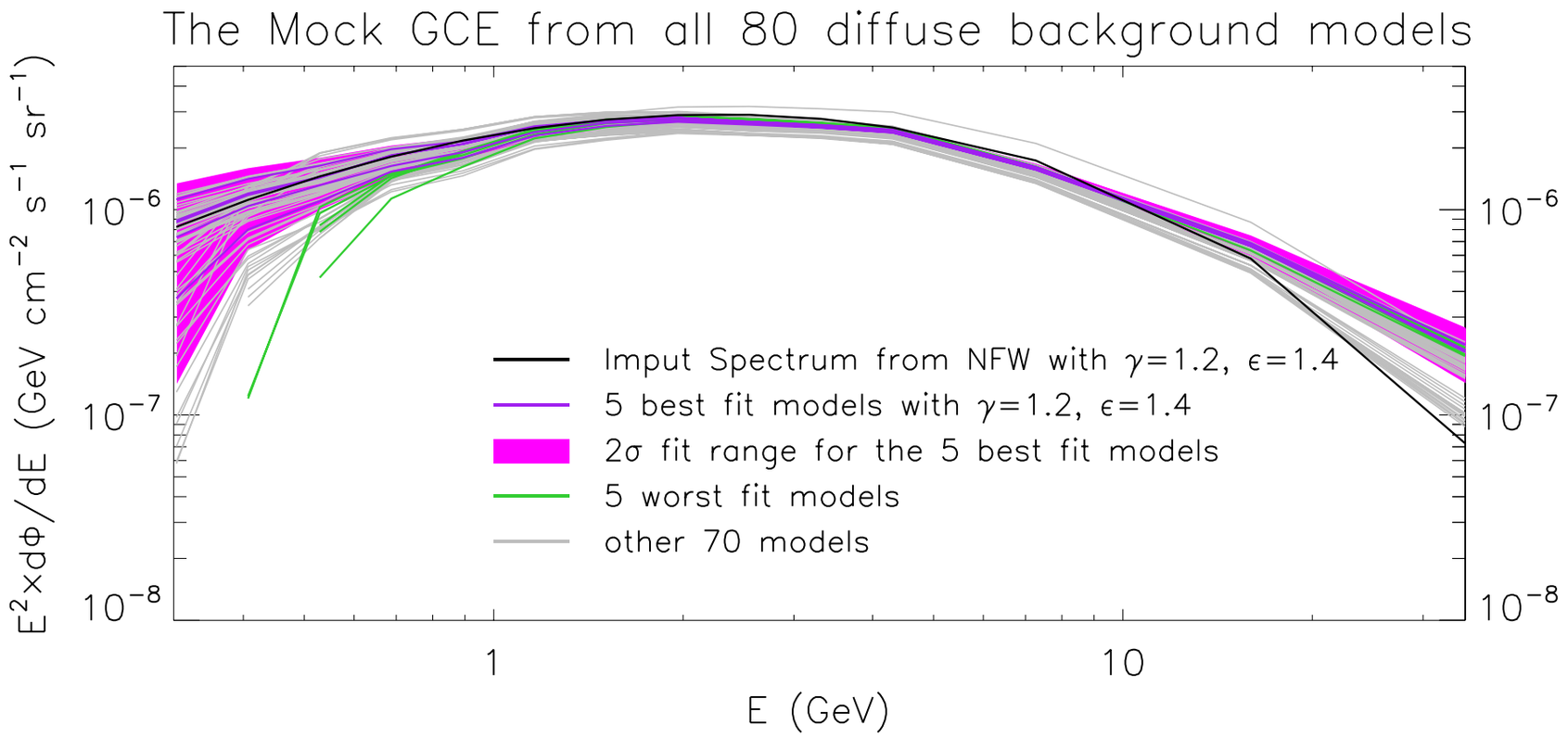

Comparison with other recent results that come to different conclusions. The ring-based approach

Works: Macias et al. Nature Astron. 2018, Macias et al. JCAP 2019,
Abazajian et al. PRD 2020, Pohl et al. ApJ 2022

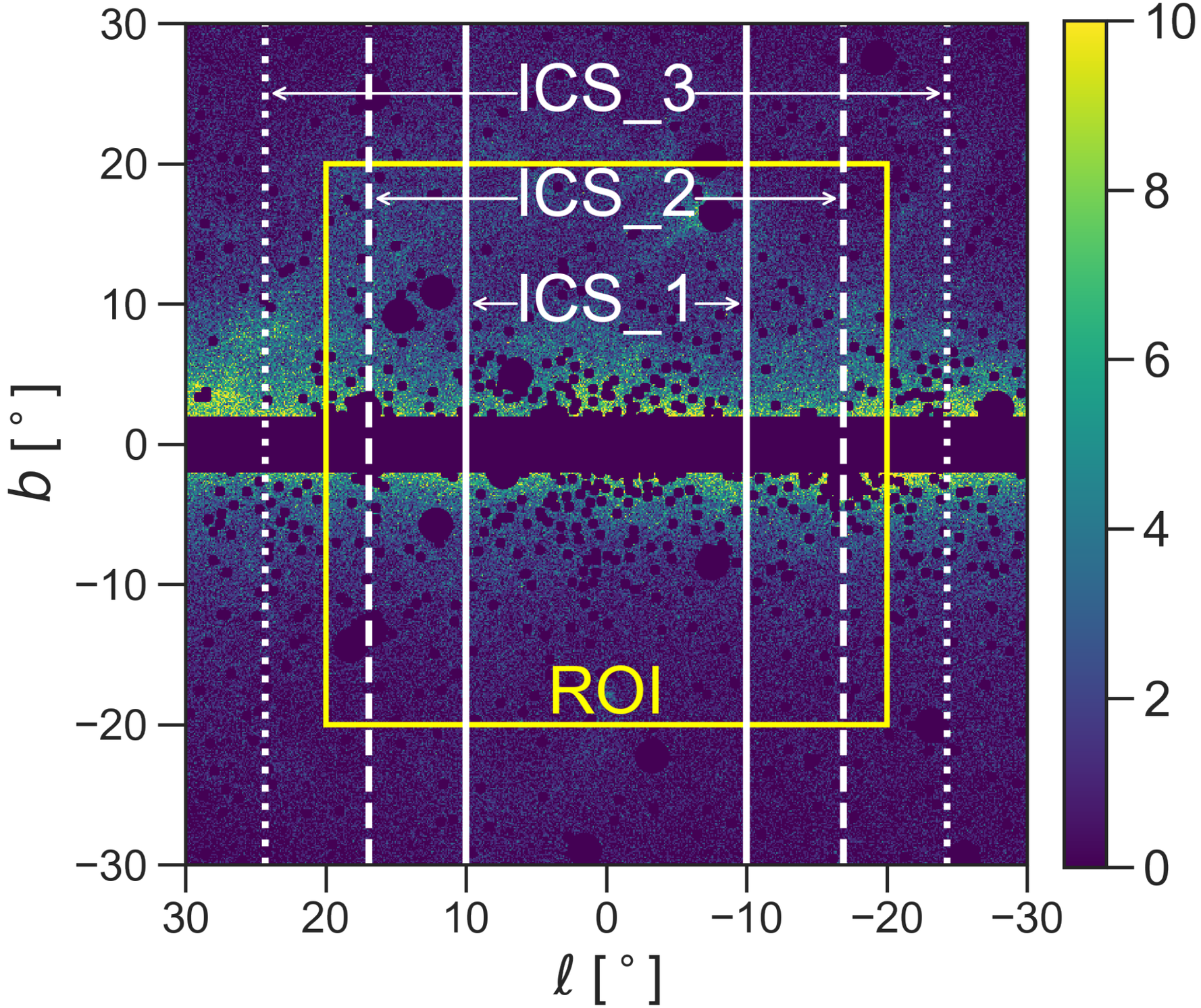

Testing how the morphology of the GCE depends on the energy of gamma-rays. Maybe it is more disky/bulgy at low energies?

Zhong, **IC** in prep. 2023

Highly uncertain at E<1 GeV

ellipticity

ϵ

2.0

1.5

1.0

0.5

elongated along to the galactic disk

spherical

elongated perpendicular to the disk

Model I
Model VI
Model X
Model XV
Model XLIX

0.275–0.464
0.464–0.784
0.784–1.32
1.32–2.24
2.24–3.78
3.78–10.8
10.0–51.9

Energy Range (GeV)

Testing how the morphology of the GCE depends on the energy of gamma-rays. Maybe it is more disky/bulgy at low energies?

Zhong, **IC** in prep. 2023

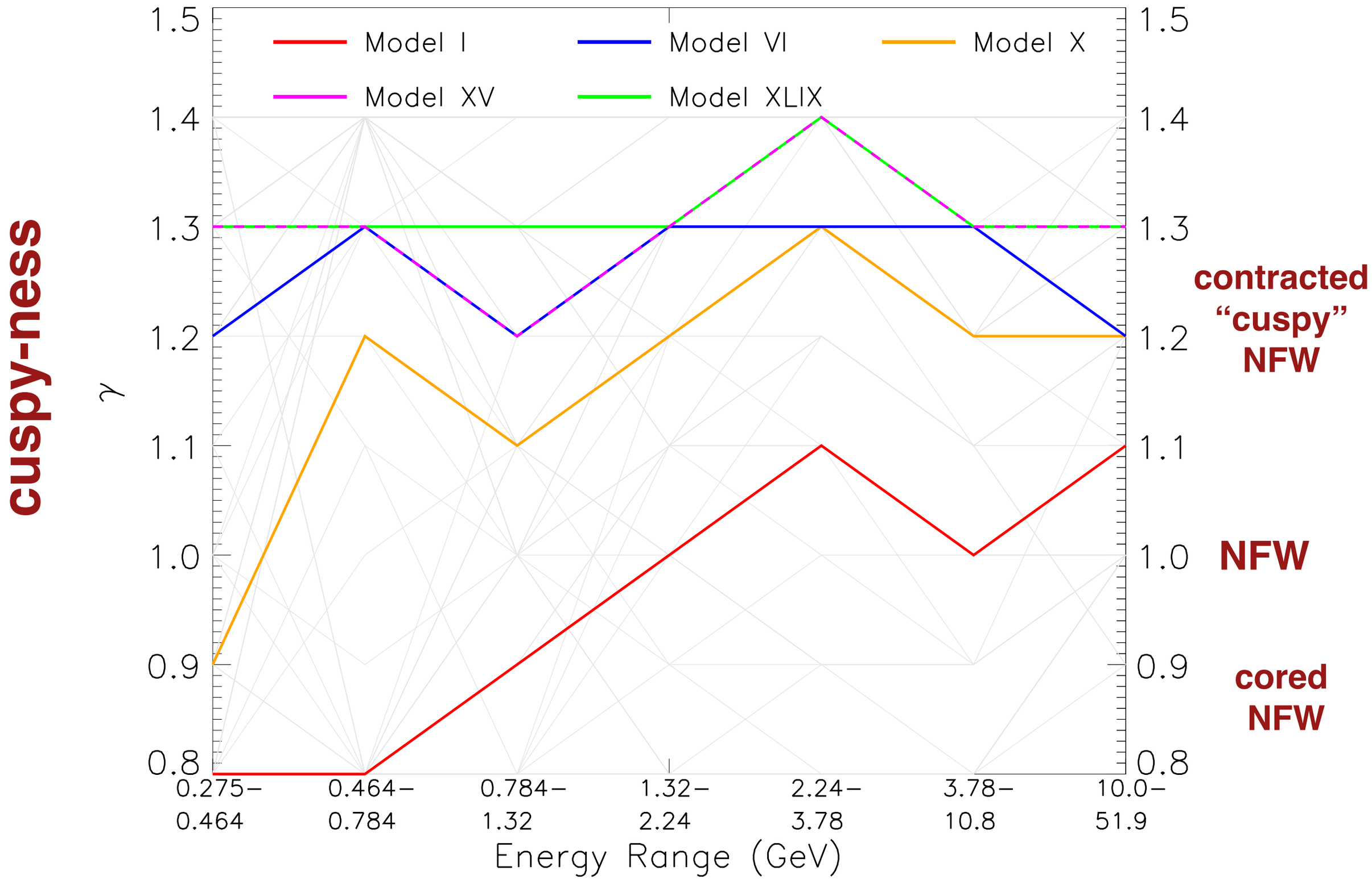

Other recently suggested bulge profiles for the GCE:

“F98”

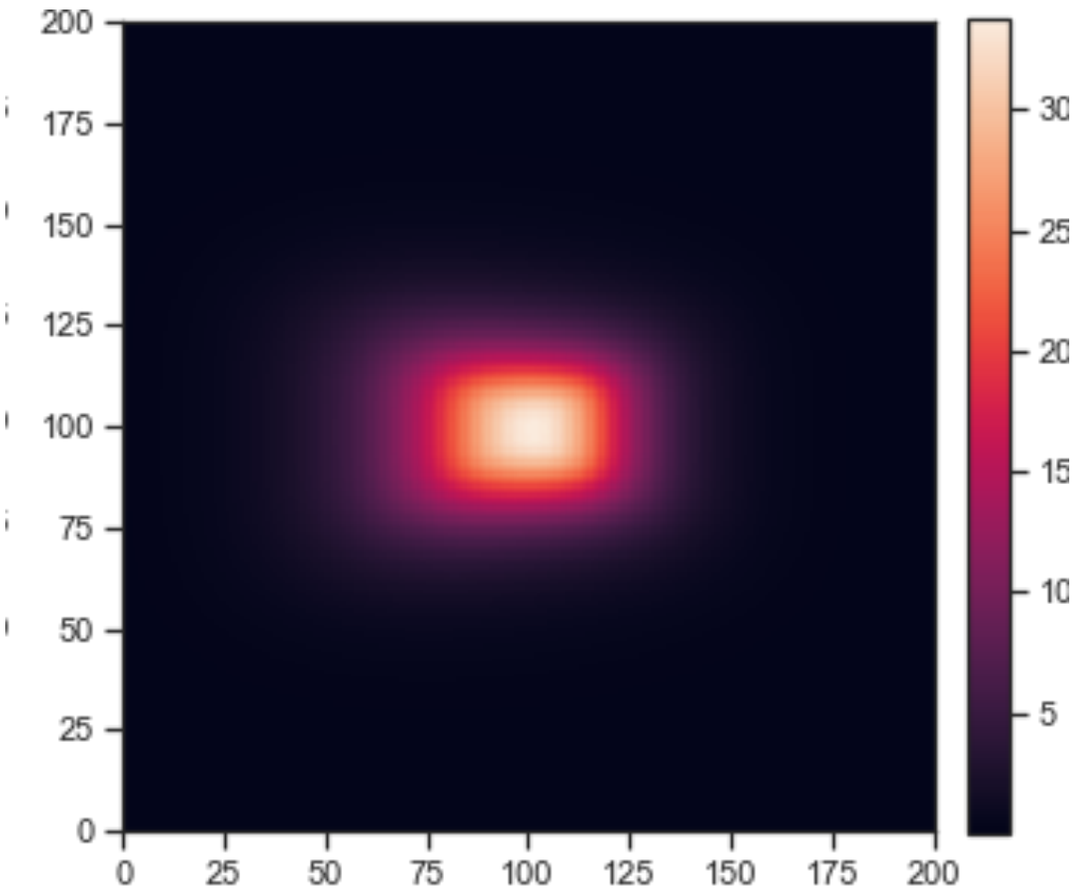

“Coleman 19” (non-parametric)

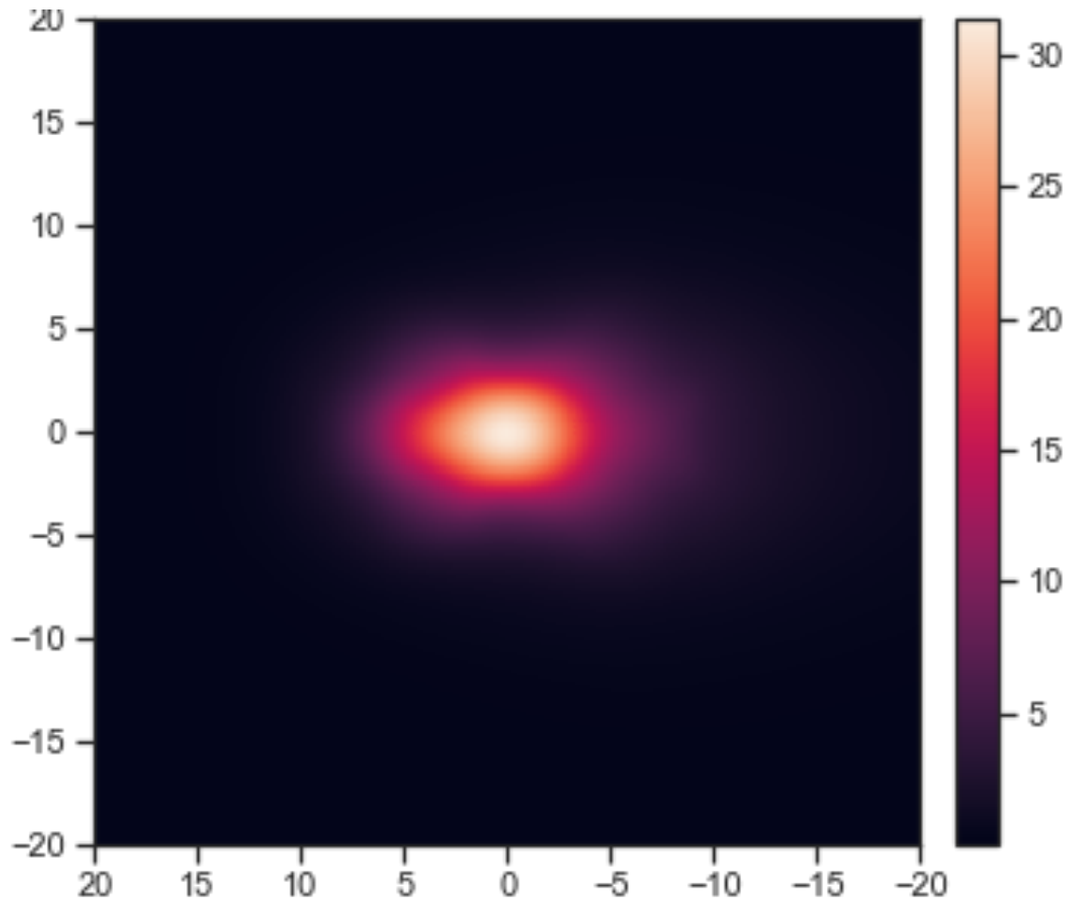

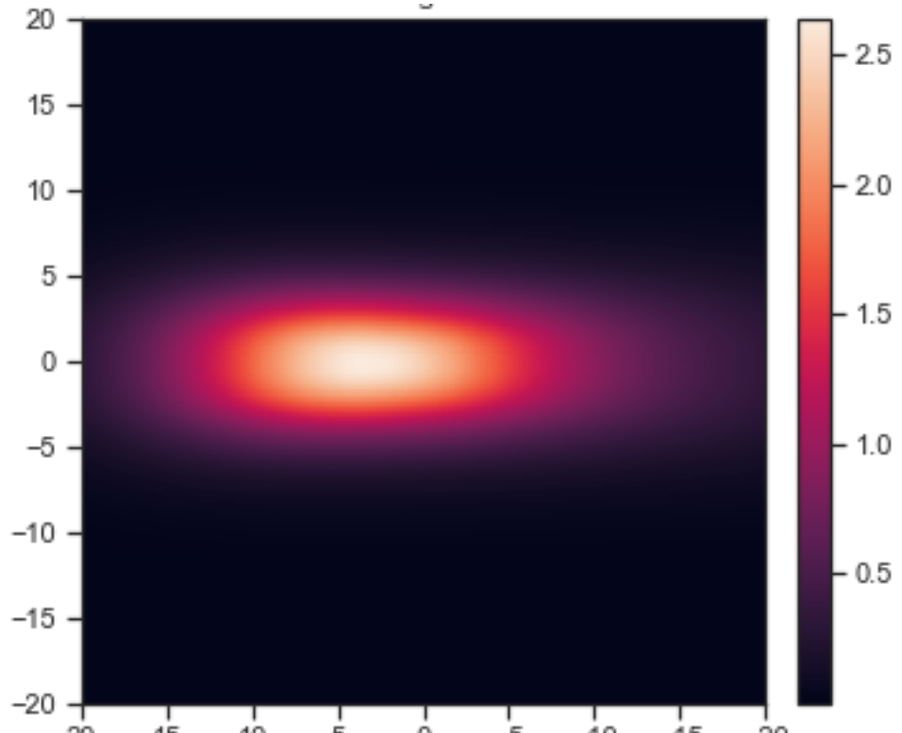

“Coleman 19” (basic para-metrization)

Ongoing Preliminary

Zhong, IC 2023 in prep

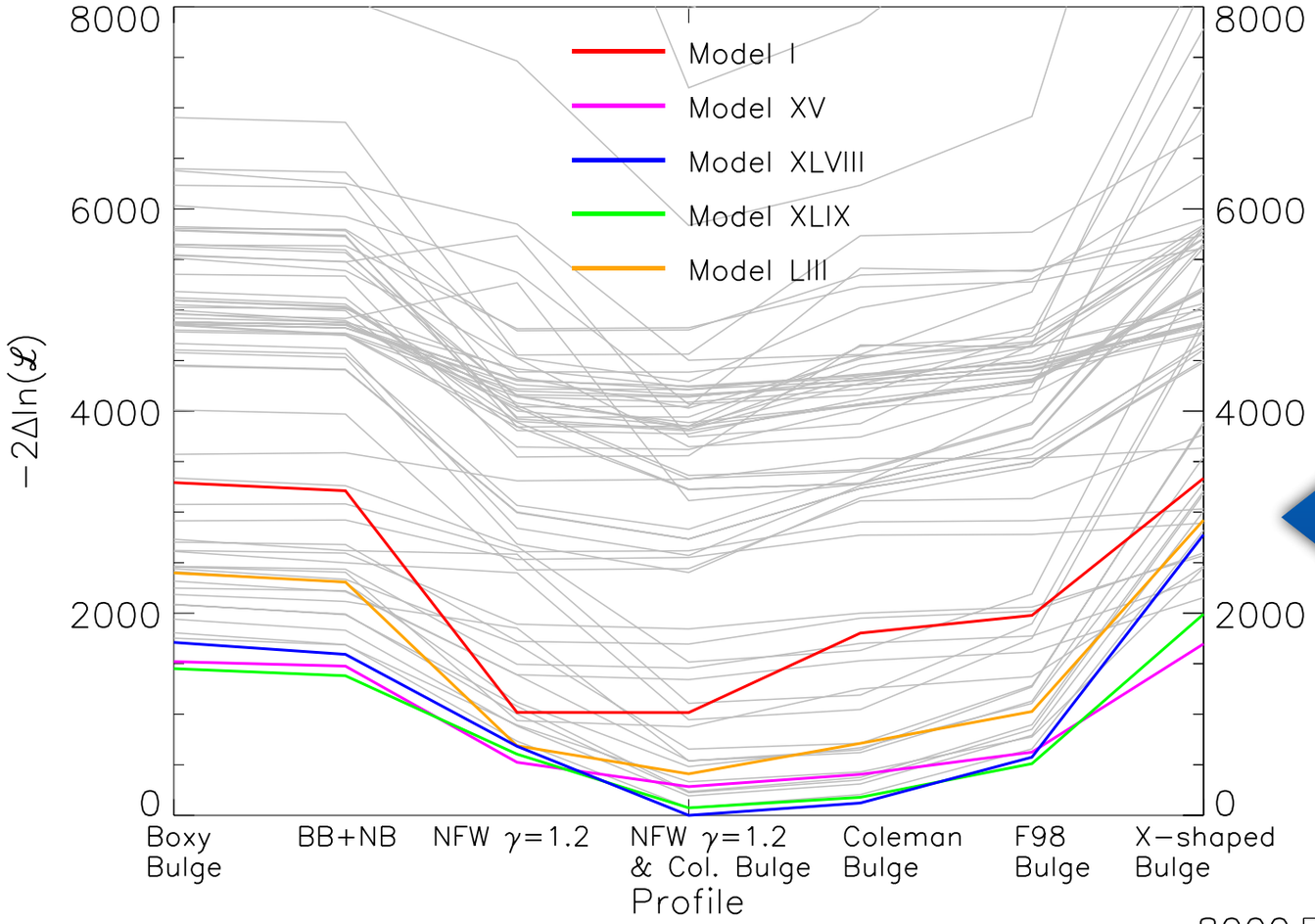

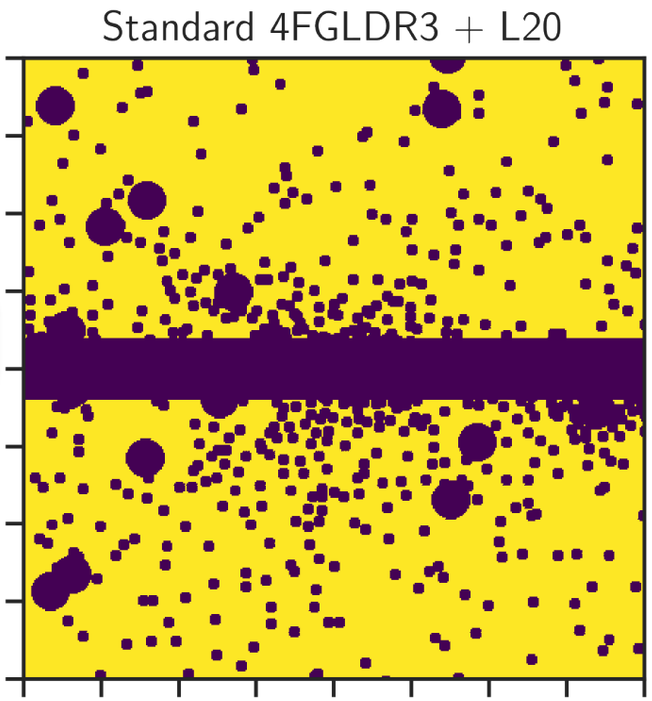

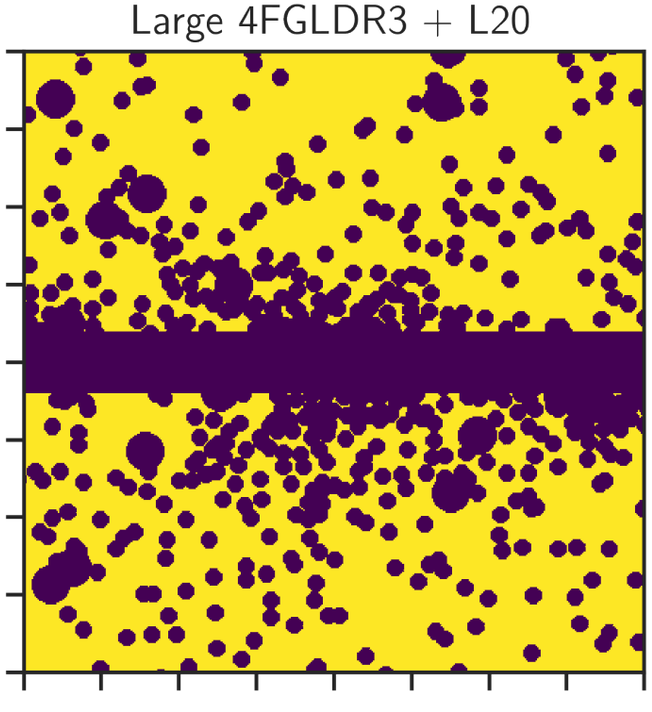

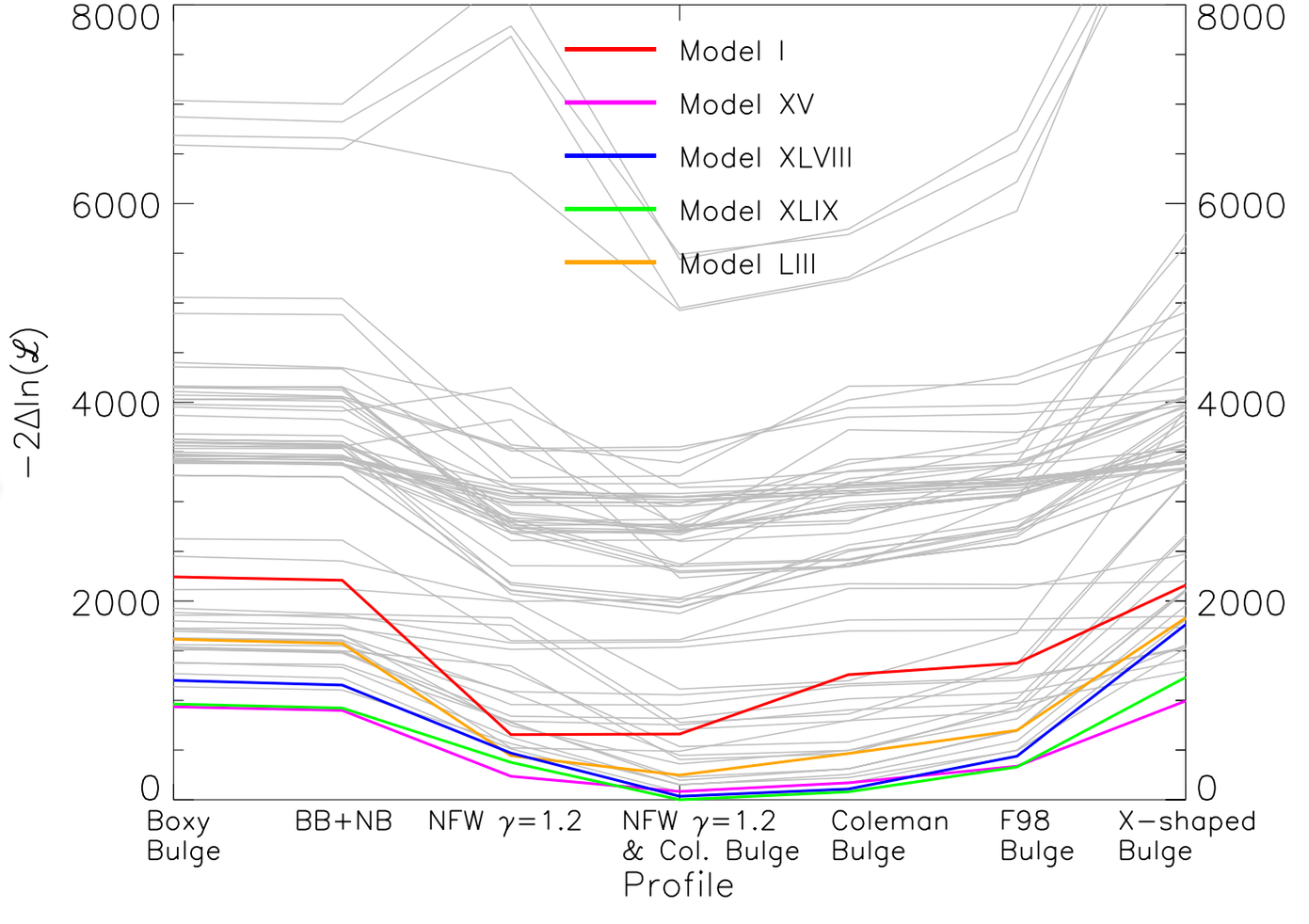

Ongoing Preliminary

Zhong, IC 2023 in prep

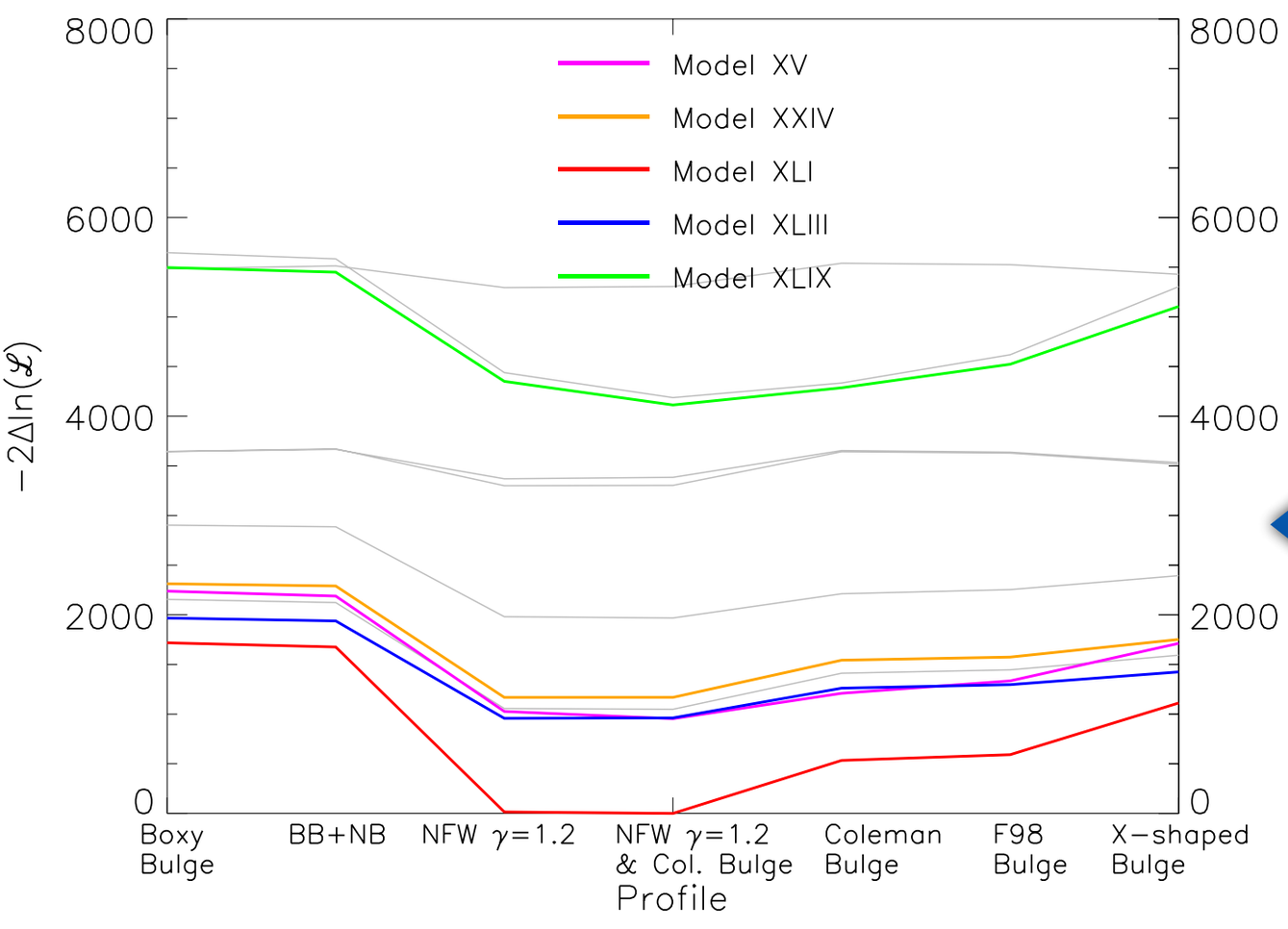

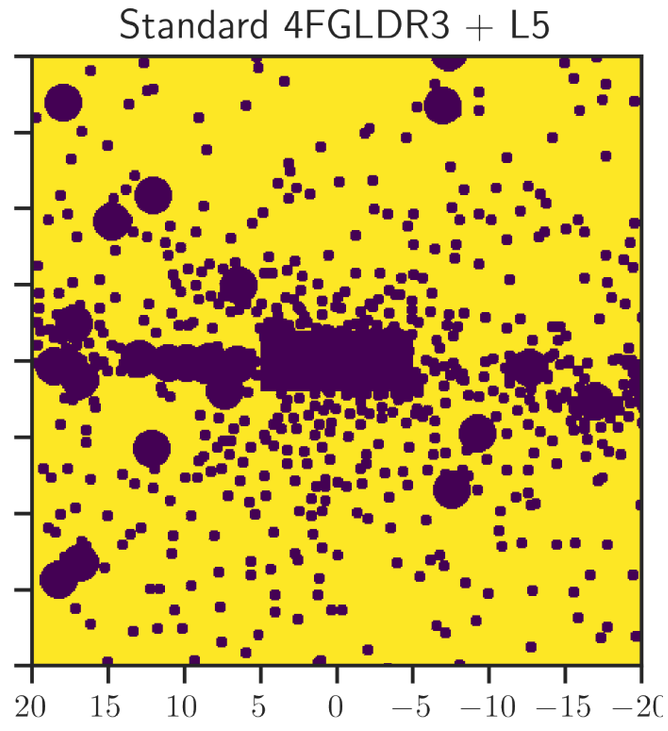

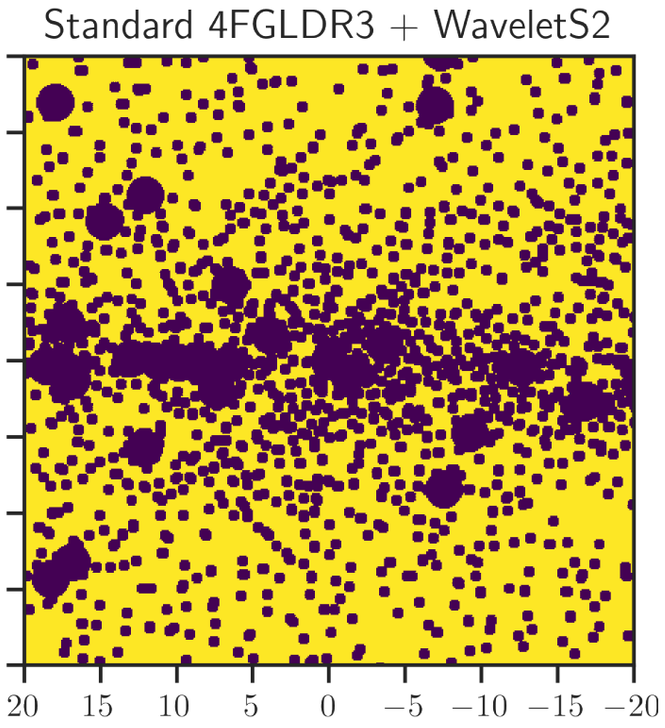

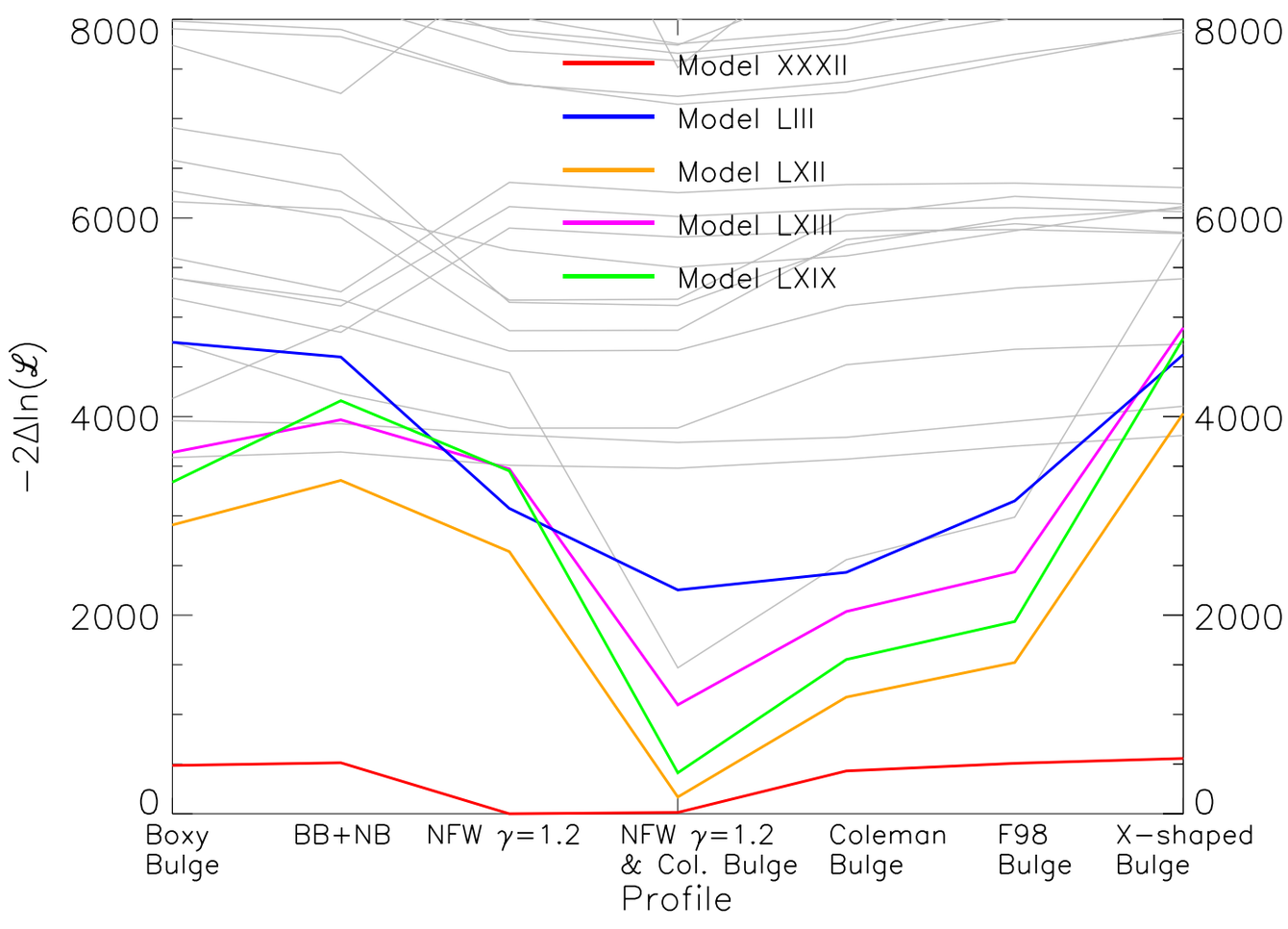

There can be a mix of BOTH MSPs and DM

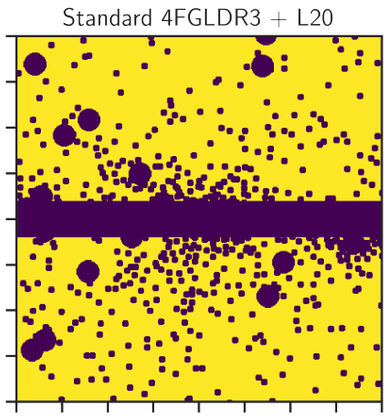

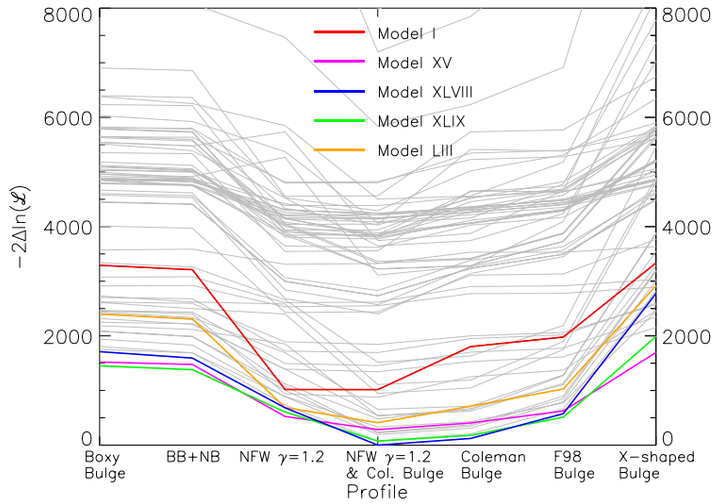

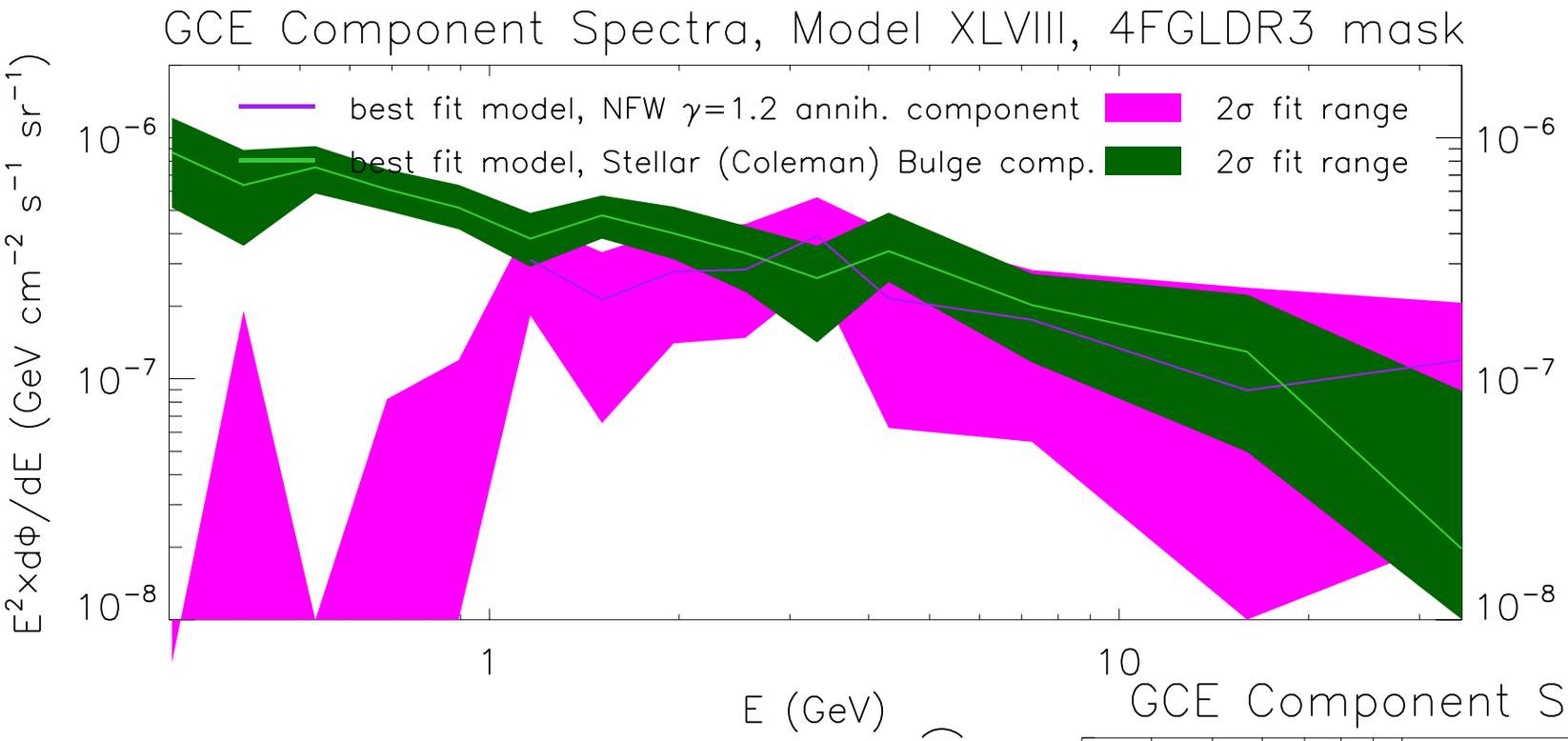

<—Model “XLVIII”

Model “I” —>

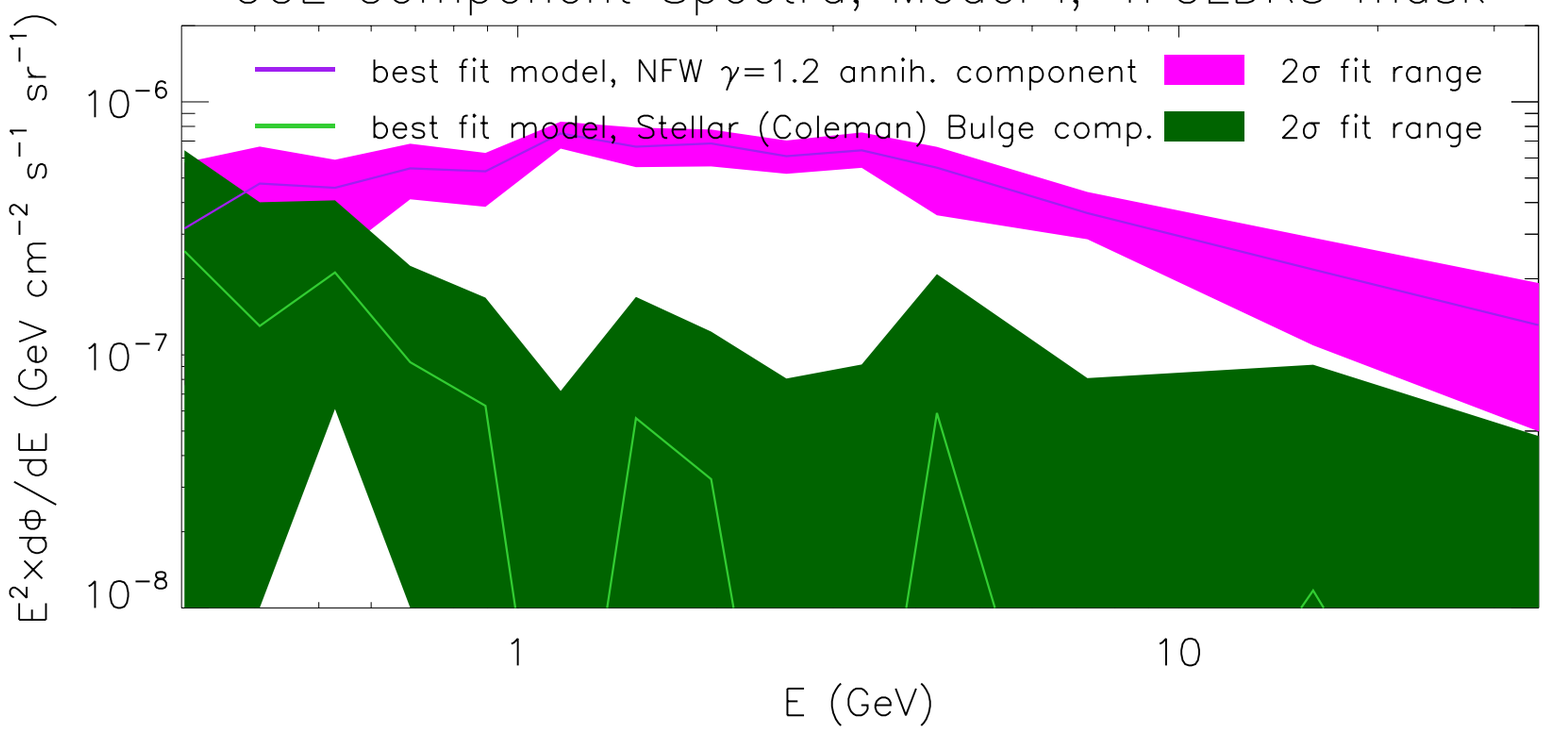

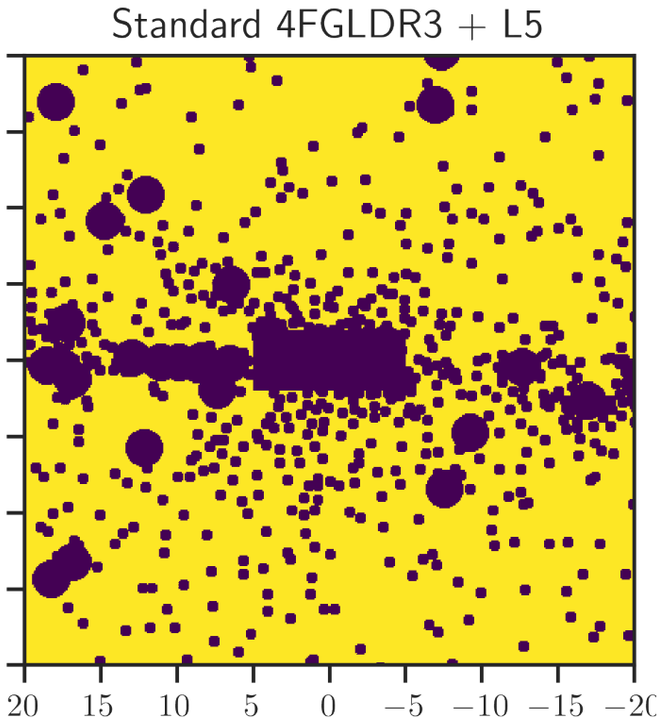
Standard 4FGLDR3 + L5
20
15
10
5
0
−5
−10
−15
−20

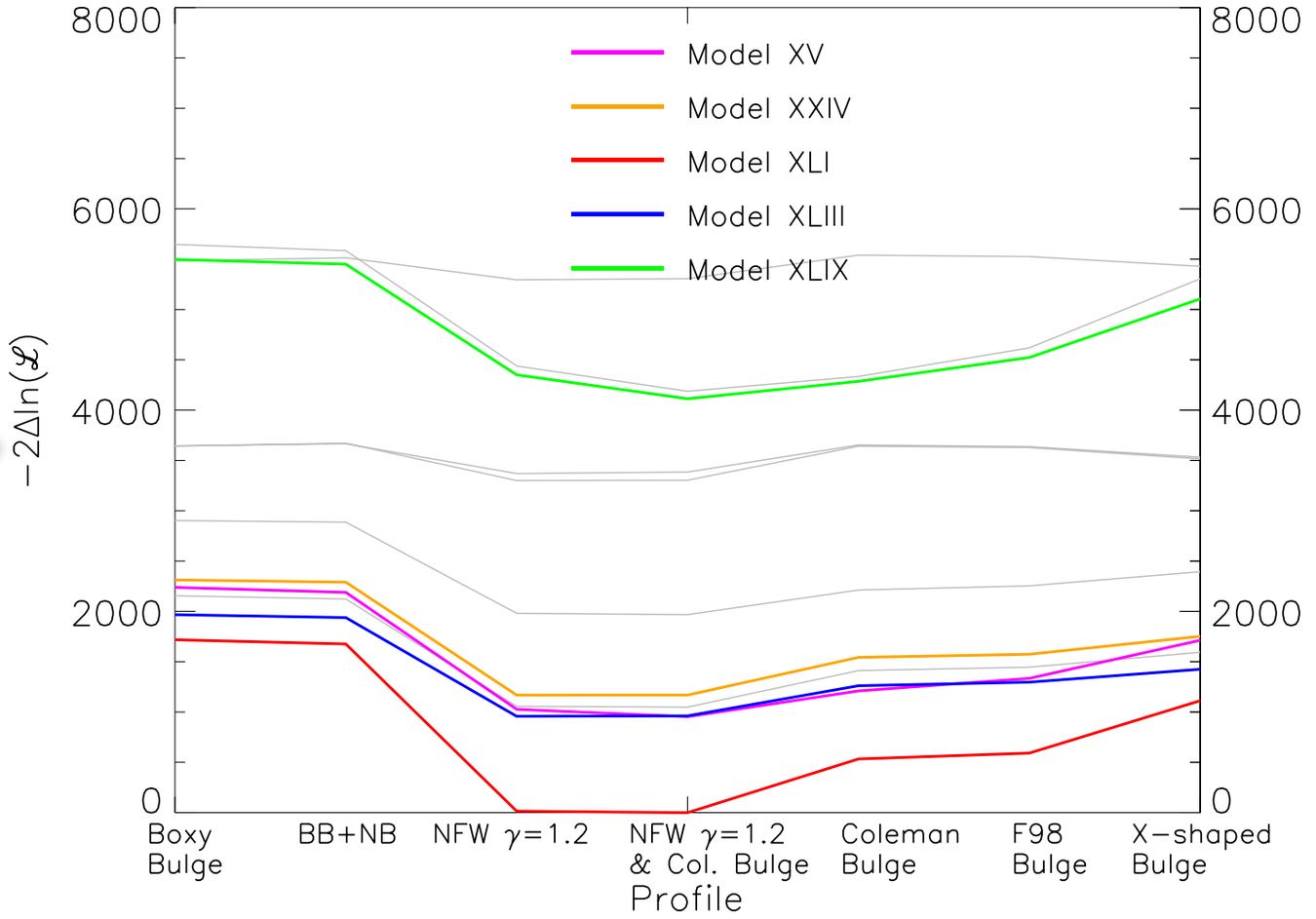
8000
6000
4000
2000
0
$-2\Delta\ln(\mathscr{L})$
Model XV
Model XXIV
Model XLI
Model XLIII
Model XLIX
Boxy Bulge
BB+NB
NFW γ=1.2
NFW γ=1.2 & Col. Bulge
Coleman Bulge
F98 Bulge
X−shaped Bulge
Profile

Model "XLI" —>

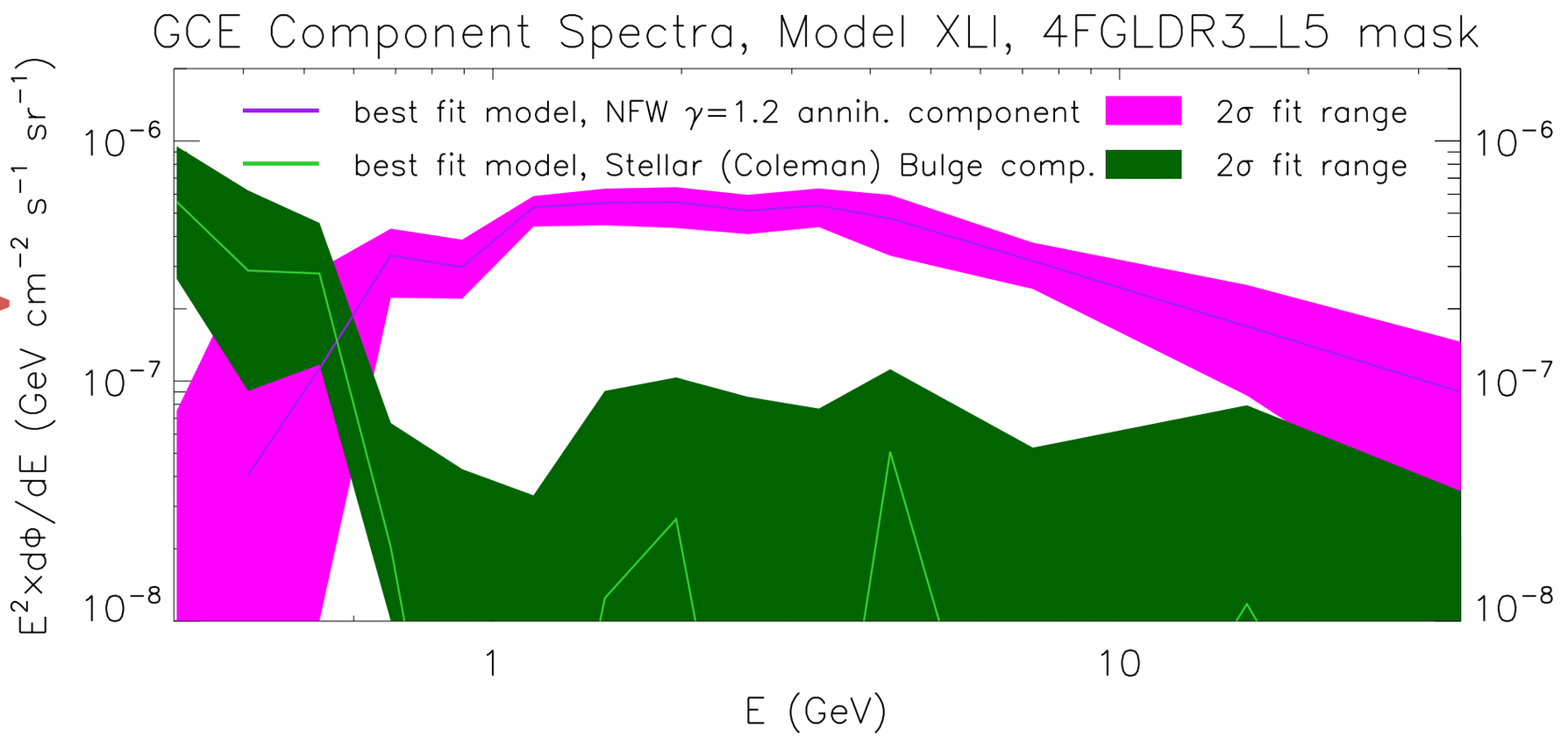
GCE Component Spectra, Model XLI, 4FGLDR3_L5 mask
best fit model, NFW γ=1.2 annih. component
2σ fit range
best fit model, Stellar (Coleman) Bulge comp.
2σ fit range
$E^2 \times d\Phi/dE$ (GeV cm^{-2} s^{-1} sr^{-1})
10^{-6}
10^{-7}
10^{-8}
1
10
E (GeV)

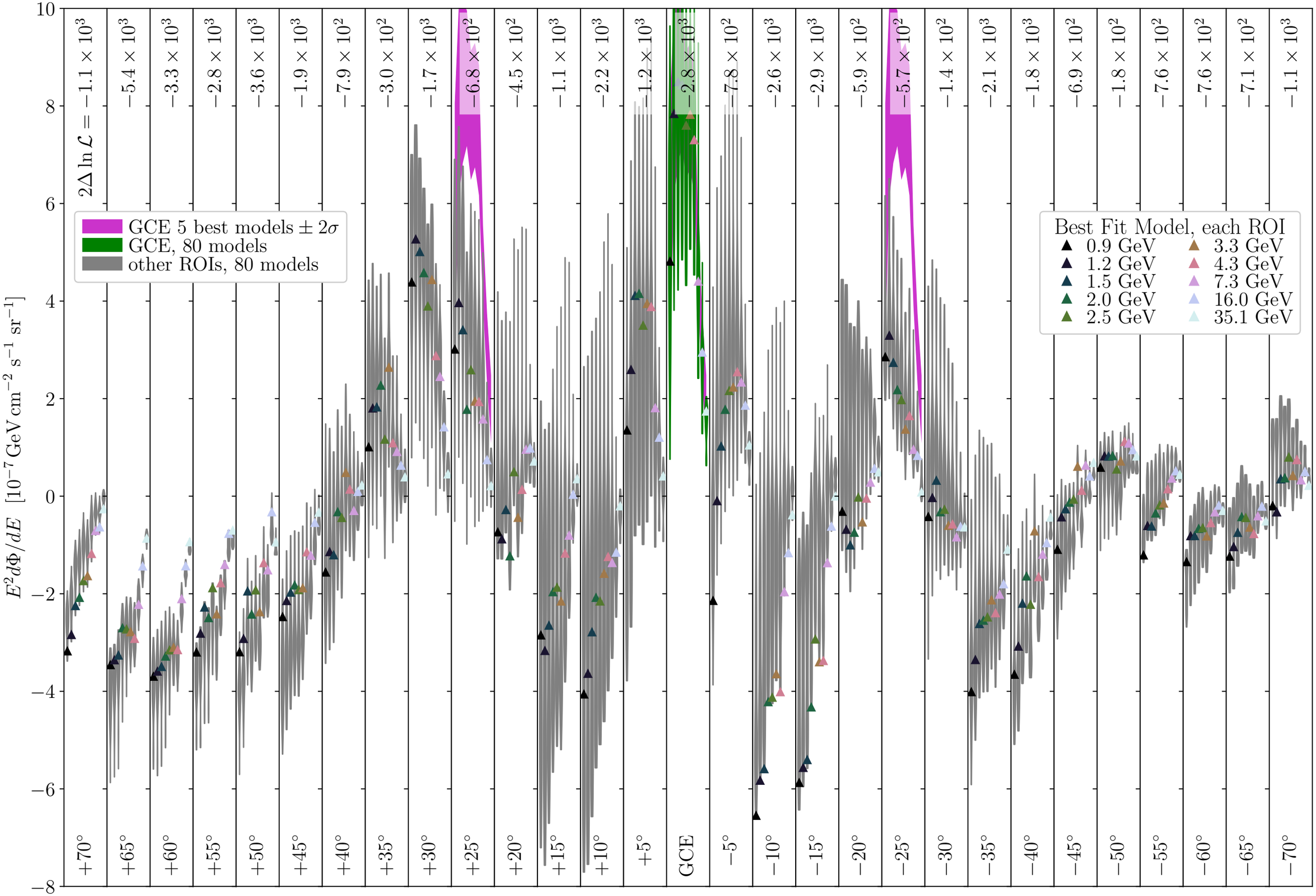

IC, Zhong, McDermott, Surdutovich, PRD 2022

IC, Zhong, McDermott, Surdutovich, PRD 2022

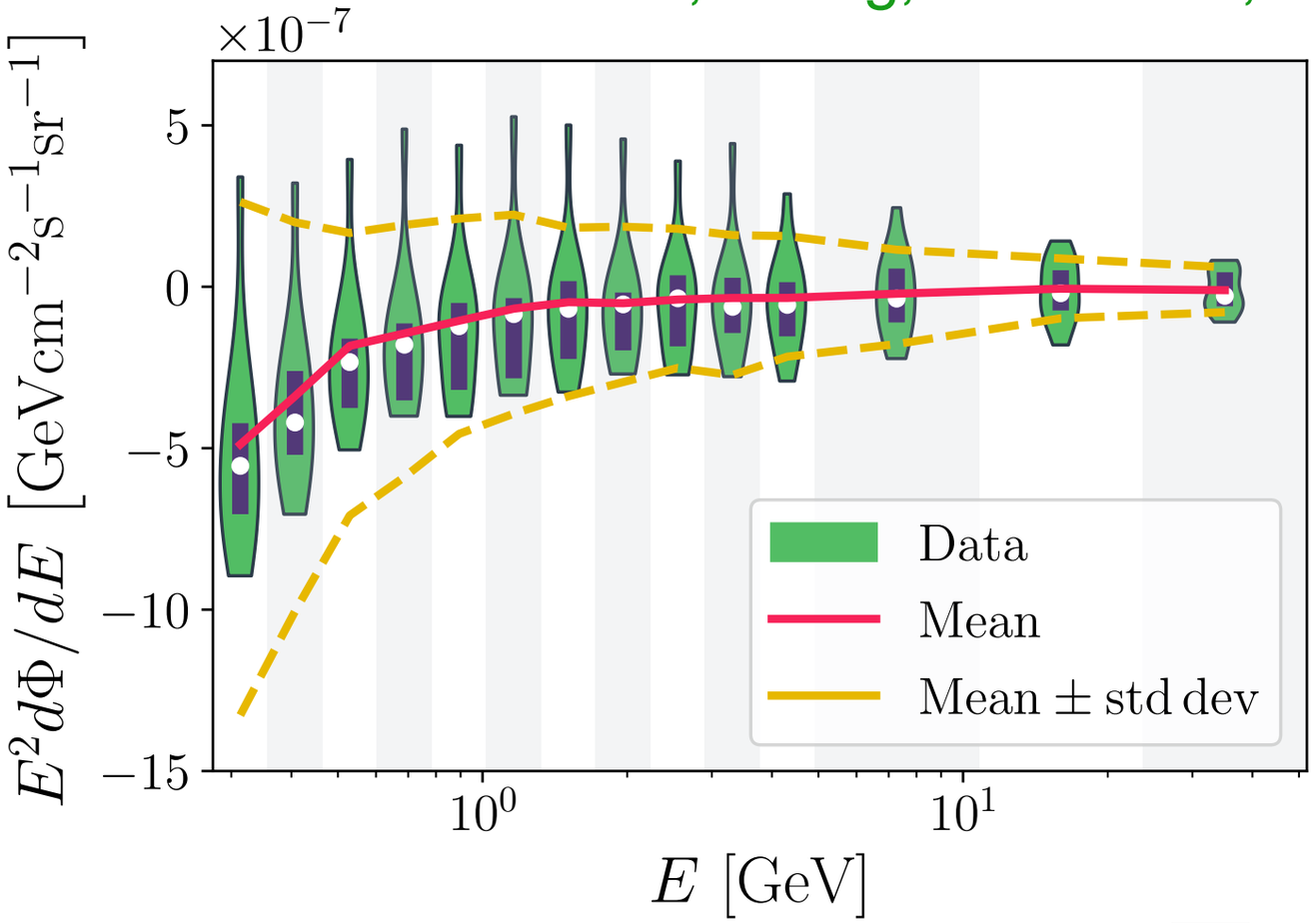

The covariance matrix:

$$\Sigma_{ij,\mathrm{mod}} = \left\langle E^4 \frac{d\Phi}{dE_i}\frac{d\Phi}{dE_j}\right\rangle - \left\langle E^2 \frac{d\Phi}{dE_i}\right\rangle \left\langle E^2 \frac{d\Phi}{dE_j}\right\rangle$$

Its truncated version:

$$\Sigma_{jk,\mathrm{mod}} \simeq \Sigma^{\mathrm{trunc}}_{jk,\mathrm{mod}} \equiv \sum_{i=1}^{3} \mathrm{PC}^{\mathsf{T}}_{ij}\mathrm{PC}_{ik}$$

The formal fit:

$$\chi^2 = \sum_{ij}\left(\mathrm{GCE}_i - \sum_k f_{ik}(\theta_k)\right) C^{-1}_{ij} \left(\mathrm{GCE}_j - \sum_\ell f_{j\ell}(\theta_\ell)\right)$$

Where:

$$C_{ij} = \sigma_i^2 \delta_{ij} + \Sigma_{ij,\mathrm{mod}}$$

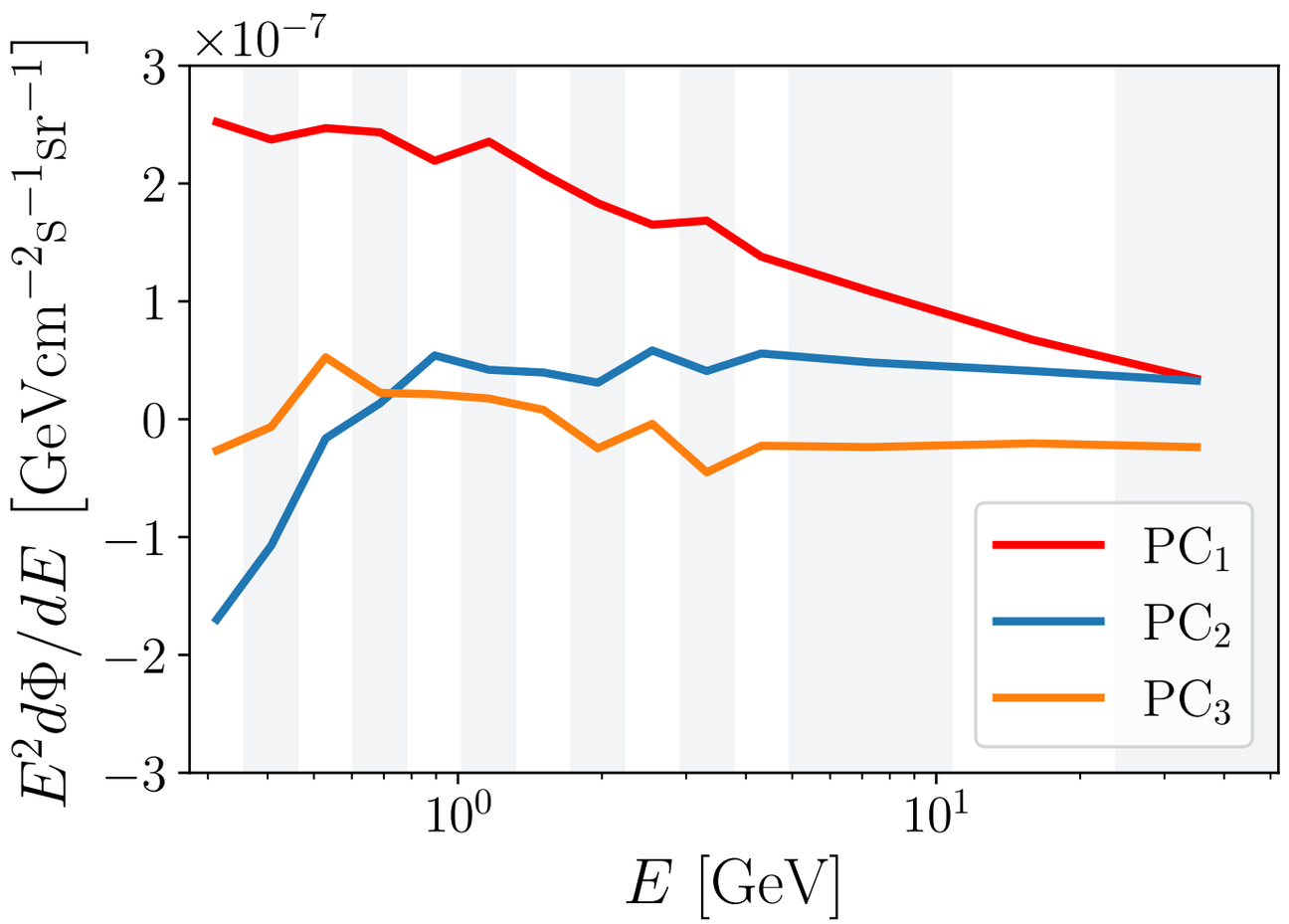

4FGLDR2 (standard mask) **IC**, Zhong, McDermott, Surdutovich, PRD 2022

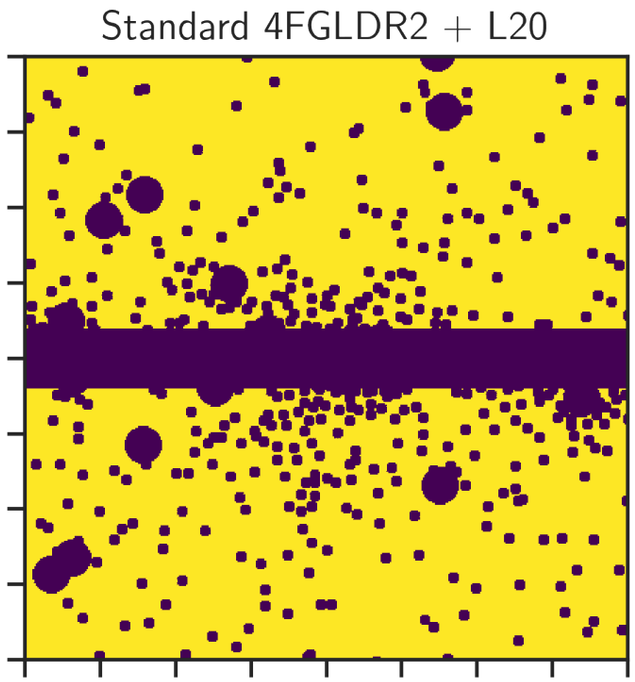

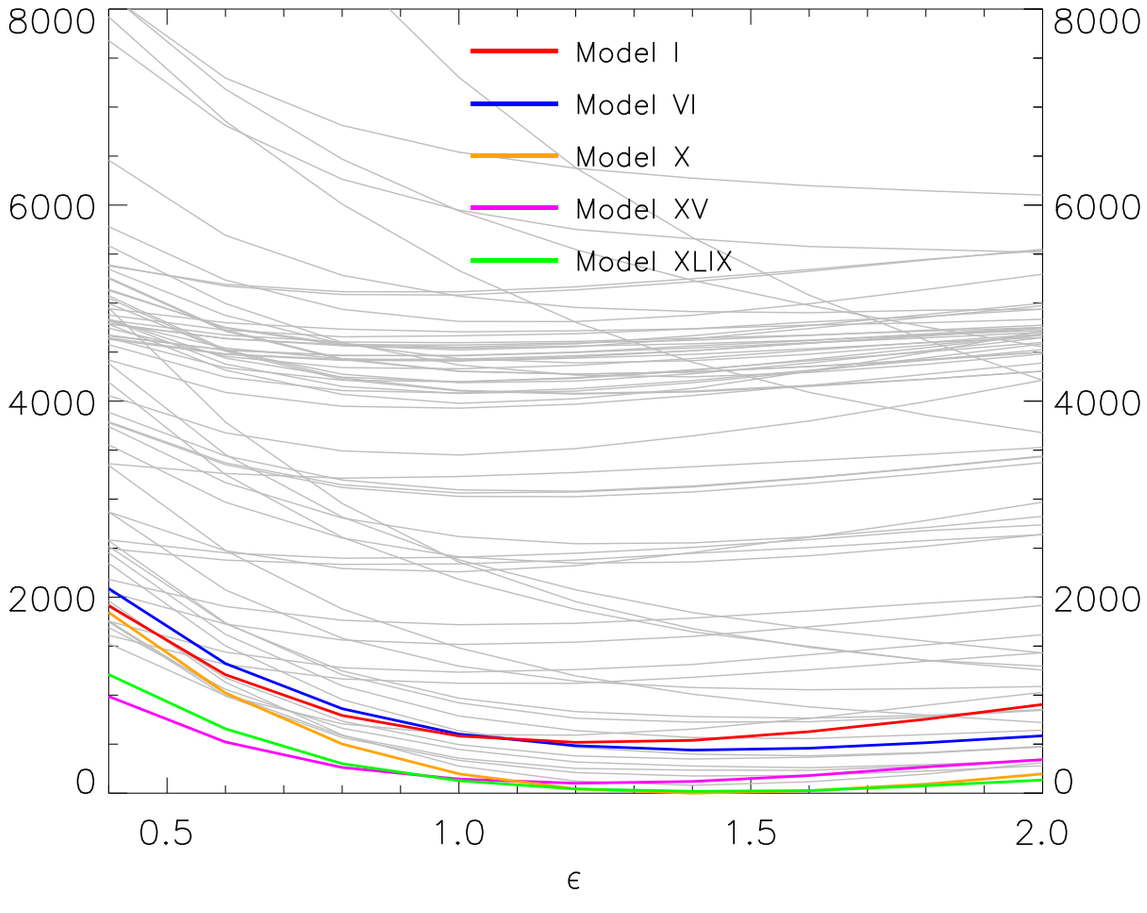

Ellipticity

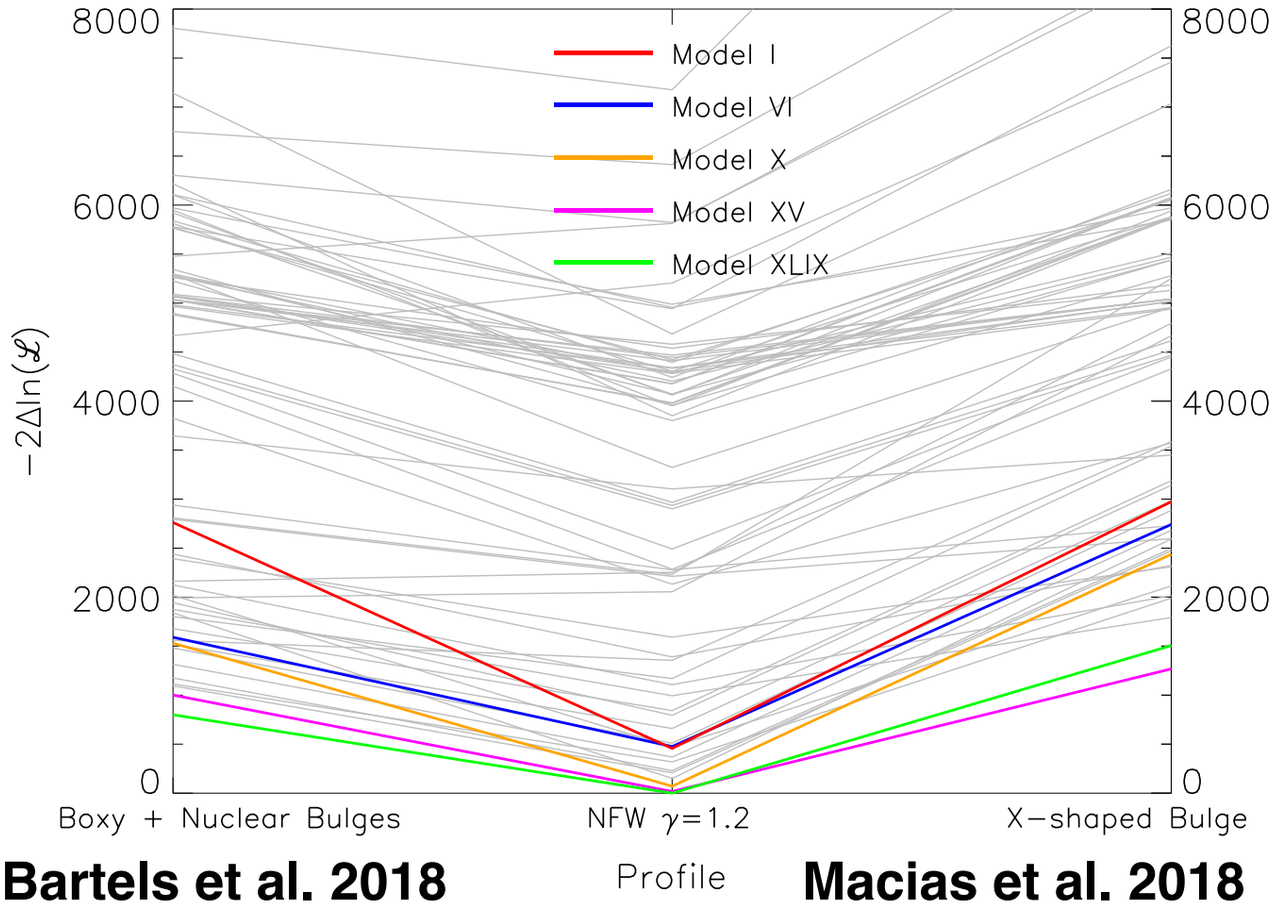

Bartels et al. 2018 **Macias et al. 2018**

Spherical NFW vs Bulges

4FGLDR3 (large mask)

Zhong, **IC** in prep. 2023

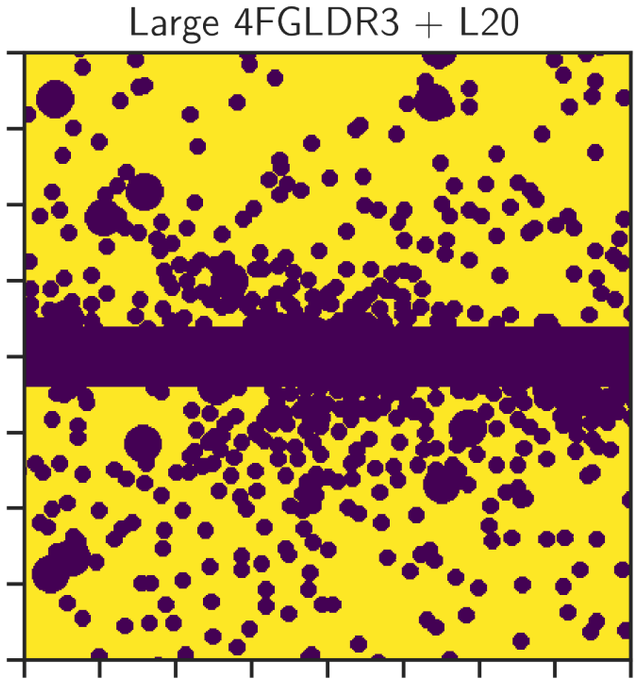

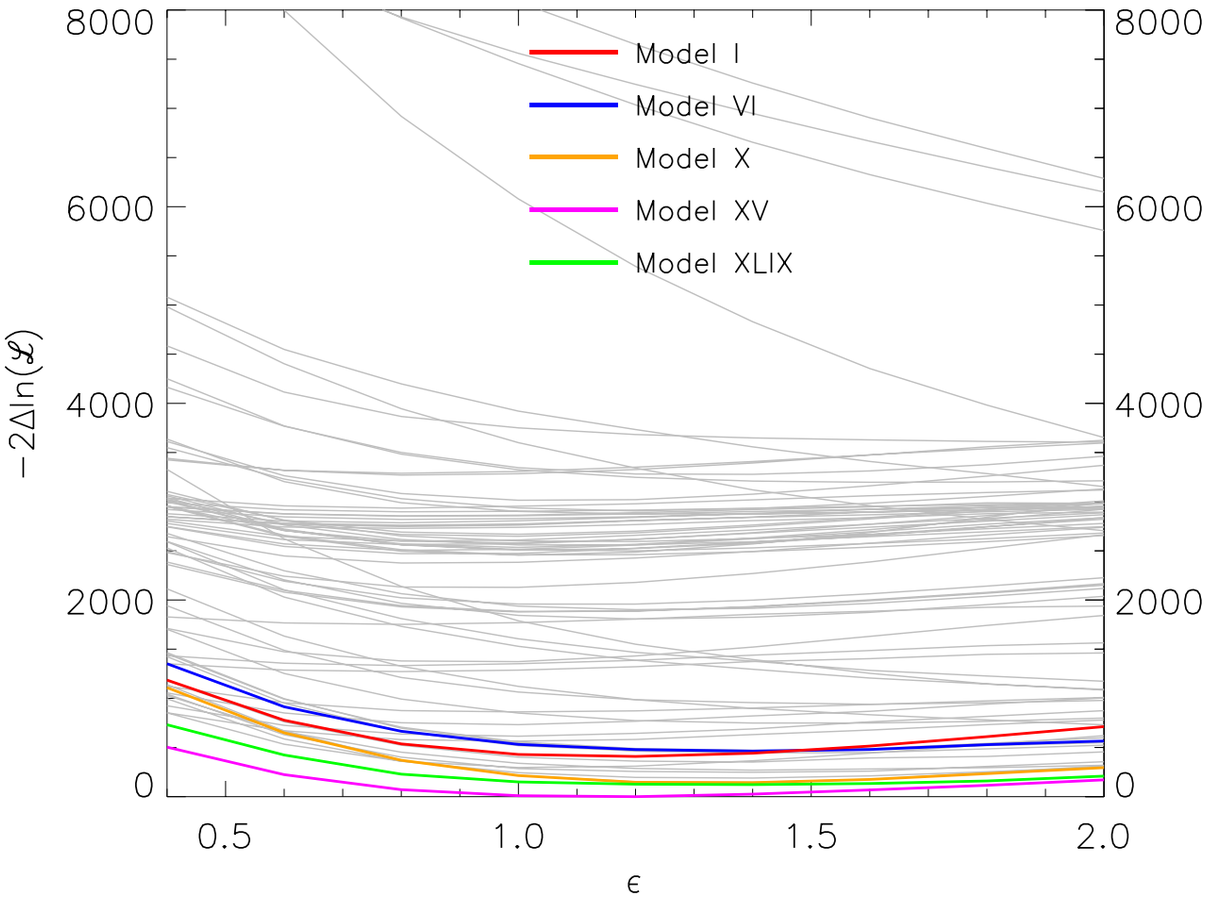

Ellipticity

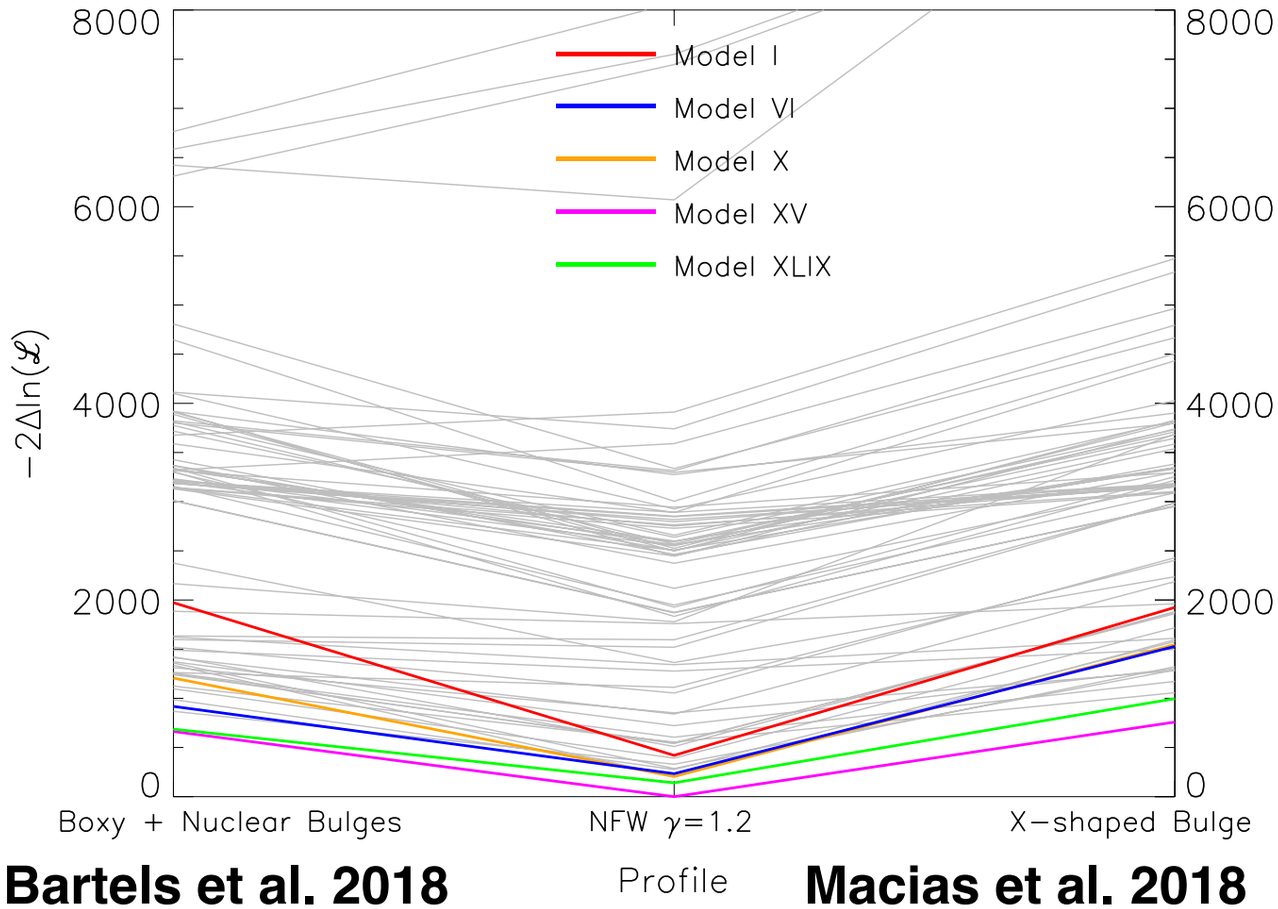

Bartels et al. 2018 Profile **Macias et al. 2018**

Spherical NFW vs Bulges

If this is a DM annihilation signal what do we learn about the particle physics?

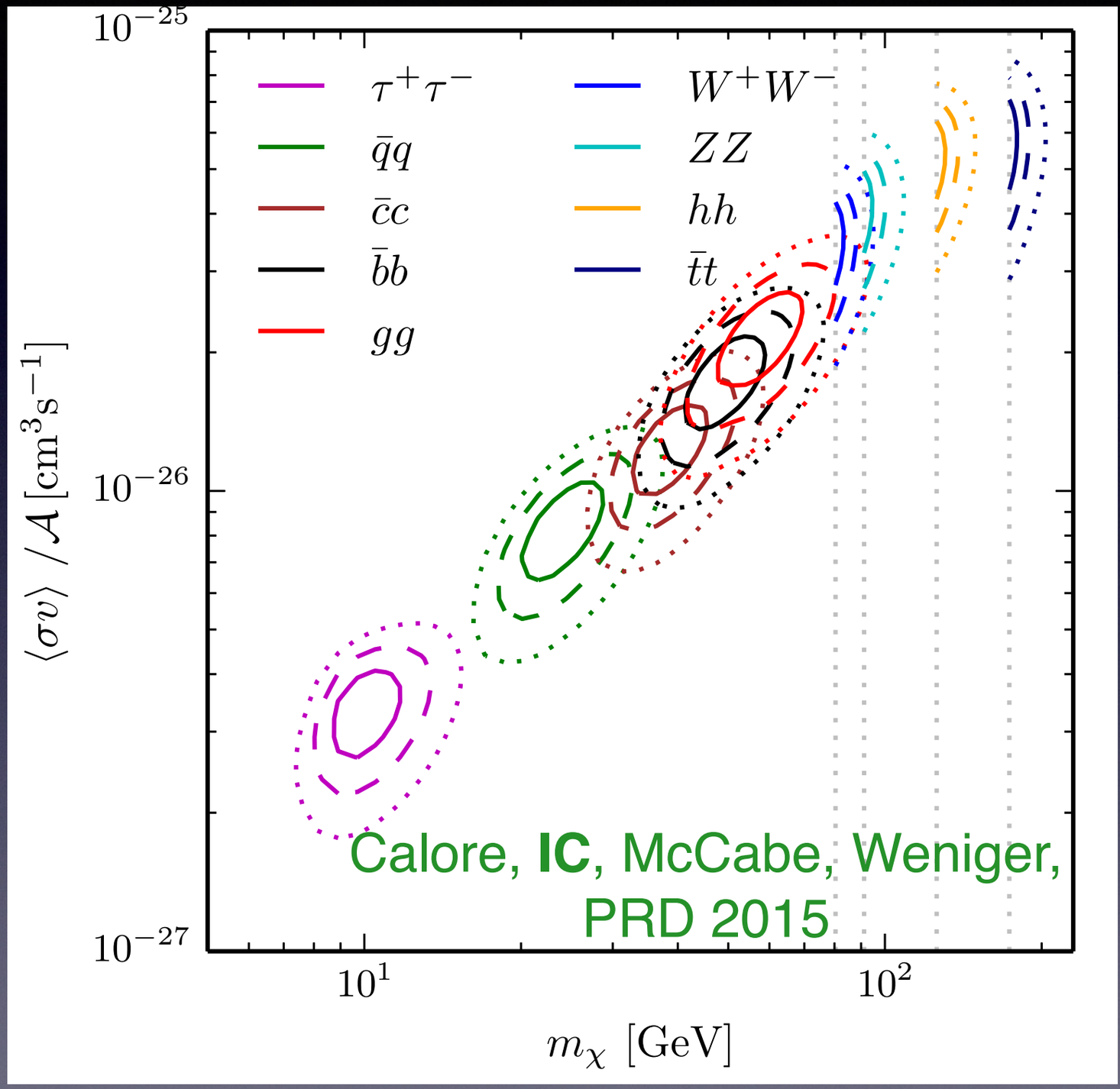

The mass range preferred very much within the WIMP range.

Looking at the antiproton to proton ratio find an the excess at~3 sigma

Supernova,

*also seen in **IC**, Hooper, Linden PRD 2017*

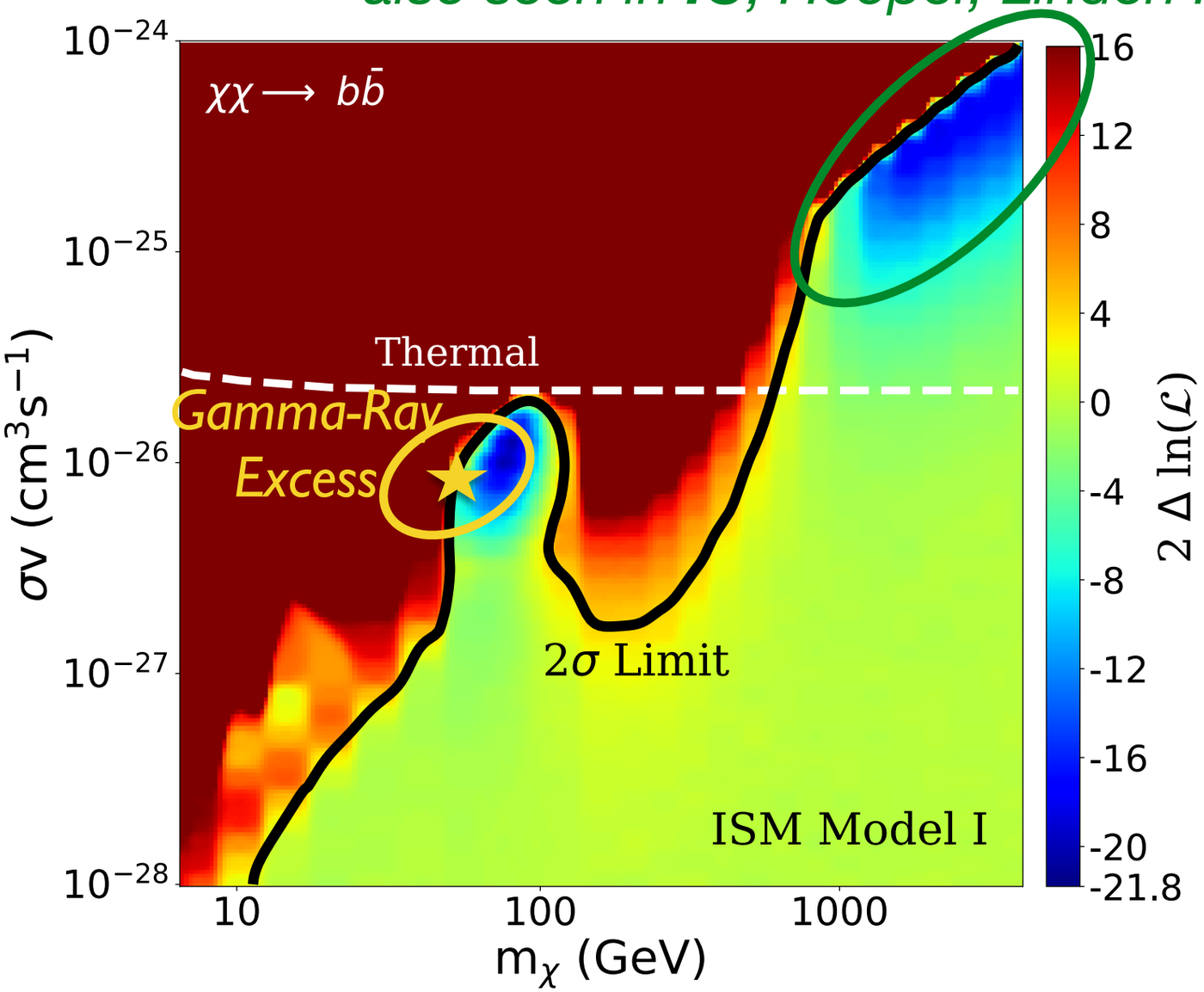

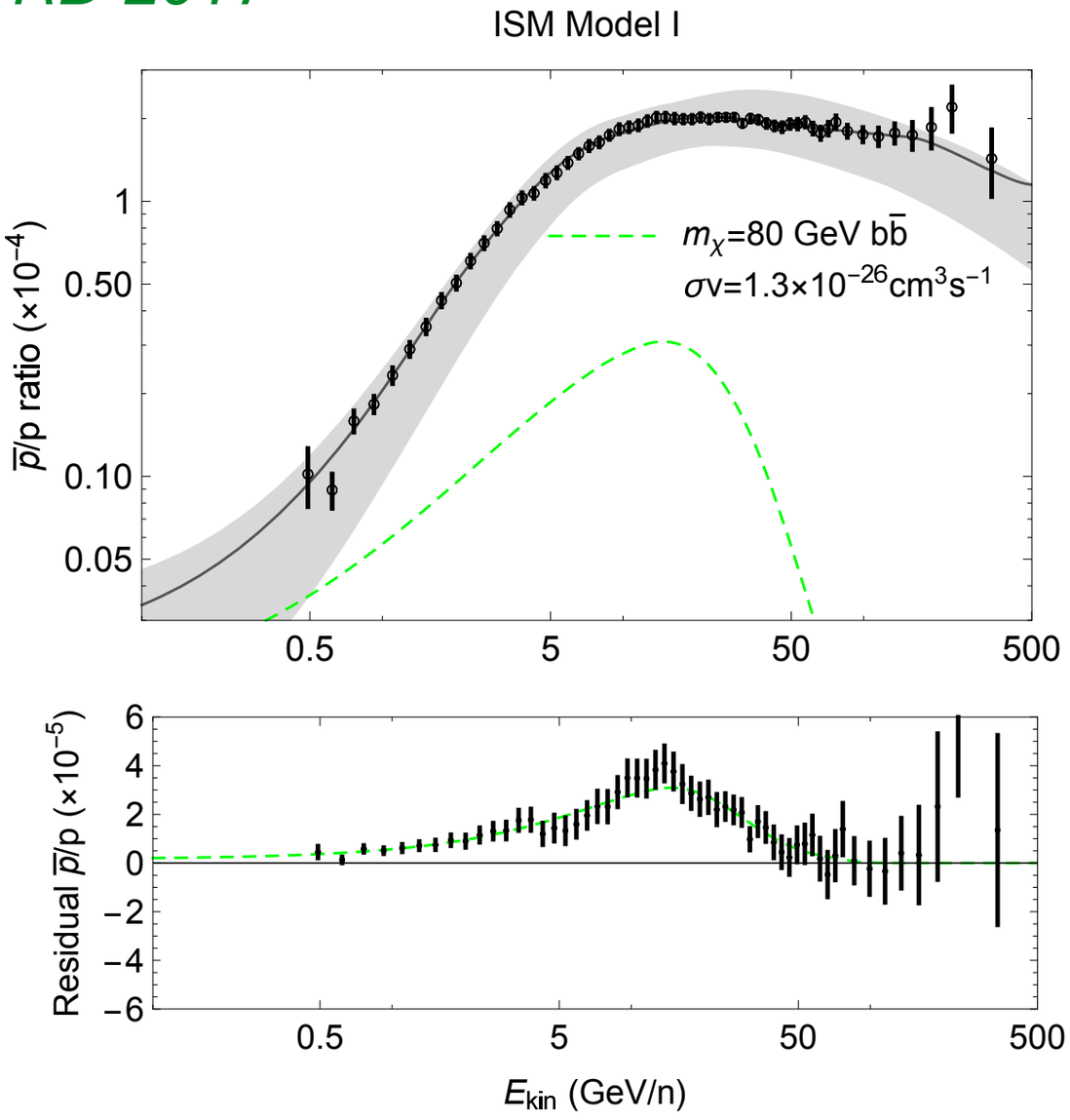

IC, Tim Linden, Dan Hooper PRD 2019

See also A. Cuoco et al. PRD 2019

Earlier results: Cuoco et al. PLR 2017,Cui et al. PRL 2017

How about heavier nuclei?

AMS, has unofficial claims of anti-He CR events (not all at the same year).

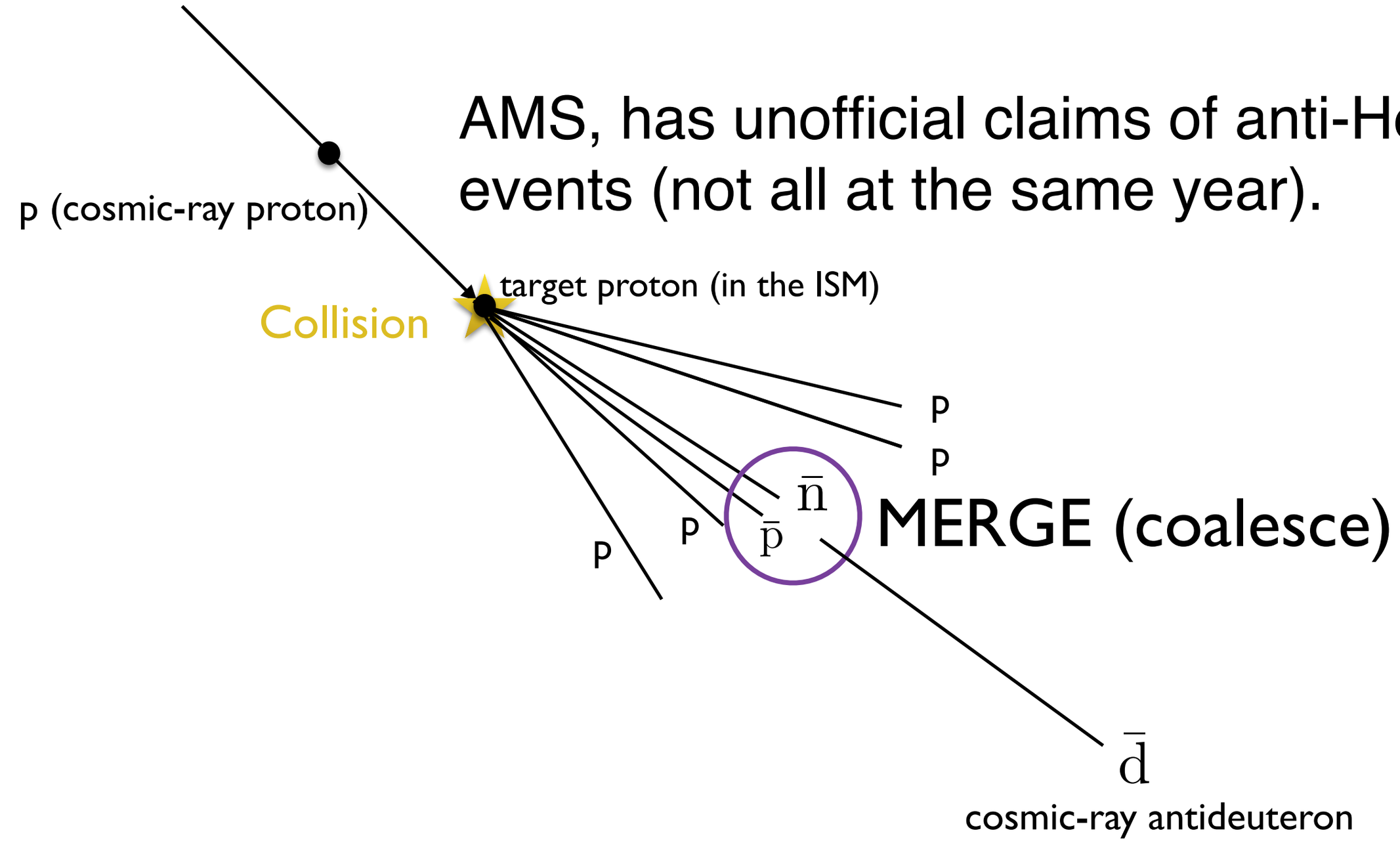

Antimatter flux Uncertainties

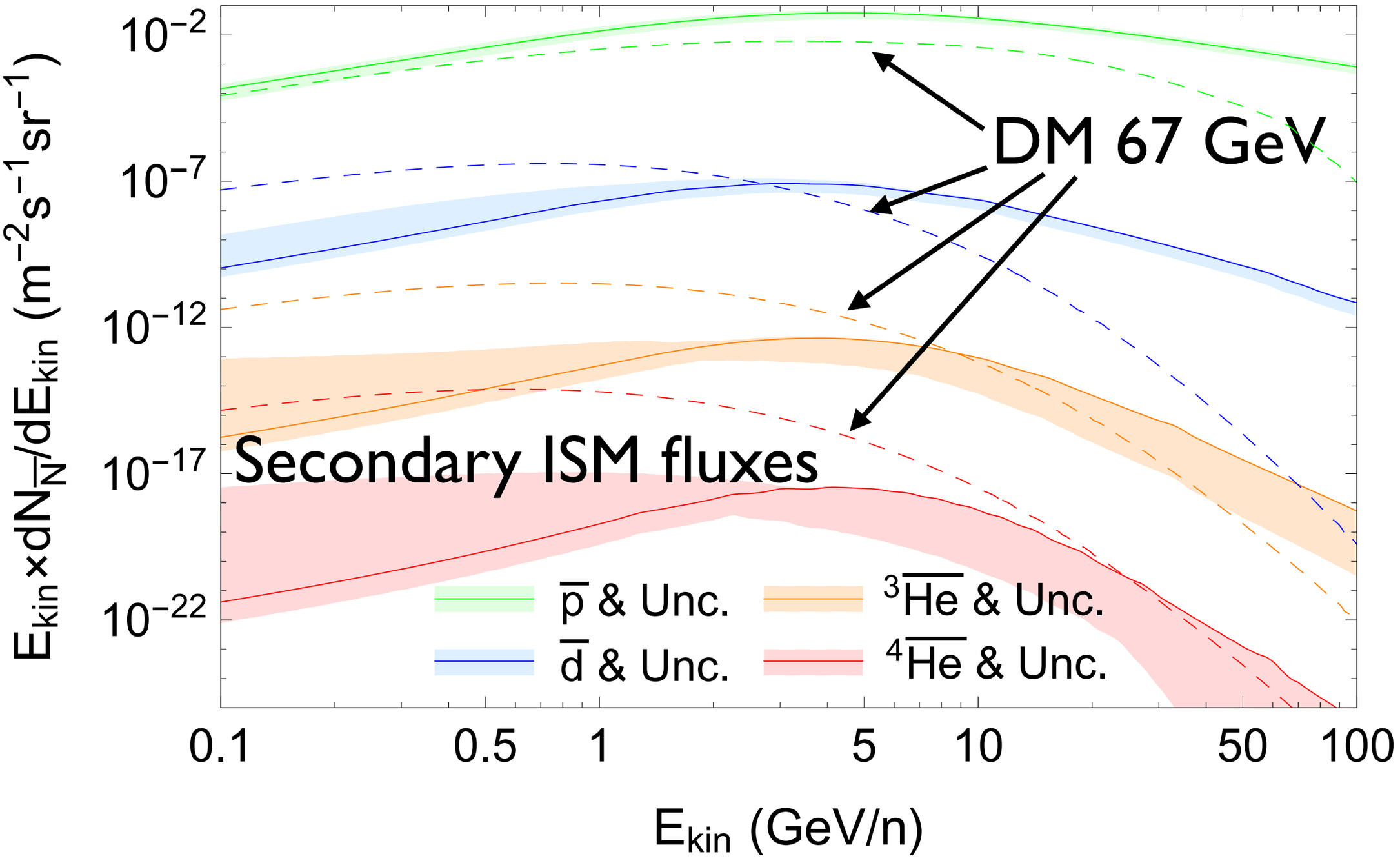

IC, Linden, Hooper PRD 2020

And a little extra positrons….

Utilizing cosmic-ray positron and electron observations to probe the averaged properties of Milky Way pulsars

Ilias Cholis[1*] and Iason Krommydas[2†]

[1]*Department of Physics, Oakland University, Rochester, Michigan 48309, USA*
[2]*Physics Division, National Technical University of Athens, Zografou, Athens 15780, Greece*

(Received 19 November 2021; accepted 4 January 2022; published 14 January 2022)

Pulsars have long been studied in the electromagnetic spectrum. Their environments are rich in high-energy cosmic-ray electrons and positrons likely enriching the interstellar medium (ISM) with such particles. In this work we use recent cosmic-ray observations from the *AMS-02*, *CALET,* and *DAMPE*

and likely release $O(10\%)$ of their rotational energy to cosmic rays in the ISM. Finally, we find at $\simeq$12 GeV positrons a spectral feature that suggests a new subpopulation of positron sources contributing at these energies.